From the Clinic of Cardiology, Pulmonology, and Vascular Medicine at Heinrich Heine University Düsseldorf Director: Univ.-Prof. Dr. med. Malte Kelm

Inhibition of Proline-rich-tyrosine kinase 2 (Pyk2) restores endothelial function and endothelium-dependent remote cardioprotection in an insulin-resistant mouse model

Dissertation

to obtain the academic title of Doctor of Philosophy (PhD) in Medical Sciences from the Faculty of Medicine at Heinrich Heine University Düsseldorf

submitted by

Amanda Brum

2023

As an inaugural dissertation printed by permission of the Faculty of Medicine at Heinrich Heine University Düsseldorf

Dean: Prof. Dr. med. Nikolaj Klöcker

Examiners: Prof. Dr. med. Malte Kelm
Prof. Dr. Eckhard Lammert

To my family

Zusammenfassung

Herz-Kreislauf-Erkrankungen sind weltweit die häufigste Todesursache. Diabetes mellitus Typ 2 und die damit zusammenhängenden Erkrankungen stehen in engem Zusammenhang mit der Entwicklung einer endothelialen Dysfunktion und kardiovaskulären Erkrankungen. Jüngste Studien haben gezeigt, dass eine endotheliale Dysfunktion mit einer erhöhten Pyk2-vermittelten Phosphorylierung von eNOS an seiner inhibitorischen Stelle (tyr656) verbunden ist. Der Einfluss von Pyk2 auf die Regulierung von eNOS in diabetischen Kontext ist jedoch noch nicht untersucht worden. Ziel dieser Studie ist es daher, die Rolle von Pyk2 für die eNOS-Regulierung, der Endothelfunktion und der kardialen Protektion im diabetischen Umfeld zu untersuchen.

New Zealand Obese (NZO) Mäuse und C57BL/6 (BL6) Mäuse im Alter von 18-20 Wochen wurden zunächst kardiovaksulär und metabolisch charakterisiert. Nach der spezifischen Hemmung von Pyk2 wurde die endotheliale Funktion und die systemische Hämodynamik mittels flussvermittelter Vasodilatation und Millar-Katheter untersucht. Der Aktivitätsstautus von Pyk2- und eNOS wurde mittels Western-Blot-Analyse bewertet. Zur Beurteilung der Infarktgrößen wurde ein Myokard-Ischämie-Reperfusions-Modell (30 Minuten/24 Stunden) eingesetzt. NZO-Mäuse zeigen eine systemische Insulinresistenz, eine Glukoseintoleranz, eine Hyperinsulinämie, einen arteriellen Bluthochdruck, einen erhöhten peripheren Widerstand und eine endotheliale Dysfunktion bei erhaltener Herzfunktion. Die Hemmung von Pyk2 stellte die endothelabhängige Dilatationsreaktion *in vivo* wirksam wieder her und normalisierte den arteriellen Blutdruck als auch den peripheren Widerstand bei diabetischen NZO-Mäusen. Die Pyk2-Hemmung mildert die funktionelle Hemmung der eNOS, indem sie die Pyk2-vermittelte Tyr657-Phosphorylierung von eNOS reduziert, was die NO-Bioverfügbarkeit wiederherstellt. Die kardioprotektiven Effekte induziert durch das rIPC-Manöver können durch Hemmung von Pyk2 in NZO-Mäusen wiederhergestellt werden, sodass die Infarktgröße sich reduziert. Dieser NO abhängige Mechanismus, der an diesem Prozess beteiligt ist, nutzt ebenso den MAPK/RISK-Signalweg, ohne das neuronale Signalwege in diabetischen NZO Mäusen eine Rolle spielen.

Pyk2 spielt eine zentrale Rolle bei der Modulation der eNOS in der Entwicklung einer endothelialen Dysfunktion bei Insulinresistenz. Darüber hinaus verbessert die Hemmung von Pyk2 die rIPC-induzierte kardiale Protektion, was darauf hindeutet, dass die Modulation von Pyk2 ein potenzieller Kandidat für die Verringerung der Belastung durch diabetesbedingte kardiovaskuläre Risiken sein kann.

Abstract

Cardiovascular disease is the leading cause of death worldwide. Type 2 Diabetes Mellitus and its related conditions are strongly associated with the development of endothelial dysfunction and cardiovascular diseases. Recent studies showed that endothelial dysfunction is associated with increased Pyk2-mediated phosphorylation of eNOS on its inhibitory site (tyr656). However, the impact of Pyk2 on eNOS regulation in diabetic conditions has not been addressed yet. Therefore, this study aims to investigate the role of Pyk2 for eNOS regulation, endothelial function, and remote cardioprotection in diabetic conditions.

Metabolic and cardiovascular characterization was performed in male 18-20 weeks old New Zealand Obese (NZO) and C57BL/6 (BL6) mice. Following Pyk2 inhibition, flow-mediated vasodilation, and Millar catheter assessed endothelial function and systemic hemodynamics. Pyk2 and eNOS activation status were evaluated by Western blot analysis, and myocardial ischemia-reperfusion (30 minutes/24h) surgery was used to investigate changes in infarct sizes associated with cardioprotection. NZO mice showed systemic insulin resistance, glucose intolerance, hyperinsulinemia, hypertension, increased peripheral resistance, endothelial dysfunction, and preserved cardiac function. Pyk2 inhibition effectively rescued endothelial-dependent dilatory response *in vivo* and normalized arterial blood pressure and peripheral resistance in diabetic NZO mice. Pyk2 inhibition alleviates eNOS abrogation by reducing Pyk2-mediated tyr657 phosphorylation on eNOS, which restores NO bioavailability. Pyk2 inhibition restores the cardioprotective effects of rIPC in NZO mice subjected to myocardial ischemia-reperfusion. The mechanism involved in this process occurs in a NO and MAPK/RISK pathway-dependent manner without the participation of neural signaling pathways in NZO mice.

Pyk2 plays a pivotal role in the modulation of eNOS and the development of endothelial dysfunction in insulin resistance conditions. In addition, Pyk2 inhibition improves rIPC-induced remote cardioprotection, suggesting Pyk2 modulation as a potential candidate for decreasing the burden of diabetes-related cardiovascular risk.

List of Abbreviations

AAR	Area at risk
Ach	Acetylcholine
ADA	American Diabetes Association
AKT	Protein kinase B
AMI	Acute myocardial infarction
Ang II	Angiotensin II
ANOVA	Analysis of Variance
AS160/TBC1D4	AKT substrate 160 kDa
ATP	Adenosine triphosphate
AUC	Area under the curve
BH4	Tetrahydrobiopterin
BL6	C57BL/6J
BSA	Bovine serum albumin
BW	Body weight
Ca^{2+}	Calcium
CABG	Coronary artery bypass grafting
CAD	Coronary artery disease
CaM	Calmodulin
CAMKII	Ca2+/calmodulin-dependent protein kinase
cGMP	Guanosine cyclic monophosphate
CO	Cardiac output
COI	Cardiac output index
CPTIO	2-4-carboxyphenyl-4,4,5,5-tetramethylimidazoline-1-oxyl-3-oxide
DAMPs	Damage-associated molecular pattern molecules
DBP	Diastolic pressure
DM	Diabetes Mellitus
DMSO	Dimethyl sulfoxide

DNA	Deoxyribonucleic acid
DPBS	Dulbecco's phosphate-buffered saline
EC	Endothelial cells
ECG	Electrocardiography
ED	Endothelial dysfunction
EDTA	Ethylenediaminetetraacetic acid
EDVI	End-diastolic volume index
EF	Ejection fraction
eNOS (NOS III)	Endothelial Nitric Oxide Synthase
eNOS KO	eNOS knockout
ERK	Extracellular signal-regulated kinase
ESVI	End-systolic volume index
ET-1	Endothelin 1
F. nerve	Femoral nerve transection
FAD	Flavin adenine dinucleotide
FAK	Focal adenosine kinase
FFA	Free fatty acids
FMD	Flow-mediated vasodilation
FMN	Flavin mononucleotide
GAPDH	Glyceraldehyde-3-phosphate dehydrogenase
GLUT-4	Glucose transporters type 4
GPCRs	G protein-coupled receptors
Grb2	Growth Factor Receptor-bound protein 2
GSK3	Glycogen synthase kinase-3
GTP	Guanosine triphosphate
GTT	Glucose tolerance test
H^+	Hydrogen ion
H_2O_2	Hydrogen peroxide
H_2S	Hydrogen sulfide

HbA1c	Haemoglobin A1C
HO-1	Heme Oxygenase-1
HPLC	High-performance liquid chromatography
HR	Heart rate
HW	Heart weight
I/R	Ischemia-reperfusion
IDF	International Diabetes Federation
iNOS (NOSII)	Inducible NOS
IR	Insulin receptor
IRS	Insulin receptor substrate
IRS1	insulin-receptor substrate 1
IS	Infarct size
ITT	Insulin tolerance test
JAK2	Janus kinase 2
LAD	Left artery descending
LANUV	Landesamt für Natur, Umwelt- und Verbraucherschutz
L-Arg	L-Arginine
L-Citr	L- Citrulline
LV	Left ventricle
MAP	Mean arterial blood pressure
MAPK	Mitogen-activated protein kinase
MEK	Mitogen-activated protein kinase kinase
miRNA	Micro RNA
mRNA	Messenger RNA
mtDNA	Mitochondrial DNA
mTOR	Mammalian target of the rapamycin
NADPH	Nicotinamide adenine dinucleotide phosphate
NEM	N-ethylmaleimide
nNOS (NOS I)	Neuronal NOS

NO	Nitric Oxide
NO_2^-	Nitrite
NO_3^-	Nitrate
NOS	Nitric oxide synthases
Nox2	NADPH oxidase 2
NZO	New Zealand Obese mice
p38 MAPK	p38 mitogen-activated protein kinase
PAI-1	Plasminogen activator inhibitor-1
Phe	Phenylephrine
PI3K	Phosphatidylinositol 3-kinase
PKA	Protein kinase A
PPCI	Primary percutaneous coronary intervention
PSLA	Parasternal long axis
Pyk2	Proline-rich tyrosine kinase 2
Pyk2-I	Proline-rich tyrosine kinase 2-inhibition
Raf	Rapidly Accelerated Fibrosarcoma
RBCs	Red blood cells
RIPA	Radioimmunoprecipitation assay buffer
rIPC	Remote ischemic preconditioning
RISK	Reperfusion injury salvage kinase
RNA	Ribonucleic acid
ROS	Reactive oxygen species
SAFE	Survivor activating factor enhancement
SAX	Parasternal short axis
SBP	Systolic blood pressure
sCG	Soluble guanylate cyclase
SEM	Standard error of the mean
Ser1177	*Serine* 1177
Ser21/9	Serine 21/9

Shc	Src homology and the Collagen
SNP	Sodium nitroprusside
STAT3	Signal transducer and activator of transcription 3
SV	Stroke volume
SVI	Stroke volume index
T1DM	Type 1 diabetes mellitus
T2DM	Type 2 diabetes mellitus
TBC1D1	TBC1 Domain Family Member 1
Thr495	Threonine 495
Thr590	Threonine 590
Thr642	Threonine 642
TNFα	Tumor necrosis factor-alpha
TPR	Total peripheral resistance
TTC	Triphenyl tetrazolium chloride
Tyr656	Tyrosine 656
Tyr657	Tyrosine 657
VCAM-1	Vascular Cell Adhesion Molecule 1
VEGF	Vascular Endothelial Growth Factor
VSMCs	Vascular smooth muscle cells

Index

1 Introduction 1
1.1 Diabetes mellitus 1
1.2 Insulin resistance and its complications 3
1.3 Insulin-mediated glucose homeostasis 5
1.4 Insulin signaling pathway 6
1.5 Endothelial nitric oxide synthase regulation and its relevance for cardiovascular homeostasis 9
1.5.1 Endothelial nitric oxide synthase regulation 11
1.6 Insulin-mediated eNOS regulation 15
1.7 Ischemia-reperfusion injury 16
1.8 Ischemic conditioning and cardioprotection 18
1.9 Remote ischemic preconditioning (rIPC) 19
1.10 Aims of thesis 23
2 Material and Methods 27
2.1 Buffers and solutions 27
2.2 Animal experiments 27
2.3 Insulin stimulation experiments 28
2.4 Pharmacological Pyk2 inhibition 28
2.5 Organ harvesting for biochemical parameters 29
2.6 Blood glucose and plasma insulin measurement 29
2.7 Metabolic tolerance tests 30
2.8 Remote ischemia-preconditioning 31
2.9 Ultrasound imaging 32
2.9.1 Assessment of cardiac function 32
2.9.2 Assessment of vascular function *in vivo* 33
2.10 Assessment of systemic hemodynamics 34
2.11 Western blot and immunoprecipitation 35
2.11.1 Protein determination 35
2.11.2 Immunoblot 35
2.11.3 Immunoprecipitation 38
2.12 Plasma levels of Nitrite and Nitrate 39

2.12.1 Sample preparation 39
2.12.2 Nitrite plasma levels 39
2.12.3 Nitrate plasma levels 40
2.13 Ischemia-reperfusion injury 40
2.13.1 Surgical procedure 40
2.13.2 Experimental groups 41
2.13.3 Infarct sizes quantification 46
2.14 Statistical analysis 47
3 Results 47
3.1 NZO mice exhibit glucose intolerance, insulin resistance, and hyperinsulinemia 47
3.2 Insulin signaling pathway in skeletal muscle and cardiovascular tissues 50
3.2.1 Skeletal muscle 51
3.2.2 Heart 57
3.3 Pyk2 inhibition leads to a regain in endothelial function in NZO mice 64
3.4 Pyk2 inhibition normalizes NZO mice´s arterial blood pressure 66
3.5 Pyk2 inhibition alleviates p-Tyr656-induced eNOS abrogation in NZO mice heart 67
3.6 Pyk2 inhibition restores the loss of cardioprotection mediated by rIPC in NZO mice 71
4 Discussion 81
4.1 Cardiometabolic characterization of the NZO mice 84
4.2 Pyk2 inhibition restores endothelial function in NZO mice 85
4.2.1 Pyk2 Inhibition and Systemic Hemodynamics 88
4.3 Pyk2-inhibition restores rIPC-induced cardioprotection in NZO mice 89
4.3.1 Remote ischemia preconditioning mediating cardioprotection 89
4.3.2 The mechanism involved in rIPC-mediated cardioprotection 91
5 References 96
6 Acknowledgments 110

1 Introduction

1.1 Diabetes mellitus

Diabetes Mellitus (DM) prevalence is increasing worldwide. According to the last International Diabetes Federation's (IDF) estimation, around 537 million people have diabetes globally. Furthermore, the predictions show that if no preventive measures are taken, those numbers will rise to 783 million people by 2045 (IDF 2021, Sun, Saeedi et al. 2022). DM is a chronic metabolic disease marked by high blood glucose, i.e., hyperglycemia and extensive impairment of energy metabolism. According to the American Diabetes Association (ADA), fasting glucose levels above 126 mg/dl or hemoglobin A1C (HbA1c) ≧6,5 % indicate DM. In contrast, values between 100-125 mg/dl and HbA1c 5,7-6,4% indicate impaired glucose tolerance, while levels below 99 mg/dl are considered normal (IDF 2021).

The primary cause of DM is impairment in insulin production, resistance to its action, or a combination of both. DM is classified into different types according to its etiology. Type 1 diabetes mellitus (T1DM) is characterized by absolute insulin deficiency, usually due to the autoimmune pancreatic β-cells destruction (IDF 2021, ElSayed, Aleppo et al. 2023). This type of DM has a robust genetic compound, usually but not only appearing at an early age (< 35 years) and affecting around 5-8% of DM patients. In contrast, type 2 diabetes mellitus (T2DM) mostly appears at late stages of life and is frequently associated with physical inactivity, overweight/obesity, unhealthy lifestyle, and aging. T2DM represents 90-95% of DM patients, and its primary cause is insulin resistance (American Diabetes Association 2014, ElSayed, Aleppo et al. 2023). Chronic insulin resistance is associated with compensatory hyperinsulinemia that can progress to pancreatic β-cells loss and decreased insulin production in the later stages of the disease (American Diabetes Association 2014).

DM is associated with several comorbidities, and its main complications are divided into macrovascular and microvascular disorders. Macrovascular complications are determined by continuous DM-associated damage to large arteries, such as coronary artery disease (CAD), acute myocardial infarction (AMI), and stroke (Chen, Ovbiagele et al. 2016, Cho, Ann et al. 2019, Baviera, Genovese et al. 2022). On the other hand, microvascular complications represent DM-induced damage to the small vessels, such as small arteries, arterioles, venules, and capillaries. Retinopathy, neuropathy, and kidney disease are among DM patients' most common microvascular complications (An, Nichols et al. 2021).

In addition, a low-grade inflammatory state associated with increased oxidative stress (Pitsavos, Tampourlou et al. 2007, Yuan, Yang et al. 2019) and an overall pro-thrombotic condition are implications of DM (Carr 2001). These aspects collectively provide aggravated pathological and immunological responses that exacerbate tissue damage and increase morbidity and mortality in those patients.

Additionally, research has demonstrated that patients with diabetes have a more than twofold increased chance of dying from cardiovascular disease than nondiabetic patients (Preis, Hwang et al. 2009). Furthermore, studies have shown that patients with diabetes have a higher chance of dying after a myocardial infarction than patients with prior cardiovascular complications (Mukamal, Nesto et al. 2001). Furthermore, DM is independently associated with reduced myocardial reperfusion, larger infarct sizes, and a higher risk of death during and after primary percutaneous coronary intervention (PCI) following an AMI (Marso, Miller et al. 2007). In addition, a recent German study demonstrated that DM is associated with a higher prevalence of several comorbidities, including obesity, depression, hypertension, coronary heart disease, and stroke (Schmidt, Reitzle et al. 2021).

Therefore, uncovering the pathophysiology of DM and its related conditions, such as insulin resistance, hyperinsulinemia, and hyperglycemia, is crucial for providing efficient therapies and strategies to decrease the burden of this disease.

1.2 Insulin resistance and its complications

Insulin resistance is defined as the impairment of insulin signal transduction, i.e., the reduction of insulin action. Insulin resistance causes several adjacent metabolic consequences, such as hyperinsulinemia and hyperglycemia, that in turn overfeed and support the insulin resistance conditions (Boucher, Kleinridders et al. 2014, Johnson 2021). Although insulin resistance is the main hallmark of T2DM, studies have demonstrated that insulin resistance may appear years prior to the onset of T2DM and independently increases the cardiovascular risk (Tabák, Jokela et al. 2009, Ormazabal, Nair et al. 2018, Adeva-Andany, Martínez-Rodríguez et al. 2019). Furthermore, studies have shown that insulin resistance/compensatory hyperinsulinemia is strongly associated with developing coronary heart disease in nondiabetic subjects (Reaven 2012). In addition, insulin resistance is a predictor of coronary arterial disease, and the maintenance of insulin sensitivity is proposed to prevent around 42% of myocardial infarct cases (Eddy, Schlessinger et al. 2009). Moreover, drugs that improve insulin sensitivity appear more effective in decreasing cardiovascular risk than glycemic control alone (Robinson, Burke et al. 1998). Furthermore, using drugs that improve insulin sensitivity, i.e., metformin, significantly improves T1DM patients' endothelial function and vascular health and decreases cardiovascular risk regardless of body weight, fat mass, and insulin dose (Bjornstad, Schäfer et al. 2018).

In addition, insulin resistance is strongly associated with the development of endothelial dysfunction (ED) and the impairment of the Phosphatidylinositol 3-kinase (PI3K)/ protein kinase B (AKT)/ endothelial Nitric Oxide Synthase (eNOS) signaling pathway. As a result, eNOS activity and its functionality are abrogated, and Nitric Oxide (NO) production is reduced, which limits eNOS-dependent remote organ protection (Symons, McMillin et al. 2009, Muniyappa, Chen et al. 2020). Evidence has demonstrated that insulin-mediated PI3K/AKT activation is responsible for antiatherogenic protective effects mediated by insulin upon cardiovascular tissues. This signaling pathway enhances NO output and increases

the expression of Vascular Endothelial Growth Factor (VEGF)/ Heme Oxygenase-1 (HO-1) proteins, decreasing the expression of inflammatory cell adhesion molecules such as Vascular Cell Adhesion Molecule 1 (VCAM-1). Thus, this pathway is known to promote anti-inflammatory, antioxidant, antiatherogenic, and cardioprotective actions necessary for maintaining cardiovascular health (Durante, Kroll et al. 1997, He, Li et al. 2021).

Furthermore, studies have shown that vascular tissues can develop selective insulin resistance, in which insulin-mediated activation of PI3K/AKT signaling pathway is impaired. In contrast, the Mitogen-activated protein kinase (MAPK) / extracellular signal-regulated kinase (ERK) remains sensitive and sometimes overstimulated. These events lead to endothelial dysfunction, increased expression of Endothelin 1 (ET-1), plasminogen activator inhibitor-1 (PAI-1), abnormal vasoconstriction, inflammation, oxidative stress, and tissue damage (Jiang, Lin et al. 1999, Kim, Montagnani et al. 2006, King, Park et al. 2016). Moreover, investigations have shown that MAPK, MAPK p38, and ERK1/2 are involved in the mechanism of damage and inflammation after ischemic events. Interestingly, the inhibition of these molecular signaling pathways alleviated ischemia-reperfusion injury and reduced cell damage (Chang, Zhao et al. 2018, Sanit, Prompunt et al. 2019). Besides that, insulin resistance also induces alterations in mitochondrial function, increasing pro-inflammatory cytokines and disrupting endothelial barrier integrity *in vitro* (Lee, Chakraborty et al. 2018). These conditions impair the endothelium's capacity to participate in remote signaling and protect the tissues against cell damage following ischemic events.

Furthermore, the blood glucose concentration is constantly high during chronic insulin resistance conditions. Hence, the pancreatic β-cells regularly receive stimuli to produce insulin to maintain glucose homeostasis. These supraphysiological insulin levels are called hyperinsulinemia (Boucher, Kleinridders et al. 2014). Hyperinsulinemia has several deleterious effects on endothelial function and cardiovascular health. Moreover, hyperinsulinemia overfeeds the atherogenic signaling described above and intensifies tissue damage (Group 2004, Chandel,

Sathis et al. 2020) and insulin resistance (Marín-Juez, Jong-Raadsen et al. 2014, Gao, Wang et al. 2020).

1.3 Insulin-mediated glucose homeostasis

Insulin is a peptide hormone secreted by the pancreatic β-cells in response to increased circulatory levels of glucose, amino acids, and fatty acids. Insulin's primary function is maintaining blood glucose levels under physiological concentration and promoting glucose uptake in insulin-dependent tissues such as skeletal muscle and adipose tissue. Furthermore, insulin has a potent anabolic effect and is essential in energy metabolism regulation, cell growth, differentiation, and gene expression (Saltiel and Kahn 2001, Boucher, Kleinridders et al. 2014).

Insulin regulates glucose homeostasis by acting in three central tissues: skeletal muscle, adipose tissue, and liver. In skeletal muscle and adipose tissue, insulin promotes glucose uptake by stimulating glucose transporters-4 (GLUT-4) translocation from intracellular vesicles to the cell membrane. In addition, insulin inhibits catabolic processes such as the breakdown of proteins, glycogen (glycogenolysis), and fat (lipolysis). In contrast, it stimulates anabolic processes such as glycogen (glycogenesis), protein and fatty acids (lipogenesis) synthases, and storage (Saltiel and Kahn 2001, Honka, Latva-Rasku et al. 2018, Silva Rosa, Nayak et al. 2020). In the liver, insulin regulates glucose homeostasis by targeting hepatic energy metabolism. Under fasting conditions, the liver plays a crucial role in maintaining blood glucose concentration by breaking hepatic glycogen and forming glucose by non-carbohydrate precursors (gluconeogenesis) (Edgerton 2006). However, insulin acts as a potent anticatabolic hormone under postprandial conditions, inhibiting catabolic mechanisms (gluconeogenesis, glycogenolysis, and lipolysis) while promoting hepatic glycogen synthesis (Edgerton 2006, Rui 2014).

Thus, the glucose intake by these tissues is essential for their energy metabolism and maintaining blood glucose concentration in homeostatic levels during the pre and postprandial period. Therefore, the failure to maintain any of these processes

due to insulin resistance or deficiency results in glucose intolerance and abnormal glucose and lipid plasma levels, consequently promoting the development of DM.

1.4 Insulin signaling pathway

Insulin mediates its activity by binding to the tyrosine kinase insulin receptor (IR). The IR is a tetrameric protein composed of two subunits $(\alpha\beta)^2$. The α subunit is an extracellular protein that undergoes modifications when bound to insulin, leading to activation and autophosphorylation of the transmembrane β subunit. The IRβ transphosphorylation initiates the phosphorylation cascade by recruiting and activating intracellular receptors substrates proteins such as insulin receptor substrate (IRS) and Shc. The phosphorylation and activation of IRS in tyrosine residues mostly lead to the activation of the PI3K/AKT signaling pathway (Boucher, Kleinridders et al. 2014). AKT mediates most of the metabolic effects of insulin. For that reason, this signaling pathway is also known as the metabolic pathway. Among the metabolic actions mediated by AKT are 1) glucose uptake by the phosphorylation of AKT substrate 160 kDa (AS160/TBC1D4) and TBC1 Domain Family Member 1 (TBC1D1) on Thr642 and Thr590, respectively. The phosphorylation of these two proteins mediates signal transduction and conformational change, resulting in GLUT-4 translocation from the intracellular vesicle to the cell surface (Sakamoto and Holman 2008, Middelbeek, Chambers et al. 2013); 2) stimulation of glycogen synthase by phosphorylation and inactivation of glycogen synthase kinase-3 (GSK3). GSK3 is a serine /threonine kinase that can inhibit glycogen synthase. After insulin stimulation, GSK3 is phosphorylated (GSk3-α/β ser21/9) and inactivated, which in turn leads to stimulate glycogen synthesis (Nikoulina, Ciaraldi et al. 2002); 3) regulation of lipid synthases (Saltiel and Kahn 2001). Furthermore, AKT also plays an important role in endothelial-dependent NO production, insulin-mediated vasodilation (Symons, McMillin et al. 2009), and cell cycle regulation and survival (Liu, Begley et al. 2014). Studies have shown that stimulation of the PI3K/AKT/eNOS signaling pathway is related to antiatherogenic and anti-inflammatory actions, resulting in organ protection and decreased

cardiovascular risk. Moreover, this signaling pathway can also lead to antiapoptotic action, improving cell survival during ischemic events by the activation of the PI3K/AKT/ mammalian target of the rapamycin (mTOR) pathway (Aikawa, Nawano et al. 2000, Gao, Gao et al. 2002, Yang, Wu et al. 2018)

Notably, insulin also regulates chronic responses by its ability to activate the MAPK)/ ERK signaling, also known as the mitogenic signaling pathway. This pathway involves the tyrosine phosphorylation of IRS in combination with the activation of Src homology and the Collagen (Shc) family. The Shc interacts with Growth Factor Receptor-bound protein 2 (Grb2) and activates Ras. Ras operates as a molecular switch, stimulating serine kinase cascade through the gradual activation of Rapidly Accelerated Fibrosarcoma (Raf) kinase, Mitogen-activated protein kinase kinase (MEK), and ERK. Once activated, ERK translocates into the cellular nucleus and initiates a transcriptional signaling response, resulting in gene expression, cell growth, and cell differentiation and proliferation (Boucher, Kleinridders et al. 2014).

Under physiological conditions, the metabolic and mitogenic signaling pathways are balanced. The activation of metabolic pathways requires small amounts of insulin concentration, whereas the activation of the mitogenic pathway requires a high insulin concentration (Bedinger and Adams 2015). However, under pathological conditions such as T2DM, obesity, insulin resistance, and increased oxidative stress, the mitogenic pathway is overactivated, which results in deleterious effects and increased cardiovascular risk (King, Park et al. 2016, Arcambal, Taïlé et al. 2019). Moreover, the excessive activation of the MAPK-ERK signaling pathway is related to an impairment of AKT-induced eNOS stimulation with concomitant vasoconstriction, endothelial dysfunction, increased ET-1 expression, and an increase in cardiovascular events (Boucher, Kleinridders et al. 2014, Tatulian 2015, Posner 2017). The insulin signaling pathway under health and insulin resistance conditions is illustrated in Figure 1.

Furthermore, researchers have shown that the abnormal activation of the MAPK-ERK pathway is related to the impairment of the metabolic signaling pathway and insulin resistance through negative regulation of IRS by serine phosphorylation (Jiang, Lin et al. 1999, Gual, Le Marchand-Brustel et al. 2005, King, Park et al. 2016). IR and IRS1 proteins can undergo serine phosphorylation, attenuating signaling by decreasing insulin-stimulated tyrosine phosphorylation. These inhibitory phosphorylations provide negative feedback to insulin signaling and serve as a mechanism for cross-talk from other pathways that produce insulin resistance (Boucher, Kleinridders et al. 2014). However, excessive serine phosphorylation can inhibit tyrosine-mediated metabolic signaling pathways and lead to pathological levels of insulin resistance. Furthermore, different risk factors associated with T2DM, such as increased Angiotensin II (Ang II), free fatty acids (FFA), and pro-inflammatory cytokines, stimulate IRS serine phosphorylation and inhibit AKT-mediated metabolic signaling (Andreozzi, Laratta et al. 2004, Andreozzi, Laratta et al. 2007, da Costa, Neves et al. 2016, Akash, Rehman et al. 2018). Furthermore, this imbalance also induces cell migration and impairment of AKT-induced eNOS stimulation with excessive vasoconstriction, endothelial dysfunction, and increased cardiovascular risk (Boucher, Kleinridders et al. 2014, Tatulian 2015, Posner 2017). Therefore, maintaining equilibrium between those two signaling pathways is crucial to preserve insulin-dependent organ protective signaling.

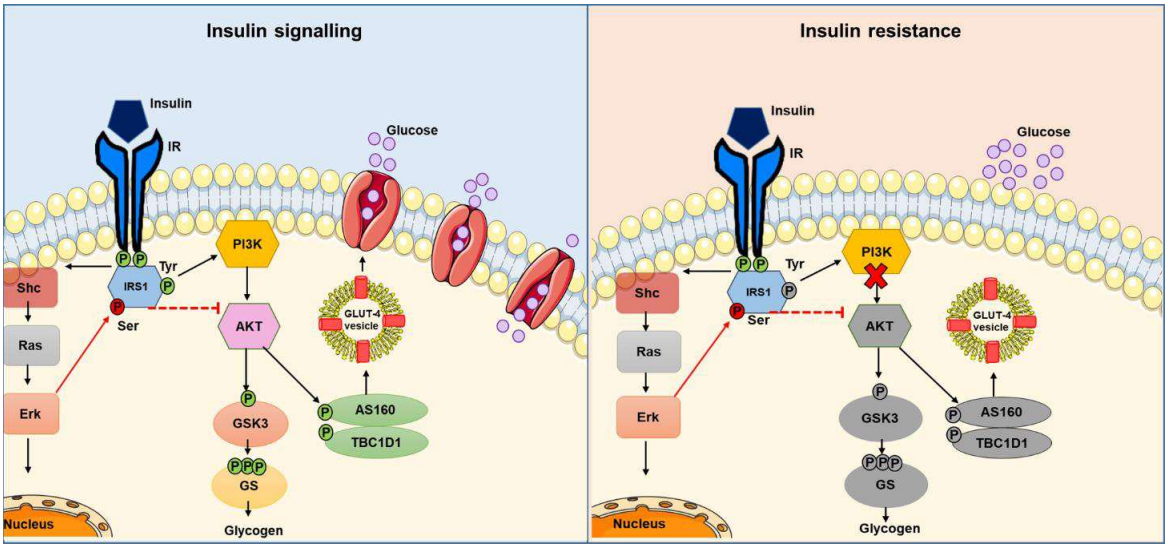

Fig. 1 Insulin signaling pathway

Insulin mediates its action upon binding to the insulin receptor (IR) in the cellular membrane. After binding, IR initiates a phosphorylation cascade by recruiting and activating insulin receptor substrate (IRS) and Shc. The phosphorylation of IRS in tyrosine residues mostly leads to activation of the phosphatidylinositol 3-kinase (PI3K) / Protein Kinase B (AKT) signaling pathway, also known as the metabolic pathway. AKT activation promotes glucose uptake by the phosphorylation of AKT substrate 160 kDa (AS160/TBC1D4) and TBC1 Domain Family Member 1 (TBC1D1), ultimately leading to GLUT4 translocation. In addition, AKT activation also stimulates glycogen synthase by phosphorylation and inactivation of glycogen synthase kinase-3 (GSK3). On the other hand, insulin can also activate the mitogenic signaling pathway consisting of mitogen-activated protein kinase (MAPK) activation. In this pathway, the tyrosine phosphorylation of IRS occurs in combination with the activation of Src homology and the Collagen (Shc) family that promotes the activation of Ras. Ras operates as a molecular switch, stimulating extracellular signal-regulated kinase (ERK). Once activated, ERK translocates into the cellular nucleus and initiates a transcriptional signaling response, resulting in gene expression, cell growth, and cell differentiation and proliferation. Under physiological conditions, both signaling pathways are in balance, as illustrated in the left scheme. However, in insulin resistance conditions, insulin fails to mediate activation of the metabolic signaling pathway, which results in abrogated glucose uptake and hyperglycemia. Insulin resistance is also followed by the overactivation of the mitogenic signaling pathway that mediates IRS phosphorylation in serine residues, intensifying the inhibition of the metabolic pathway (right scheme). Created by Amanda Brum with elements of molecular biology at smart-server medical art (https://smart.servier.com/).

1.5 Endothelial nitric oxide synthase regulation and its relevance for cardiovascular homeostasis

The endothelium is a monolayer of cells that surround the vascular wall. For a long time, it was believed that the endothelium's only function was to be a physical

barrier between the blood and the tissues. However, in 1980, Furchgott and Zawadski discovered that the endothelium plays a pivotal role in the modulation of vascular homeostasis and tone (Furchgott and Zawadzki 1980, Cahill and Redmond 2016). Endothelial cells (EC) act as a signal transducer that reacts and releases circulating factor that modifies the vessel wall. EC can respond to physical and chemical signals by producing a wide range of factors that regulate vascular tone, cell adhesion, thrombus resistance, smooth muscle proliferation, and vessel wall inflammation (Fleming 2010, Heiss, Rodriguez-Mateos et al. 2015, Sun, Wu et al. 2019). The main vasoactive molecules produced by EC are NO and ET-1, which mediate vascular relaxation and constriction, respectively. NO is a gaseous molecular messenger responsible for multiple positive responses in the cardiovascular system. In endothelial cells, NO is generated by the action of eNOS in response to cellular events such as Ca^{2+} influx, phosphorylation, and protein interactions. Several events and molecules have been described to regulate eNOS function and NO output. Among them, fluid shear stress (physical forces), neuromodulators (acetylcholine (Ach) and phenylephrine (Phe)), and hormones (insulin, estrogen, and bradykinin) are the most common (Fleming and Busse 2003, Siragusa and Fleming 2016).

NO plays a pivotal role in the control of vascular tone in large and small arteries (Leo, Suvorava et al. 2021). After synthesis within the EC, NO diffuses to the vascular smooth muscle cells and activates guanylate cyclase, which mediates guanosine-cyclic monophosphate (cGMP)-mediated vasodilation. Furthermore, NO plays a pivotal role in maintaining the vascular wall's quiescent state by inhibiting inflammation, cellular proliferation, and thrombosis (Fleming 2010, Cahill and Redmond 2016). Therefore, maintaining NO bioavailability is crucial for healthy endothelial and vascular function.

1.5.1 Endothelial nitric oxide synthase regulation

Nitric oxide synthases (NOS) are a family of enzymes that mediate the conversion of L-arginine (L-Arg) into L-citrulline (L-Citr) and NO. These enzymes come in three different isoforms according to their function and tissue, which was first characterized. NOS I, or neuronal NOS (nNOS), was the first described and is most expressed in neural tissue. NOS II, also known as inducible NOS (iNOS), is essentially activated during immune responses, and NOS III, also called endothelial NOS (eNOS), is predominantly expressed in endothelial cells. NOS I and NOS III are continuously expressed and are generally modulated by phosphorylation and Ca^{2+}/calmodulin (CaM) interaction, whereas NOS II is only expressed when there are stimuli such as inflammation and immune reactions (Fleming, 2010).

The eNOS is a multi-domain enzyme that contains an oxidase and a reductase domain. The oxidase domain has binding sites for heme, L-Arg, and the co-factor tetrahydrobiopterin (BH4), whereas the reductase domain has binding sites for CaM and reduced nicotinamide adenine dinucleotide phosphate (NADPH), flavin mononucleotide (FMN), and flavin adenine dinucleotide (FAD). The generation of NO occurs when NADPH-derived electrons from the reductase domain are transferred to the oxidase domain, facilitating the binding of heme iron and O_2, which catalyzes the synthesis of NO + citrulline from L-Arg (Siragusa and Fleming 2016).

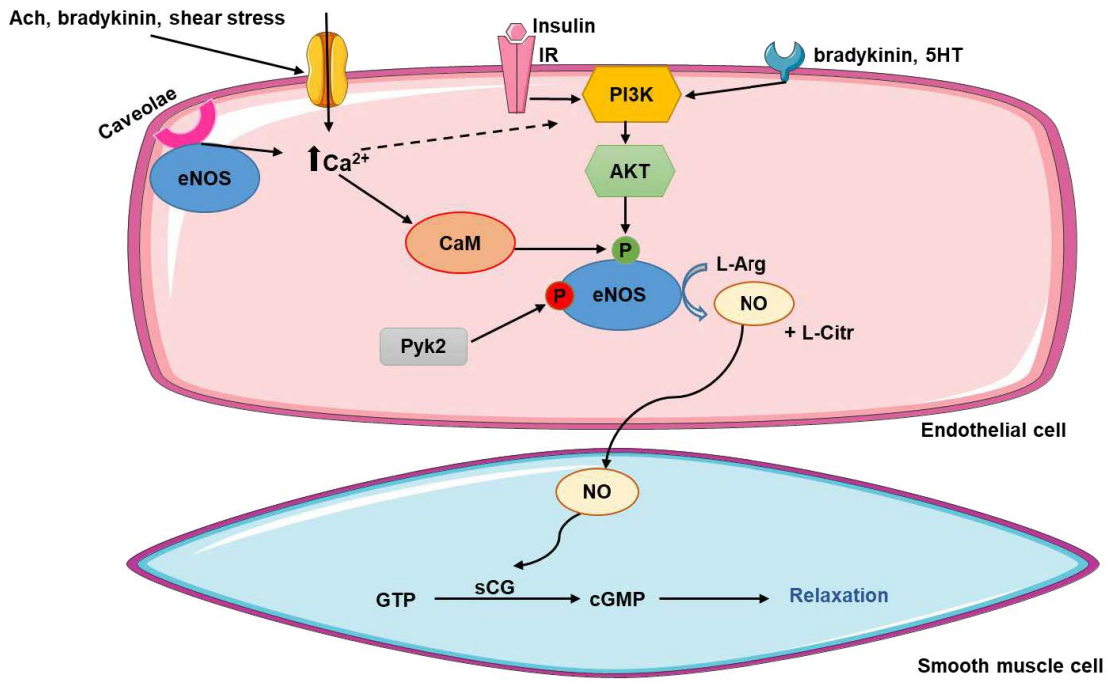

Fig. 2 Endothelial nitric oxide synthase

Several molecular events have been described to regulate the activation of endothelial nitric oxide synthase (eNOS) function, such as fluid shear stress, acetylcholine (Ach), insulin, bradykinin, and 5-hydroxytryptamine. The activation of eNOS involves three primary mechanisms: increased intracellular calcium (Ca^{2+}) concentrations, calmodulin (CaM) binding, and phosphorylations. These processes work in synchrony to promote the activation of eNOS and the production of nitric oxide (NO). Subsequently, NO diffuses to the smooth muscle cells and promotes activation of guanylate cyclase, which mediates Guanosine 3',5'-cyclic monophosphate (cGMP)-mediated vasodilation. Insulin receptor (IR), phosphatidylinositol 3-kinase(PI3K), protein kinase B (AKT), proline-rich tyrosine kinase 2 (Pyk2), L-Arginine (L-Arg), L-Citrulline (L-Citr), guanosine triphosphate (GTP), soluble guanylate cyclase (sCG).Created by Amanda Brum with elements of molecular biology at smart-server medical art (https://smart.servier.com/).

The eNOS activation is mediated by three main mechanisms: 1) increase intracellular calcium concentrations; 2) protein interactions, i.e., CaM binding; and 3) phosphorylations. This process occurs in a coordinate system, leading to enzymatic activity and NO synthesis (Fleming and Busse 2003, Jin, Chennupati et al. 2021). Furthermore, the bioavailability of substrates and co-factors are essential for the eNOS accurate catalytic activity. Since the deficiency of any of these molecules promotes eNOS uncoupling and enhances oxidative stress (Alp, Mussa

et al. 2003, Alp, Mcateer et al. 2004). The regulation of the eNOS function is illustrated in Figure 2.

Several molecular events have been described to regulate eNOS function, such as fluid shear stress (mechanoforces), neurotransmitters (Ach and Phe), and hormones (insulin and bradykinin).

A) Shear stress

Fluid shear stress is the phenomenon in which the blood flow mediates hemodynamic mechanical friction on the vascular wall. This event results in endothelial cell activation and the release of vasoactive factors such as NO. Fluid shear stress-mediated NO production regulates vascular tone, peripheral resistance, and tissue perfusion. Shear stress implicates the actions of several mechanosensing molecules that affect eNOS in specific subcellular locations (Förstermann and Sessa 2012, Roux, Bougaran et al. 2020). The main mechanosensors involved in eNOS activation are located either on the plasma membrane (Caveolae, ionic channels) or intracellular (i.e., cytoskeleton). Those molecules recognize this mechanical stimulus and mediate a cascade of signaling pathways, ultimately leading to increased calcium influx with the formation of Ca2+/CaM complexes, followed by stimulatory phosphorylation events that increase eNOS catalytic activity and increase eNOS sensibility to calcium which promote its enzymatic activity to occurs in resting Ca^{2+} levels (Balligand, Feron et al. 2009, Wang, Chennupati et al. 2016). Furthermore, G protein-coupled receptors (GPCRs) and junction complexes have been shown to participate in endothelial cell mechanosensing by activating the PI3K/AKT pathway and promoting eNOS phosphorylation. Together, those mechanisms ultimately mediate NO production and, consequently, vasorelaxation (Erkens, Suvorava et al. 2017).

B) Neuromodulators (Ach, Phe)

It is widely known that neurotransmitters such as acetylcholine (Ach) and phenylephrine (Phe) impact vascular tone regulation. For instance, vascular reactivity to Ach is one of the main methods used to determine endothelial function

in large vessels, e.g., aorta (aortic rings) (Waldron, Ding et al. 1999, Akther, Razan et al. 2021). In endothelial cells, Ach binds to the muscarinic receptor, promoting Ca^{2+} influx and eNOS-dependent NO production and vasodilation. On the other hand, Phe binds to alpha-adrenergic receptors in the vascular smooth muscle cells (VSMCs), promoting vasoconstriction (Terwoord, Racine et al. 2021).

C) Phosphorylation

The regulation of eNOS by phosphorylation is a complex process. The eNOS can be phosphorylated in serine, threonine, and tyrosine residues that coordinate the stimulation and inhibition of the enzyme catalytic activity (Fleming and Busse 2003).

Serine 1177 (ser1177) is the primary eNOS stimulatory residue (within the reductase domain). This residue is known to mediate the catalytic function of eNOS and increase the sensibility of the enzyme to calcium concentration. Furthermore, this residue phosphorylation is commonly used to determine enzyme activity. Several stimuli mediate eNOS stimulation through Ser1177 phosphorylation. Notably, shear stress, insulin, VEGF, and bradykinin promote rapid phosphorylation of eNOS on ser1177 by different mechanisms. Shear stress mediates ser1177 phosphorylation by protein kinase A (PKA) activity, whereas insulin, estrogen, and VEGF mainly phosphorylate eNOS by AKT action. On the other hand, Bradykinin, Ca^{2+}, and ionophore mediate serine phosphorylation by activating Calcium-Calmodulin Kinase II (CAMKII) (Chen, Druhan et al. 2008, Fleming 2010). Furthermore, eNOS can also be phosphorylated on threonine 495 (Thr495) residue (within the CaM-binding domain). This residue is constitutively phosphorylated and is associated with reduced enzymatic activity. The dephosphorylation of this residue promotes the binding of CaM complexes, elevates endothelial Ca^{2+} sensibility, and increases eNOS activity and NO production (Fleming, Fisslthaler et al. 2001). The central stimuli associated with threonine dephosphorylation are bradykinin, histamine, and Ca^{2+} ionophores. Moreover, the phosphorylation of eNOS on tyrosine 657 (Tyr657) (FMN-binding domain) has been shown to be the primary negative regulator of its enzymatic

activity (Fisslthaler, Loot et al. 2008, Bibli, Zhou et al. 2017). This residue is associated with shear stress stimulation and activation of proline-rich tyrosine kinase 2 (Pyk2). Studies have shown that Ang II, hydrogen peroxide (H_2O_2), and insulin can induce endothelial dysfunction by Pyk2-mediated eNOS inhibition. Interestingly, eNOS phosphorylation on tyr657 abrogates eNOS functionality regardless of other stimulatory events, such as phosphorylation on ser1177 or Ach stimulation, suggesting that this residue applies a dominant inhibitory effect over the eNOS function (Andreozzi, Laratta et al. 2004, Loot, Schreiber et al. 2009, Bibli, Zhou et al. 2017).

1.6 Insulin-mediated eNOS regulation

Insulin has been reported to mediate vasodilation *in vivo*. However, the detection of eNOS activation and increase in cyclic guanosine cyclic monophosphate (cGMP) levels in fresh arteries remain inconclusive. Evidence has demonstrated that insulin can mediate the concomitant phosphorylation of eNOS on ser1177 by AKT and on tyr657 by Pyk2. Furthermore, studies have shown that this parallel phosphorylation leads to enzyme abrogation, reduced NO output, and endothelial dysfunction (Fisslthaler, Loot et al. 2008, Bibli, Zhou et al. 2017, Viswambharan, Yuldasheva et al. 2017). Pyk2 is a non-receptor tyrosine kinase member of the focal adenosine kinase (FAK) family, mainly expressed in epithelial cells, hematopoietic cells, and neural tissue. Its main function involves cell migration, proliferation, and survival (Zhao, Finlay et al. 2016). However, studies have shown that Pyk2 can inhibit eNOS function by phosphorylating eNOS on its inhibitory site (tyr657 human; tyr656 mice). Furthermore, Pyk2 downregulation improves insulin-mediated eNOS activity. In addition, Pyk2 inhibition improves endothelial function and increases NO production in cells stimulated with insulin, Ang II, or H_2O_2 (Fisslthaler, Loot et al. 2008, Bibli, Zhou et al. 2017). Viswambharan et al. showed that the increase in endothelial cell-specific insulin sensitivity led to endothelial dysfunction mediated by an increase of eNOS phosphorylation on tyr656 (mice) and exacerbation of NADPH oxidase 2 (Nox2)-derived superoxide. Furthermore, Pyk2 inhibition

normalizes insulin-induced eNOS activity and increases NO output (Viswambharan, Yuldasheva et al. 2017). This data highlights the relevance of Pyk2-mediated eNOS inhibition by insulin.

Moreover, Bibli and colleagues (Bibli, Zhou et al. 2017) demonstrated that ischemic events mediate early activation of Pyk2, resulting in reduced NO production and consequently intensifying cell damage. The inhibition of Pyk2 enhances NO output and limits cardiac damage following myocardial ischemia-reperfusion (I/R) injury. Besides improving eNOS activity and enhancing NO output (Siragusa and Fisslthaler 2017), Pyk2 inhibition can also alleviate endothelial inflammation by modulation of immune responses and cytokine gene expression (Murphy, Jeong et al. 2019). Taken together, these studies highlight the potential role of Pyk2 in modulating endothelial function, endothelial-dependent organ protection, and inflammation.

1.7 Ischemia-reperfusion injury

Ischemic diseases such as AMI, stroke, and peripheral vascular disease are the leading cause of death and disability worldwide (Roth, Mensah et al. 2020). The primary therapeutic approach for treating these conditions is reperfusion therapy, such as primary percutaneous coronary intervention (PPCI) or Coronary artery bypass grafting (CABG), followed by thrombolytic therapy (Doenst, Haverich et al. 2019, Lawton, Tamis-Holland et al. 2022). However, restoring the blood supply itself can lead to a series of cellular and molecular pathological events causing even more tissue injury and cell death, called I/R injury (Kalogeris, Baines et al. 2012). Nevertheless, reperfusion treatment is essential for improving patient survival and recovery. Therefore, strategies to decrease infarct sizes and promote a better prognosis after ischemic insult are crucial.

During ischemia, the blood supply is interrupted, and the oxygen is insufficient for maintaining aerobic metabolism (Eltzschig and Eckle 2011). Therefore, cell metabolism and survival depend on adenosine triphosphate (ATP) production

through anaerobic glycolysis (Chouchani, Pell et al. 2016, Lan, Geng et al. 2016). However, prolonged anaerobic metabolism results in intracellular acidification due to the accumulation of lactate and hydrogen ions (H^+). The intracellular acidification, in combination with insufficient ATP, impairs the ATP-dependent activation of ion exchange channels, promoting an intracellular ions imbalance, mitochondrial dysfunction, Ca^{2+} overload, cell swelling and rupture, and ultimately, cell death (Cadenas 2018, Wang, Toan et al. 2020). Upon restoration of the blood flow, the dysfunctional mitochondria receive a burst of oxygen, resulting in abnormal production of reactive oxygen species (ROS).

Furthermore, the reverse electron transport within the mitochondria, in combination with Ca^{2+} imbalance and reduced ATP production, increases mitochondrial permeability, resulting in the leakage of mitochondrial DNA (mtDNA) and generating a sterile proinflammatory response due to the release of damage-associated molecular pattern molecules (DAMPs), followed by apoptotic and necrotic cell death (Foster, Van Eyk et al. 2009, Chouchani, Pell et al. 2016, Liu, Cao et al. 2017). The magnitude of the I/R injury depends on the extension and time of ischemia. The longer the ischemic insult, the more extensive the injury and tissue damage. Furthermore, I/R injury causes functional consequences that lead to morphological adaptation and function, such as remodeling and left ventricular (LV) dysfunction that dictates the resolution and prognosis of the disease and the probability of progression to heart failure. An important determinant of patient prognosis and recovery is infarct size. The infarct size determines whether the recovery or further cardiovascular complications occur. Larger infarct sizes are related to poor prognosis, LV dysfunction, and reduced ejection fraction, whereas smaller infarct sizes are associated with better outcomes and recovery (Minicucci, Farah et al. 2014).

Substantial data have shown that insulin resistance and T2DM increase the susceptibility to aggravate I/R injury outcomes. This event occurs due to three main mechanisms: 1) the impairment of eNOS activity and thereby decreased NO bioavailability (Symons, McMillin et al. 2009, Bibli, Zhou et al. 2017); 2) oxidative

stress (Viswambharan, Yuldasheva et al. 2017, Arcambal, Taïlé et al. 2019); and 3) increase of pro-inflammatory cytokines (Andreozzi, Laratta et al. 2004, da Costa, Neves et al. 2016, Arcambal, Taïlé et al. 2019). Altogether, these conditions lead to greater tissue damage, cell apoptosis, and worsened cardiovascular outcomes following ischemic events. Therefore, finding new treatments and strategies to decrease the burden of cardiovascular complications in diabetic and nondiabetic patients is essential.

1.8 Ischemic conditioning and cardioprotection

The concept of ischemic conditioning was first described by Murry and colleagues in 1986, which demonstrated that brief, nonlethal cycles of ischemia followed by reperfusion increased organ tolerance to ischemic insult (Murry, Jennings et al. 1986). Over the years, the ischemic conditioning protocol evolved into different protocols depending on the area and time point related to the ischemic episode. For instance, the ischemic conditioning protocol can be performed directly on the target organ before (preconditioning) or after (postconditioning) the ischemic insult. Alternatively, ischemic conditioning can also be performed in a remote area, before (remote ischemic preconditioning, rIPC), during (remote ischemic per conditioning), or after (remote ischemic postconditioning) an ischemic event (Heusch 2015, Heusch, Bøtker et al. 2015).

Ischemic conditioning has been shown to protect the heart (Munk, Andersen et al. 2010, Chai, Liu et al. 2014) and other organs (Basalay, Davidson et al. 2018, Wu, Chen et al. 2020) against ischemic insults. The most beneficial effects of ischemic conditioning involve the reduction of infarct sizes, which is a significant predictor of functional recovery and future ischemic events (Minicucci, Farah et al. 2014). In addition, studies have demonstrated that ischemic conditioning, besides decreasing infarct sizes, also reduces inflammation, oxidative stress, and cell death

in several organs subjected to ischemic insult (Bromage, Pickard et al. 2017, Cho, Min et al. 2017, Pearce, Davidson et al. 2021, Landman, Uthman et al. 2022).

Furthermore, in clinical studies, the use of ischemic conditioning in combination with standard protocols has been shown to improve myocardial salvage index and ventricular systolic function following myocardium infarction (Bøtker, Kharbanda et al. 2010, Munk, Andersen et al. 2010). However, translating these results into clinical practice focusing on decreasing infarct sizes remains challenging (Heusch 2013, Hausenloy, Kharbanda et al. 2019). Furthermore, this approach has been shown to fail in inducing protective effects in DM animal models and patients (Miki, Itoh et al. 2012, Wider, Undyala et al. 2018) as well as in elderly patients (van den Munckhof, Riksen et al. 2013).

1.9 Remote ischemic preconditioning (rIPC)

The rIPC maneuver consists of brief cycles of ischemia followed by reperfusion on a remote area, e.g., limbs or arms. Several studies have shown that remote conditioning is an efficient, safe, noninvasive, and easily feasible protocol to decrease infarct sizes and improve survival following ischemic events (Heusch, Bøtker et al. 2015). Johnsen and colleagues established that the ideal rIPC protocol to promote cardioprotection is between 4-6 cycles of 2-5 minutes of ischemia followed by reperfusion (Johnsen, Pryds et al. 2016). This approach has been shown to promote whole-body protection against ischemic events and positively impact vascular health (Manchurov, Ryazankina et al. 2014, Gu, Liu et al. 2021). In addition, studies have shown that this approach improves endothelial function (Rassaf, Totzeck et al. 2014, Maxwell, Carter et al. 2019) and promotes endothelial participation in remote cardioprotection (Cho, Min et al. 2017, Rossello, He et al. 2018, Liang, Lin et al. 2019). Interestingly, rIPC has been shown to fail in elderly patients with endothelial dysfunction (van den Munckhof, Riksen et al. 2013). Furthermore, this phenomenon was also observed by Heinen et al. (Heinen,

Behmenburg et al. 2018), which also demonstrated that a healthy endothelium is essential for rIPC-induced cardioprotective humoral factor release.

The mechanism involved in rIPC-induced organ protection involves two main theories: neural and humoral signaling. Neural signaling involves somatic and sympathetic nerves that stimulate the valgus nerve and induce organ protection (Yang, Shakil et al. 2019). On the other hand, the humoral theory consists of a sender tissue, e.g., endothelial cells or skeletal muscle, that activates or releases humoral factors that travel through the circulation and mediate its action in the target organ. Several studies hypothesize that these two theories work together in neurohumoral signaling, leading to organ protection (Heusch, Bøtker et al. 2015, Basalay, Davidson et al. 2018, Lassen, Just et al. 2021). Nevertheless, the rIPC-mediated cardioprotection involves four main processes: the rIPC stimulus (1) that triggers the sender tissues (2) to activate or release messengers (3) molecules that mediate modification in the target organ (4) and promote cell survival and protection against the ischemic insult. This mechanism is illustrated in Figure 3.

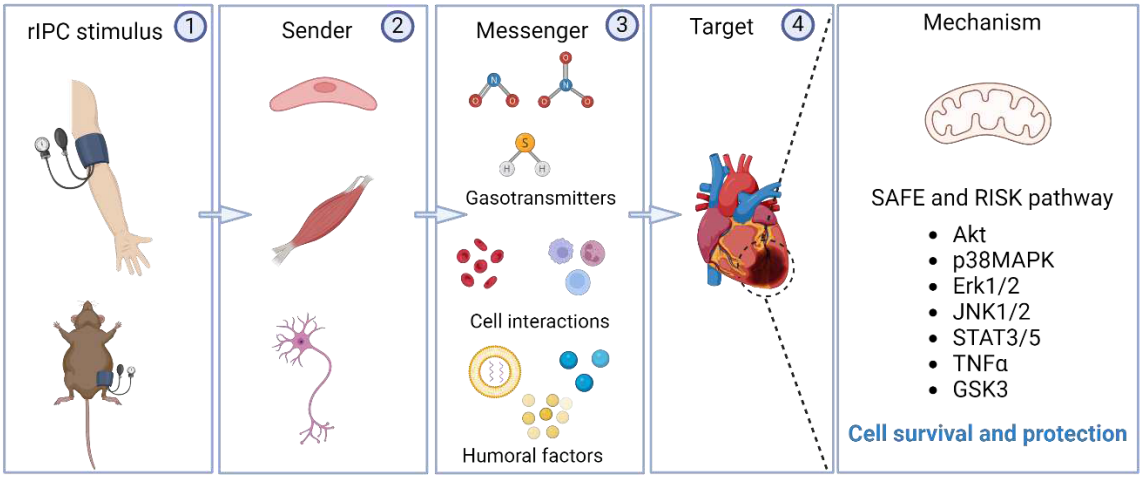

Fig. 3 Remote ischemic preconditioning

The mechanism involved in rIPC-mediated cardioprotection. 1)The rIPC stimulus is performed in humans or mice. 2) the activation of sender tissues such as endothelial cells, skeletal muscle and neural tissue to activate or release protective messenger factors. 3) Messenger molecules such as gasotransmitters nitrite (NO_2^-), nitrate (NO_3^-) and hydrogen sulfide (H_2S); Cell interactions, red blood cells (RBCs), and immune cells; Humoral factors, miRNAs, cytokines and microvesicles. 4) Target organ that receives signals to promote cell survival and protection against the ischemic insult.

Mechanism triggers in the target organ by the messenger that mediates organ protection. Mitochondrial transitions pores modifications, activation of reperfusion injury salvage kinase (RISK) pathway that involves the PI3K, AKT, ERK, and GSK3β. The survivor activating factor enhancement (SAFE) pathway SAVE involves STAT3 activation in combination with AKT and TNFα. Created by Amanda Brum and Ralf Erkens with Biorender.

The rIPC maneuver stimulus triggers cellular events and tissues, such as endothelial cells, skeletal muscle, and activation of neural tissue. In addition, cell interactions, such as red blood cells (RBCs) and immune cell activation, have also been implied to participate in rIPC-induced organ protection (Heusch, Bøtker et al. 2015, Tomschi, Niemann et al. 2018). The activation of these cells and tissues results in the release and activation of circulating messengers that transmit a protective signal to the target organ. Among the messenger's molecules studies, the most important are molecules such as gasotransmitters nitrite (NO_2^-), nitrate (NO_3^-) and hydrogen sulfide (H_2S), and humoral factors, such as micro RNAs (miRNAs), cytokines and microvesicles (Rassaf, Totzeck et al. 2014, Andreadou, Iliodromitis et al. 2015, Lassen, Just et al. 2021).

Research indicates that the mechanism involved in the cardioprotective effects of rIPC occurs mainly due to the activation of endothelial cells in the remote area (Rassaf, Totzeck et al. 2014, Cao, Wang et al. 2018). The rIPC maneuver promotes the alteration of shear stress, which mediates endothelial-dependent NO production. Thus, NO contributes to endothelial function and mediates its local effect by leading to smooth muscle relaxation and vasodilation (Andreadou, Iliodromitis et al. 2015, Heiss, Rodriguez-Mateos et al. 2015, Erkens, Suvorava et al. 2017). Furthermore, NO is released to the blood, oxidized to nitrite, and promotes a cross-talk between different cells, i.e., heterocellular communication. At the target organ (e.g., the heart), nitrite is reduced to NO by myoglobin and converted to S-nitrosation on mitochondrial complex I. This process improves mitochondrial function, reduces oxidative stress, and alleviates tissue damage following I/R injury (Hendgen-Cotta, Merx et al. 2008, Rassaf, Totzeck et al. 2014). Interestingly, more than 2/3 of circulating nitrite is produced by the oxidation of endothelial-derived NO (Kleinbongard, Dejam et al. 2003), highlighting the

relevance of endothelium for cardiovascular homeostasis and organ protection. Moreover, rIPC can also modulate immune responses, regulate ROS generation and decrease pro-inflammatory cytokine gene expression by downregulating the Janus kinase 2 (JAK2)/ Signal transducer and activator of transcription 3 (STAT3) signaling pathway (Turrell, Thaitirarot et al. 2014, Zhao, Xue et al. 2019). Furthermore, endothelial cells have been shown to mediate crosstalk by releasing microRNAs (miRNAs) (Dellett, Brown et al. 2017, Fernández-Hernando and Suárez 2018). The miRNAs are small noncoding RNAs capable of modulating gene expression. MiRNAs act by downregulating target genes by binding to messenger RNA (mRNAs) and silencing the translation of genes into proteins (Treiber, Treiber et al. 2019). Interestingly, Davidson and colleagues proposed that endothelial-derived extracellular vesicles are partially responsible for the ischemic conditioning cardioprotection (Davidson, Riquelme et al. 2018). Furthermore, Cheng and colleagues (Cheng, Zhu et al. 2010) confirmed this assumption, demonstrating the relevance of miRNAs and microvesicles in endothelial-mediated cellular crosstalk. The skeletal muscle has also been shown to release humoral factors in response to rIPC stimulus. Chen et al. demonstrated that rIPC led to the release of the myokine irisin from the skeletal muscle into the bloodstream. Irisin acts directly in the mitochondria of the target organ, protecting the mitochondrial function from the oxidative stress caused by I/R (Chen, Xu et al. 2017).

Furthermore, Gourine and colleagues proposed that rIPC mediates its cardioprotection effects by activating a neural signal transmission called “remote preconditioning reflex” (Gourine, Gourine et al. 2010). According to the Gourine hypothesis, rIPC stimulus triggers sensory afferent nerves in the remote area that send the information to the central nervous system. Then, the protective signals are transmitted to the target organ by vagal efferent parasympathetic innervation. This assumption was corroborated by other studies that demonstrated that denervation, transection, or blockage of nerves abolishment of rIPC-mediated cardioprotection (Loukogeorgakis, Panagiotidou et al. 2005, Steensrud, Li et al. 2010). Moreover, Redington and colleague's findings also support the relevance of neural signaling for organ protection, in which femoral nerve stimulation and topical

capsaicin induce the release of cardioprotective humoral factor that mimics the cardioprotective effects of rIPC (Redington, Disenhouse et al. 2012). However, more studies are needed to fully understand the role of neural signaling in rIPC-induced organ protection.

Moreover, studies have shown that the rIPC maneuver enhances the expression of proteins involved in the cell survival pathway, such as the reperfusion injury salvage kinase (RISK) and the survivor-activating factor enhancement (SAFE) pathway in the target organ (Kalakech, Hibert et al. 2014, Wang, Zhang et al. 2016, Heusch 2017). The RISK pathway is composed of PI3K, AKT, and ERK activation that, in combination, phosphorylates GSK3β, promoting cell survival by inhibiting the opening of mitochondrial transitioning pores. On the other hand, the SAVE signaling pathway promotes cell survival signals by activating STAT3 activation in combination with AKT and TNFα. STAT3 activation promotes survival by promoting the expression of cardioprotection proteins, improving mitochondrial respiration, and alleviating cell death (Heusch 2017, Heinen, Behmenburg et al. 2018). Overall, these two signaling pathways regulate the opening of mitochondrial transitioning pores, which are mainly responsible for mitochondrial leaking and induction of necrosis and cell death signaling (Turrell, Thaitirarot et al. 2014).

1.10 Aims of thesis

Cardiovascular disease is the primary cause of death worldwide. Diabetic patients have a higher probability of death by cardiovascular complications than non-diabetic patients. Insulin resistance and hyperinsulinemia are hallmarks of the development of T2DM and are strongly associated with endothelial dysfunction and cardiovascular disease. Endothelial dysfunction occurs mainly due to impairment of eNOS function and reduced endothelial-dependent vasorelaxation. Pyk2 has been identified as the primary negative regulator of eNOS and, consequently, impaired NO production. Pyk2 inhibition alleviates endothelial dysfunction and

enhances NO output *in vivo* and *in vitro*. However, to our knowledge, the role of Pyk2-regulates eNOS function under insulin resistance and hyperinsulinemic conditions has not been addressed yet. Therefore, this study hypothesized that Pyk2 plays an essential role in the development of endothelial dysfunction and impaired endothelial-dependent remote cardioprotection in insulin resistance and hyperinsulinemia. In addition, it is hypothesized that Pyk2-inhibition improves endothelial function and remote cardioprotection under diabetic-related conditions. To address this hypothesis, four major aims have been proposed:

1. Perform the cardiovascular and metabolic characterization of a murine model of hyperinsulinemia and insulin resistance. The first aim was to characterize the cardiometabolic system of NZO mice and determine the suitability of this mouse model for our study. Therefore, body weight, heart weight, blood glucose, and plasma insulin were measured. Furthermore, metabolic tolerance tests and Western blot analysis of protein involved in the insulin signaling pathway were investigated. In addition, echocardiography and flow-mediated vasodilation determined cardiac and endothelial function, respectively.

2. Determine the effect of Pyk2-inhibition on endothelial function in insulin resistance conditions. The second aim was to investigate the impact of Pyk2 inhibition on endothelial function and blood pressure regulation. Therefore, endothelial-dependent vasodilation *in vivo* was assessed by Flow-mediated vasodilation (FMD) analysis. In addition, an invasive Millar catheter was used to determine the effect of Pyk2 inhibition on systemic hemodynamics.

3. Investigate the role of Pyk2-induced eNOS regulation and function in an insulin-resistant condition. Western blot analysis determined the cardiac expression and activity of Pyk2 and eNOS. In addition, immunoprecipitation experiments were conducted to measure eNOS phosphorylation levels at its inhibitory site (Tyr656). Furthermore, Nox analyzer experiments (CLD and ENO30) were used to quantify nitrite and nitrate plasma levels.

4. Analyse the role of Pyk2 and its inhibition on eNOS-dependent remote cardioprotection mediated by rIPC maneuver. Myocardial ischemia-reperfusion protocol investigated how Pyk2 affects rIPC-mediated cardioprotection in insulin resistance conditions. Furthermore, the rIPC-induced cardioprotection mechanism was investigated, and the influence of NO, neural signaling, and activation of the RISK pathway was determined.

A summary of the aims is illustrated in Figure 4.

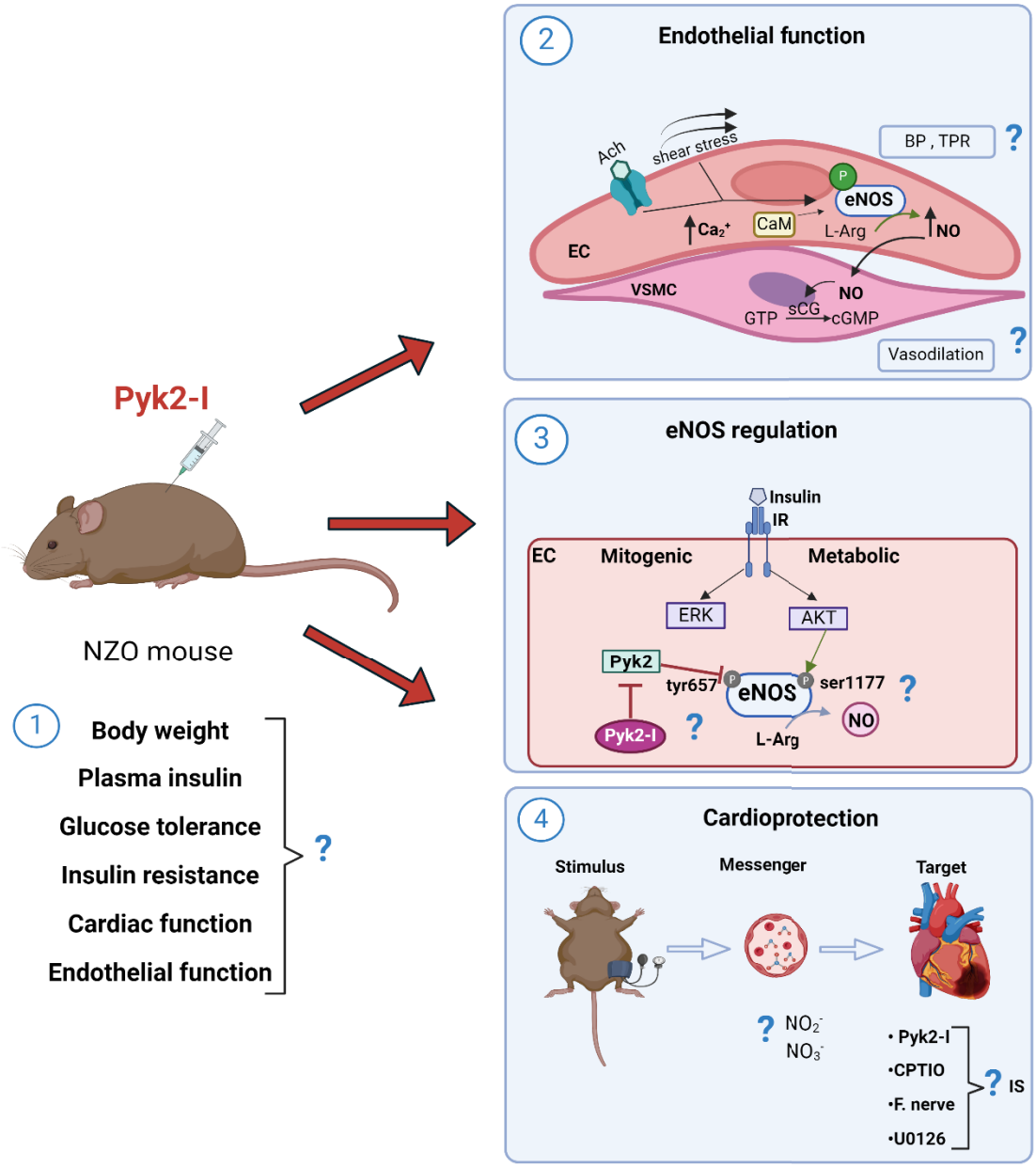

Fig. 4 Graphic Aims

The four major aims of this study are: 1. Perform the cardiovascular and metabolic characterization of a murine model of hyperinsulinemia and insulin resistance (NZO mice). 2. Determine the effect of Pyk2-inhibition on endothelial function in insulin resistance conditions. Furthermore, it investigates the impact of Pyk2 inhibition on endothelial function and blood pressure regulation. 3. Investigate the role of Pyk2-induced eNOS regulation and function in an insulin-resistant condition. In addition, analyze the levels of eNOS phosphorylated in its stimulatory(ser1177) and at its inhibitory site (Tyr656). 4. Analyse the role of Pyk2 and its inhibition on eNOS-dependent remote

cardioprotection mediated by rIPC maneuver. Endothelial cell (EC), vascular smooth muscle cells (VSMC), Blood pressure (BP), total peripheral resistance (TPR), Nitrite (NO_2-), nitrate (NO_3-), Infarct size (IS), 2-(4-carboxyphenyl)-4,4,5,5-tetramethylimidazoline-1-oxyl-3-oxide. (CPTIO), femoral nerve transection (F.nerve). Created by Amanda Brum with Biorender.

2 Material and Methods

2.1 Buffers and solutions

Unless otherwise indicated, all reagents were purchased from Sigma Aldrich (St. Louis, USA), Merck (Darmstadt, Germany), or Carl Roth GmbH (Karlsruhe, Germany). Buffers and solutions were prepared using distilled or ultrapure water (MilliQ®, Merck, Darmstadt, Germany), calcium and magnesium-free Dulbecco's phosphate-buffered saline (DPBS), pH 7.4 (Sigma Aldrich, St. Louis, USA), or an isotonic saline solution (0.9% NaCl, Fresenius Kabi, Germany).

2.2 Animal experiments

Animal experiments were approved by the local animal ethics committee “Landesamt für Natur, Umwelt- und Verbraucherschutz” (LANUV, Northrhine-Westfalia, Germany) under the file numbers G432/14 (Erkens, AZ 84-02.04.2014.A2432), G117/20 (Kelm, AZ81-02.04.2020.A117) and O32/19. Animal welfare was consistent with the European Convention on the Protection of Vertebrate Animals Used for Experimental and Other Scientific Purposes (Council of Europe Treaty Series No. 123). The animals were kept in standard housing conditions following institutional guidelines. The housing environment was maintained at constant temperature and humidity. Mice were exposed to a 12:12 hour light-dark cycle routine and received ad libitum drinking water and a standard rodent diet.

Male 18-20 week-old C57BL/6J (BL6) mice were purchased from Janvier Labs (Janvier Labs, Le Genest-Saint-Isle, France) and used in the lean control group. Furthermore, male age-matched New Zealand Obese mice (NZO/HILtJ) acquired from Professor Hadi Al-Hasani (Deutsches-Diabetes-Zentrum, Düsseldorf, Germany) were used in the insulin resistance/hyperinsulinemia group.

2.3 Insulin stimulation experiments

To investigate metabolic responses to insulin, insulin stimulation experiments were carried out. Mice were randomly divided into insulin or control (fasting) groups. Mice were placed in new, clean cages and fasted for five hours, with access only to drinking water. After fasting, the insulin group received an intraperitoneal injection of 1IU/kg of insulin solution (Humulin R, Lilly, USA) containing 0.25IU/ml insulin and isotonic saline (v/v), while the control group was euthanized. The mice in the insulin group were euthanized after 15 minutes of insulin administration. Both groups were euthanized by cervical dislocation to avoid anesthesia-induced metabolic disturbances. Tissues were harvested after extensive perfusion with cold DPBS, immediately frozen in liquid nitrogen, and stored at -80°C until further analysis.

2.4 Pharmacological Pyk2 inhibition

To determine the role of Pyk2 for eNOS regulation in insulin resistance conditions, we used a well-established Pyk2 inhibitor, PF-431396 hydrate (Sigma-Aldrich, St.Louis, USA) (Han, Mistry et al. 2009, Bibli, Zhou et al. 2017). PF-431396 is a competitive inhibitor that binds to the active site of Pyk2, blocking its action. PF-431396 was administrated intraperitoneally at a concentration of 5µg/g in 100 µl of a 10% DMSO/saline solution (v/v). Unless otherwise specified, the Pyk2 inhibitor was administered 15 minutes prior to the start of each experimental protocol. The control group received 100 µl of a vehicle solution containing 10% DMSO/saline solution (v/v).

2.5 Organ harvesting for biochemical parameters

The euthanasia method used in the present work varies according to the experiment's aim. Therefore, each method section in which a different protocol of euthanasia was required specified the method used. Regardless of the euthanasia protocol used, tissues were collected after systemic perfusion with cold DPBS. In cases where perfusion was not feasible, such as for infarct size quantification, the tissue was washed with cold DPBS. Subsequently, tissue samples were immediately placed in 2 mL Eppendorf safe-lock tubes (Eppendorf, Germany), frozen in liquid nitrogen, and stored at -80°C until further analysis.

2.6 Blood glucose and plasma insulin measurement

To measure fasting glucose and insulin levels, mice were placed in a clean cage with access only to drinking water and fasted for six hours. Subsequently, the mouse's tail vein was punctured, and blood glucose was measured on a glucose meter (glucose meter: Contour XT; Bayer Health Care, Leverkusen, Germany). Furthermore, fasting insulin plasma levels were also measured. After six hours of fasting, around 30µl of blood samples were collected from the tail vein using a Greiner Bio-One MiniCollect™ tube. Next, the samples were centrifuged at 4 ° C for 20 minutes at 2000x g, and plasma was collected and placed in the -80 freezer until further measurement of insulin.

Insulin plasma levels were determined by an ultrasensitive mouse ELISA kit (Crystal Chem, USA) following the manufacturer's instructions for a low-range assay. In brief, 95µl of sample diluent was dispensed into antibody-coated microplate wells, followed by 5µl of sample or mouse insulin standard (0,1- 6,4 ng/ml) and incubated for two hours at 4°C. After the washing step (5x 300 µl of wash buffer per well), 100µl of anti-insulin enzyme conjugate was dispensed in each well and incubated for 30 min at room temperature. Next, after one more washing step (7x 300 µl of wash buffer per well), 100µl per well of enzyme substrate

solution was dispensed in the microplate and incubated for 40 minutes in the dark at room temperature. Afterward, 100µl per well of enzyme reaction stop solution was added, and the absorbance was measured at a wavelength of 450 nm (A450) and 630 nm (A630) (FLUOstar Omega, BMG Labtech, Germany). The absorbance was measured using A450 values and subtracting A630 values. Finally, insulin concentration was determined using a standard curve and the mean absorbance value for each sample.

2.7 Metabolic tolerance tests

Metabolic tolerance tests were performed to investigate glucose and insulin homeostasis *in vivo* and identify potential metabolic differences between groups in dynamic conditions. The glucose tolerance test (GTT) and insulin tolerance test (ITT) were performed according to the guidelines established by Benedé-Ubieto et al.(Benedé-Ubieto, Estévez-Vázquez et al. 2020). Mice were placed in a clean cage with access only to drinking water and fasted for six hours. Afterward, baseline body weight and blood glucose levels were measured using a glucose meter (Contour XT; Bayer Health Care, Leverkusen, Germany) by puncturing the mouse's tail vein. Subsequently, intraperitoneal injections of 1.5 g/kg of D-glucose solution glucose (Sigma-Aldrich, St. Louis, USA) (20% D-glucose/DPBS (w/v)) were administered to the mice. Blood glucose levels were measured 15, 30, 60, and 120 minutes after glucose administration.

To perform the insulin tolerance test (ITT), mice were placed in a clean cage and fasted for six hours, similar to the GTT test. Baseline body weight and blood glucose levels were measured using a glucose meter (Contour XT; Bayer Health Care, Leverkusen, Germany). Subsequently, mice received an intraperitoneal injection of 1IU/kg of 0, 25 IU/ ml of insulin solution (insulin/saline (v/v)). Next, blood glucose concentrations were measured at 15, 30, 60, and 90 minutes after insulin administration.

2.8 Remote ischemia-preconditioning

The rIPC maneuver is a noninvasive protocol for inducing remote cardioprotection by transient nonlethal episodes of ischemia applied to a limb. First, mice were anesthetized with (2-3% induction and 1.5-2% maintenance) isoflurane and placed on a 37 ° C warm platform. Next, the mice's limbs were secured with adhesive tape, and an 8 mm diameter vascular occluder (Harvard Apparatus, Harvard, Boston, MA, USA) was placed around the mouse's left hindlimb. Next, the occluder was inflated supra systolic pressure (250 mmHg) using a KAL 84 pressure calibration device (Halstrup Walcher, Kirchzarten, Germany) to occlude blood flow for five minutes. Subsequently, the occluder was deflated, allowing tissue reperfusion for five minutes. The entire procedure was repeated four times to achieve the desired effect. Figure 5 illustrates the rIPC manoeuvre protocol.

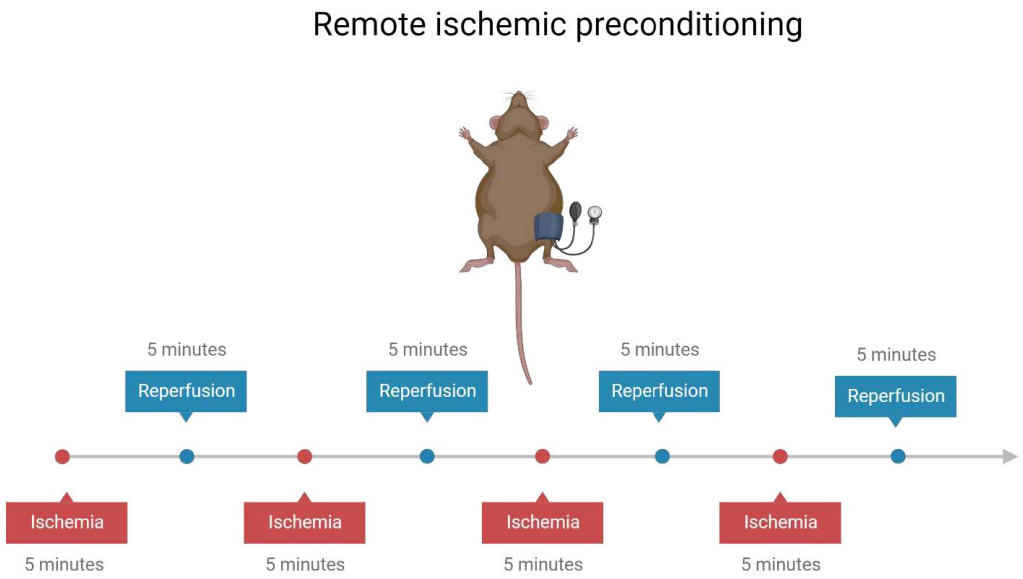

Fig. 5 Remote ischemic preconditioning maneuver protocol

Remote ischemic preconditioning protocol was performed with four cycles of 5 minutes of ischemia (>250 mmHg) followed by four cycles of 5 minutes of reperfusion. Created by Amanda Brum with Biorender.

2.9 Ultrasound imaging

High-resolution micro-ultrasound imaging was used to assess cardiac and endothelial function *in vivo*. The imaging measurements, *i.e.,* echocardiography and flow-mediated vasodilation (FMD), were performed under constant inhalation anesthesia (2-3% induction and 1.5-2% maintenance). To prevent any cardiac disturbances during the measurements, the mice's basal parameters, such as heart rate (400-500 beats per minute), breathing rate (100 breaths per minute), and body temperature (37°C), were carefully maintained at constant levels.

2.9.1 Assessment of cardiac function

Cardiac function was assessed using a high-resolution ultrasound imaging system (Vevo 3100, Visual Sonics, Fujifilm, Japan). First, mice were placed into an induction chamber containing a mixture of isoflurane and oxygen (2-3% isoflurane). Once anesthetized, the mice were positioned in a supine position on a heating pad with electrocardiography (ECG) electrodes to monitor heart rate and maintain body temperature. In order to ensure continuous sedation during the imaging sessions, a face mask with continuous inhalation anesthesia (2-2.5% isoflurane) was placed on the mice's snouts. Next, conducting cream was applied to the mice's paws and taped to metal ECG electrodes. Subsequently, the mice's thorax fur was removed with a hair removal cream (Veet, Reckitt Benckiser, United Kingdom), and a layer of pre-warmed ultrasound gel was applied to the mice's thorax. Finally, the mice were positioned in a supine position, slightly upright, and an MX-400 transducer (20-46 MHz; Vevo 3100) was placed on the thorax.

First, the left ventricle parasternal long axis (PSLA) was visualized, and B-mode and M-mode imaging was acquired. Then, the transducer was rotated 90 degrees clockwise to obtain imaging of the left ventricle parasternal short axis (SAX), and B-mode and M-mode imaging were acquired. Next, transmitral blood flow Doppler

was recorded using an apical four-chamber view. Finally, in the suprasternal position, the aortic valve flow was measured using a pulse wave Doppler. Angle corrections were used to measure flow profiles and velocity accurately. The data analysis was performed using the Vevo Lab software (Visual Sonics, Fujifilm, Japan), and the LV-Trace tool was used to analyze the ventricular function in the PSLA view. The calculation of Left ventricle (LV) volume, stroke volume (SV), cardiac output (CO), and ejection fraction (EF) was performed using the B-mode view. End-systolic volume (ESV), end-diastolic volume (EDV), SV, and CO were indexed to body surface area (Lang, Badano et al. 2015, Bansal and Sengupta 2017).

2.9.2 Assessment of vascular function *in vivo*

A flow-mediated vasodilation protocol assessed *in vivo* vascular function using a high-resolution ultrasound system using a 30-70 MHz linear array Microscan transducer (Vevo 2100, Visual Sonics Inc., Toronto, Canada). This method was based on measuring changes in vessel diameter in response to shear stress following vascular occlusion (Erkens, Kramer et al. 2015). First, mice were anesthetized and placed in a warm platform, as described in the cardiac function assessment section. Next, the fur of the left hindlimb was removed, and a 5 mm diameter vascular occluder (Harvard Apparatus, Harvard, Boston, MA, USA) was placed around the limb. Subsequently, the transducer was placed on the mouse's left hindlimb using a stereotactic holder and manually adjusted to visualize the external iliac artery. Baseline imaging was acquired in B-mode and pulse wave Doppler mode. Afterward, the vascular occluder was inflated above the systolic pressure using a KAL 84 pressure calibration device (Halstrup Walcher, Kirchzarten, Germany) to occlude blood flow. Images were recorded in B-mode and pulse wave Doppler-mode every 30 seconds during 5 minutes of vascular occlusion and every 20 seconds for 5 minutes after tissue reperfusion. Data analysis was performed using the Brachial Analyzer for Research (Medical Imaging

Applications, LLC, USA). Measurements of vessel diameter were calculated as percent ratio (%) = [diameter(max) / diameter (baseline)] x100. Maximal dilation measurements were calculated as Δ%= [diameter(max) – diameter (baseline)/diameter (baseline)] x 100.

2.10 Assessment of systemic hemodynamics

Approximately 30 minutes before the experiment began, mice were administered subcutaneously with buprenorphine (0.1 mg/kg) to induce analgesia during the procedure. Mice were intubated, placed on a warm operation table (37,5ºC), and submitted to constant inhalation anesthesia (2-3% isoflurane) using a murine respirator (micro ventilator, UNO, The Netherlands) throughout the experiment. The mouse's fur was removed from the mouse's neck, and an incision was made below the mandible to the thoracic inlet. The right carotid artery was exposed and isolated from adjacent tissues. The catheter was inserted into the right carotid artery and placed in the left ventricle according to the closed chest method described by Pacher et al. (Pacher, Nagayama et al. 2008). Invasive hemodynamic parameter evaluation was performed using a 1.4 F pressure conductance catheter (SPR-839, Millar Instrument, Houston, TX, USA). Heart rate (HR), systolic blood pressure (SBP), and diastolic pressure (DBP) were recorded by a Millar Box and analyzed with LabChart 7 (AD Instruments, Oxford, UK). Furthermore, mean arterial blood pressure (MAP) was calculated using the following equation above.

$$\mathrm{MAP} = \frac{(\mathrm{SBP} + 2 * \mathrm{DBP})}{3}$$

The total peripheral resistance (TPR) was calculated by dividing the mean arterial blood pressure by the cardiac output. These experiments were performed with the support of Stefanie Becher.

2.11 Western blot and immunoprecipitation

2.11.1 Protein determination

For tissue disruption and sample homogenization, the heart and soleus samples were placed in 2 ml safe-lock tubes and settled in the Retch tube adapter for single-use vials (Retsch, Haan, Germany). Stainless steel beads were added to each tube and placed in the Mixer Mill (MM 400, Retsch, Haan, Germany), setting a vibration frequency of 20 Hz for one minute. Radioimmunoprecipitation assay buffer (RIPA) (150 mM NaCl, five mM EDTA, 50 mM Tris, 1 % NP-40, 0.5 % sodium deoxycholate, 0.1 % SDS) added to protease, and phosphatase inhibitor (Pierce, Thermo Fisher Scientific, Waltham, USA) was added to each tube and homogenized in a protocol of 30 Hz for 3 min. Subsequently, the samples were placed in an ultrasonic bath for 10 minutes at 4 ° C and centrifuged at 13300G for 15 minutes at 4 ° C. The supernatant was collected, and the total protein concentration was determined by the Bio-Rad DC protein assay (Bio-Rad Laboratories Inc., Hercules, USA) following the manufacturer's instructions. Briefly, the samples were diluted in RIPA buffer in a ratio of 1:25 (heart and soleus). The standard protein curve was prepared using bovine serum albumin (BSA) (Sigma-Aldrich St. Louis, USA) at 0,2-2,0 mg/ml concentration. Next, five µl of samples and standards were added to a 96-well plate in duplicate. Next, 25 µl of working reagent A (reagent A+S) and 200 µl of solution B were added to each well. The microplate was incubated at room temperature, in the dark, for 15 minutes. The sample absorbances were measured at a wavelength of 740 nm using the FLUOstar Omega plate reader (BMG Labtech, Germany). The protein concentration was determined according to the standard curve.

2.11.2 Immunoblot

For SDS-page preparation, 75-100µg of protein were added to the LDS sample buffer (NuPAGE™, Invitrogen™, Waltham, USA) and sample reducing agent

(NuPAGE™, Invitrogen™, Waltham, USA) and denatured for 15 minutes at 75ºC. Samples were loaded in NuPAGE™ 4-12% Bis-Tris, Pre-cast gels (Invitrogen™, Waltham, USA), and PageRuler™(Plus Prestained Protein Ladder, Thermofisher, Waltham, USA) were used to determine protein migration during electrophoresis. Electrophoresis was carried out in the XCell SureLock™ system (Invitrogen™ Waltham, USA) with a MOPS (3-(N-morpholino) propane sulfonic acid) SDS running buffer (Invitrogen™ Waltham, USA) at 150mV for 60 minutes. After electrophoresis, proteins were transferred to nitrocellulose membrane Hybond P 0,2 (Amersham Biosciences, Munich, Germany) at 80 mV for 90 minutes using a wet electroblotting system (Bio-rad Laboratories, Inc. Hercules, USA).

The membranes were blocked for 1 hour at room temperature with Intercept Blocking Buffer TBS (LI-COR Biosciences GmbH, Germany), followed by overnight incubation at 4 °C with the primary antibody. The primary antibodies were diluted in blocking buffer 0,1%, Tween 20, according to Table 1. Subsequently, the membranes were washed with TBS (1x dilution of pH 7,5 20X TBS: 121,14 g Trizma®-Base, 175,32 g NaCl, and 1000 ml distilled water) and incubated in a secondary antibody for 1 hour in the dark, at room temperature. The secondary antibody was diluted in in blocking buffer 0,1%, Tween 20, according to Table 2. After washing, the membranes were detected at 700 nm or 800 nm in the Odyssey Fc Imaging System (LI-COR Biosciences GmbH, Bad Homburg, Germany). Data analysis was performed using Image Studio™ Lite 5.2 software supplied by LI-COR.

Table 1 Primary antibody list.

Primary Antibody	Dilution	Source	Brand (Product number)
PYK2/ Pyk2(5E2)	1:1000	rabbit/mouse	CST(3292)/(3480)
Phospho-PYK2 (Tyr402)	1:1000	rabbit	CST(3291)
Anti-eNOS/NOS Type III	1:500	mouse	BD Biosciences (610297)
Phospho-eNOS (Ser1177)	1:500	rabbit	CST(9571S)
Phospho-eNOS (tyr657)	1:500	rabbit	Biotrend (NP4031)
AKT	1:1000	rabbit	CST(9272)
Phospho-AKT (ser473)	1:1000	rabbit	CST(9271)
ERK 1/2	1:1000	rabbit	CST (4695)
Phospho-ERK1/2	1:1000	rabbit	CST(9101)
TBC1D1 (V796)	1:1000	rabbit	CST(4629S)
Phospho-TBC1D1 (Thr590)	1:1000	rabbit	Thermofisher (PA5-104667)
AS160(C69A7) mAB	1:1000	rabbit	CST (2670)
Phospho-AS160 (Thr643)	1:1000	rabbit	CST(4288)
Glut4(1F8) mAB	1:1000	mouse	CST (2213S)
GSK-3α/β(D75D3) mAB	1:1000	rabbit	CST (5676S)
Phospho-GSK-3α/β (Ser21/9)	1:100	rabbit	CST(9331S)
GAPDH (6C5) mAB	1:2000	mouse	Abcam (ab8245)

Cell signalling technology (CST), Monoclonal antibody (mAB), Tyrosine (Tyr), Serine (Ser), Treonine (Thr), glyceraldehyde-3-phosphate dehydrogenase (GAPDH).

Table 2 Secondary antibody

Secondary Andibody	Dilution	Sorce	Brand (Product number)
IRDye® 800CW anti-Rabbit	1:10000	Goat	LI-COR Biosciences (926-32211)
IRDye® 800CW anti-Mouse	1:10000	Goat	LI-COR Biosciences (926-32210)
IRDye® 680 RD anti-Rabbit	1:10000	Goat	LI-COR Biosciences (926-68071)
IRDye® 680 RD anti-Mouse	1:10000	Goat	LI-COR Biosciences (926-68070)

2.11.3 Immunoprecipitation

Immunoprecipitation was performed to determine the levels of eNOS phosphorylated on the tyr656 site. Therefore, heart samples were pulverized in dry ice, collected, and lysed in a lysis buffer. For eNOS precipitation, 2mg of protein lysate was incubated overnight with an Anti-NOS III antibody (BD Bioscience 610297; 2 µg/mg protein lysate). After that, agarose immunoprecipitation was performed. In brief, after elution, 25µl of the sample was loaded onto 8% SDS gels, and standard immunoblot protocol was performed. Finally, membranes were incubated overnight with tyr656 eNOS antibody (custom-made by Eurogentec, freshly diluted 1:500 in Rotiblock). The bands were visualized by chemiluminescence signal with Western Blotting Detection Reagent (GE Healthcare Amersham™ ECL Select™) in Chemidoc imaging (Biorad Califórnia, EUA). Band intensity quantification was performed using ImageJ software, and the Phospho-tyr656-eNOS/eNOS ratio was expressed as a fold change of BL6 mice. These experiments were performed in collaboration with Prof. Dr. Ingrid Fleming and Dr. Mauro Siragusa from the Vascular Research Center Frankfurt am Main.

2.12 Plasma levels of Nitrite and Nitrate

2.12.1 Sample preparation

In order to prevent contamination, all tubes and labware were rinsed with ultrapure water. Mice fasted for 3 hours with only access to drinking water to avoid any diet-induced disturbances in nitrite and nitrate levels. Next, mice were anesthetized with isoflurane and placed on a warm pad as previously described. Blood samples (900 µl) were collected by heart puncture and placed in 2 ml tubes containing 100 µl of N-ethylmaleimide (NEM; 100 mM), ethylenediaminetetraacetic acid (EDTA; 20 mM), and DPBS solution. Samples were centrifuged at 3000g for 2 minutes at 4ºC, and plasma samples were collected. The samples were immediately frozen on liquid nitrogen and stored at -80 ° C until further analysis.

2.12.2 Nitrite plasma levels

Plasma samples were thawed on ice, and nitrite concentrations were quantified by a chemiluminescence detector (CLD 88 e, Eco Physics GmbH, Munich, Germany) as previously described by Bryan (Bryan, Rassaf et al. 2004). Briefly, the nitrite levels were measured in a 60ºC reaction chamber filled with a solution of potassium iodide (45 mM) and iodine (10 mM) in 93 % acetic acid. Then, 100 µl of samples or a standard nitrite curve were injected into a septum by a Hamilton syringe (Hamilton Company, USA). Following the CLD method, the NO contained in the sample will be released and passed across a cooling system in the CLD analyzer using helium as carrier gas. The reaction between NO and ozone (O^3) forms nitrogen dioxide (NO_2), emits light, and the chemiluminescence produced is detected by a photomultiplier tube. Then, the CLD output voltage will be proportional to the nitrite concentration in the sample. A standard nitrite curve of 0-1200nM determined the nitrite concentration. Data analysis was performed by eDAQ Powerchrome software (eDAQ, Colorado Spring, USA).

2.12.3 Nitrate plasma levels

Plasma nitrate concentrations were measured by high-performance liquid chromatography (HPLC) in ENO-30 (AMUZA INC, San Diego, USA), following the manufacturer's instructions. First, samples were thawed on ice, and 10 µl of sample or nitrate standard curve were injected into ENO-30 without dilution. For that reason, the precolumn was changed every 15 samples. Then, the carrier collected and pushed the sample across the separation columns responsible for separating nitrite from nitrate. Next, the samples passed through the reduction column, which is responsible for converting nitrate to nitrite. Finally, Griess's reagent N-(1-naphthyl) ethylenediamine is added, and the two peaks are detected at 540nm. The area under the curve was measured using the Clarity 8.2.02.094 software package (DataApex, The Czech Republic).

2.13 Ischemia-reperfusion injury

2.13.1 Surgical procedure

Approximately 30 minutes before the experiment, mice were administered subcutaneously with buprenorphine (0.1 mg/kg) to induce analgesia during the procedure. Mice were intubated (Venous cannula 20G), placed on a warm operation table (37,5ºC), and submitted to constant inhalation anesthesia (2% induction, 3% maintenance isoflurane v/v) using a murine respirator (micro ventilator, UNO, The Netherlands). Regardless of the group, all animals were kept for 40 minutes under inhalation anesthesia before the ischemia. The respiratory rate (about 120-140 breaths/min) and the body temperature (37.5°C) were kept constant throughout the experiment. Electrocardiogram recordings were performed by PowerLab 4.0 (AD Instruments, UK). The mouse's fur was removed from the mouse's chest using a hair removal cream (Veet, Reckitt Benckiser, United Kingdom), and Betaisodona was applied to the chest to disinfect the incision area. A thoracotomy was performed between the fourth and fifth ribs, and the pericardium

was carefully retracted. After that, the left descendent artery (LAD) was occluded (Prolene suture 8,0) for 30 minutes and confirmed by ST elevation on the electrocardiogram recorded during the ischemic phase and the first minute after reperfusion, followed by 24 hours of reperfusion as described (Erkens, Suvorava et al. 2018). These experiments were performed with the support of Stefanie Becher.

2.13.2 Experimental groups

The experimental groups were randomly divided into two phases. Phase I consisted of investigating whether Pyk2 affects infarct sizes and rIPC-induced cardioprotection. Phase II involved investigating the mechanism by which Pyk2 inhibition affects infarct sizes.

Phase I

Phase I was divided into six groups: 1) IR group, mice received only a standard surgical procedure as described above; 2) rIPC group, in this protocol, mice were submitted to rIPC maneuver 40 minutes before surgery; 3) nitrite group, this group was subjected to the application of 48 nmol sodium nitrite (50µl) into the left ventricular cavity 5 min before LAD ligation. This group was used as a positive control of NO-dependent cardioprotection. 4) Pyk2-I group, in this group Pyk2 inhibitor (PF-431396), was administered intraperitoneally 15 minutes prior to LAD ligation; 5)Pyk2-I+rIPC group, in this group Pyk2 inhibitor, was administered intraperitoneally 15 minutes before the rIPC protocol was performed and 55 minutes before LAD ligation; 6)Pyk2+nitrite group, in this group Pyk2 inhibitor, was administered and sodium nitrite, as described above, 15 minutes and 5 minutes before LAD ligation, respectively. A scheme with all the operation settings for phase I is illustrated in Figure 6.

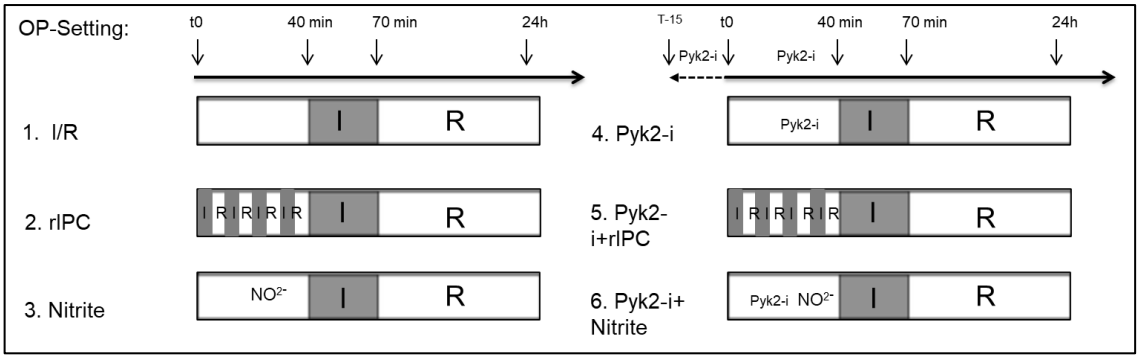

Fig. 6 Phase I operating settings

Myocardial ischemia-reperfusion (I/R) surgical groups. 1-I/R group, 2-remote ischemic preconditioning maneuver (rIPC) group, 3- nitrite group, 4-Proline-rich tyrosine kinase 2 (Pyk2) inhibition group, 5-Pyk2 inhibition and rIPC maneuver group, 6-Pyk2 inhibition, and nitrite group. Ischemia (I) 30 minutes, Reperfusion (R) 24 hours, Nitrite (NO_2^-). Created by Amanda Brum using elements of Microsoft PowerPoint.

Phase II

Phase II was divided into three primary protocols: 1) the use of a NO scavenger, 2-4-carboxyphenyl-4,4,5,5-tetramethylimidazoline-1-oxyl-3-oxide (CPTIO), 2) the transection of the femoral nerve (F. nerve) and 3) the use of a MAPK inhibitor (U0126).

1) In the CPTIO protocol, mice received a 100µl intravenous injection of 1mg/kg of CPTIO/saline solution through the tail vein. The CPTIO protocol was divided into three groups: 1A) CPTIO+rIPC, in this group, mice received CPTIO injection 5 minutes prior to the beginning of the rIPC maneuver; 1B) CPTIO+Nitrite, in this group, mice received CPTIO injection 5 minutes prior to nitrite injection as described previously; 1C) CPTIO+Pyk2+rIPC, in this group mice, received Pyk2 inhibitor and injection of CPTIO 15 and 5 minutes prior to rIPC maneuver. The CPTIO groups op settings are illustrated in Figure 7.

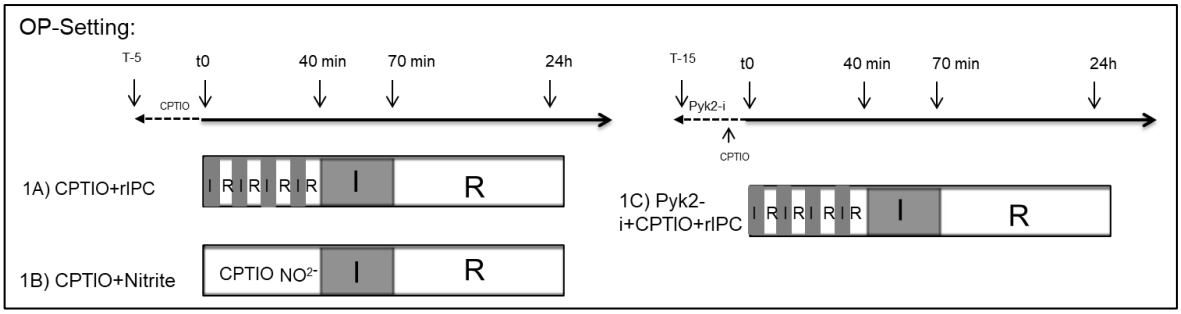

Fig. 7 CPTIO protocol setting

Myocardial ischemia-reperfusion (I/R) CPTIO groups. 1A- CPTIO and remote ischemic preconditioning maneuver (rIPC) group, 1B- CPTIO and nitrite group, 1C-Proline-rich tyrosine kinase 2 (Pyk2) inhibition, CPTIO and rIPC maneuver group. Ischemia (I) 30 minutes, Reperfusion (R) 24 hours, Nitrite (NO_2^-), 2-4-carboxyphenyl-4,4,5,5-tetramethylimidazoline-1-oxyl-3-oxide (cPTIO). Created by Amanda Brum using elements of Microsoft PowerPoint.

2) In the femoral nerve protocol, the transection of the F. nerve was performed after 5 minutes of intubation of the mice. First, an incision was made in the internal left hindlimb, and the skeletal muscle was carefully retracted. Subsequently, the femoral nerve was carefully isolated from the femoral artery and vein, and a nerve transection was performed. Subsequently, the hindlimb skin was closed by sutures, and when required, a cuff was placed on the hindlimb to facilitate the rIPC maneuver. The F. nerve protocol was divided into three groups: 2A) F.nerve group, in this group mice, had the F. nerve transected and received a standard surgical procedure as described above; 2B) F.nerve+rIPC group, in this group, mice had the F.nerve transected and were submitted to rIPC maneuver; 2C)F.nerve+Pyk2+rIPC, in this group mice, received Pyk2 inhibitor had the F.nerve transected 15 and 5 minutes prior to rIPC maneuver. The femoral nerve transection groups' op settings are illustrated in Figure 8.

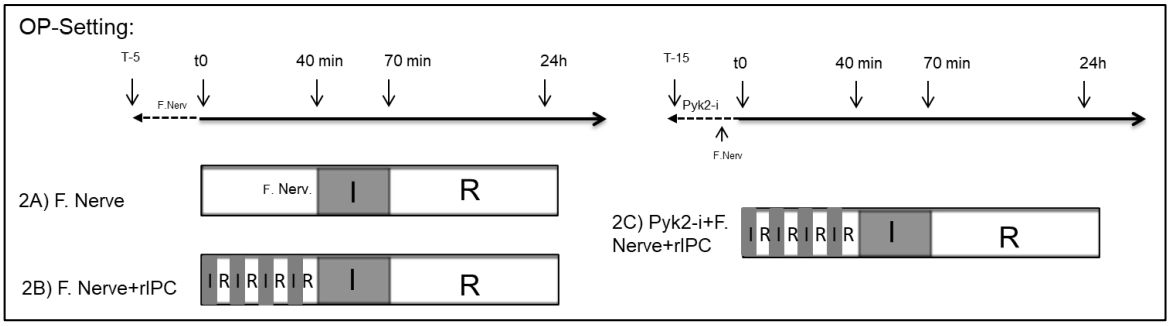

Fig. 8 Femoral nerve transection protocol

Myocardial ischemia-reperfusion (I/R) Femoral nerve transection groups. 2A- Femoral nerve transection (F. nerve) group, 2B- F.nerve and remote ischemic preconditioning maneuver (rIPC) group, 2C-Proline-rich tyrosine kinase 2 (Pyk2) inhibition, F.nerve, and rIPC maneuver group. Ischemia (I) 30 minutes, Reperfusion (R) 24 hours. Created by Amanda Brum using elements of Microsoft PowerPoint.

3) The MAPK inhibitor protocol (U0126) followed the protocol performed by Wang et al. (Wang, Zhang et al. 2016). A summary of the U0126 targeting action is illustrated in Figure 9. In this protocol, mice received pretreatment with U0126 (3mg/kg body weight diluted in DMSO) intraperitoneally 30 minutes before LAD ligation. The MAPK inhibitor protocol was divided into four groups: 3A) U0126 group, in this group, mice received the U0126 injection prior to standard surgical procedure as described above; 3B) U0126+rIPC, in this group, mice were submitted to the rIPC maneuver, and U0126 was administrated 10 minutes after the rIPC manner beginning; 3C) U0126+Pyk2, in this group mice received the U0126 and Pyk2 injection 30 and 15 minutes prior to LAD ligation; 3D) U0126+Pyk2+rIPC, in this protocol mouse, receive Pyk2 inhibitor 15 minutes prior to rIPC maneuver and U0126 30 minutes before LAD ligation. A scheme with all the groups above is demonstrated in Figure 10.

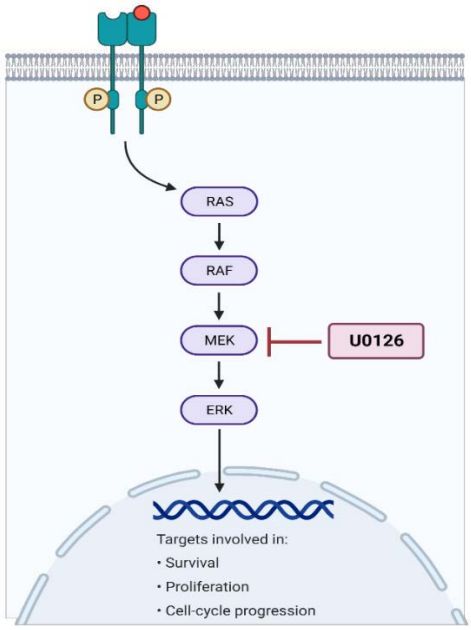

Fig. 9 *MAPK inhibition by U0126*

The inhibitor U0126 inhibits the activation of extracellular signal-regulated kinase (ERK ½) and its consequences by inhibiting the activity of the Mitogen-activated protein kinase kinase (MEK ½). Created by Amanda Brum with Biorender.

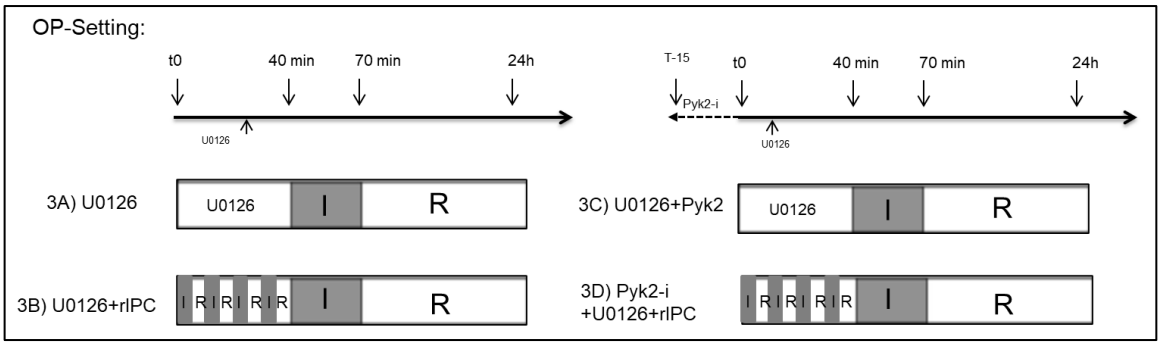

Fig. 10 MAPK inhibitor protocol setting

Myocardial ischemia-reperfusion (I/R) MAPK inhibitor groups. 3A- U0126 inhibitor group, 3B- U0126 inhibitor and remote ischemic preconditioning maneuver (rIPC) group, 3C- U0126 inhibitor and Proline-rich tyrosine kinase 2 (Pyk2) inhibitor group, 3D-Pyk2-I, U0126 inhibitor, and rIPC maneuver group. Ischemia (I) 30 minutes, Reperfusion (R) 24 hours, Mitogen-activated protein kinase (MAPK). Created by Amanda Brum using elements of Microsoft PowerPoint.

2.13.3 Infarct sizes quantification

After 24h of surgical procedure, mice were anesthetized by intraperitoneal administration of 100 mg/kg ketamine (Ketanest®) and 10 mg/kg xylazine (Rompun®). Furthermore, 200 µl of heparin (250 IU) was administered intraperitoneally to avoid blood anticoagulation during heart preparation. The thorax was opened, and the heart was carefully harvested and rinsed with saline solution. LAD was reoccluded at the exact location, and 1% Evans Blue dye was injected into the aortic root to delineate the area at risk (AAR) from the not-at-risk myocardium. The tissue was wrapped in a clear food wrap and stored in a -20°C freezer for one hour. The heart was then serially sectioned perpendicularly to the long axis in 1-mm slices, and each slice was weighed. The sections were incubated in 1% triphenyl tetrazolium chloride (TTC) for 5 min at 37°C to demarcate the viable and nonviable myocardium within the risk zone. The areas of infarction, AAR, and no ischemic left ventricle were assessed with computer-assisted planimetry. The size of the myocardial infarction was expressed as a percentage of the AAR. The Myocardial ischemia-reperfusion protocol and infarct size quantification is illustrate in Figure 11.

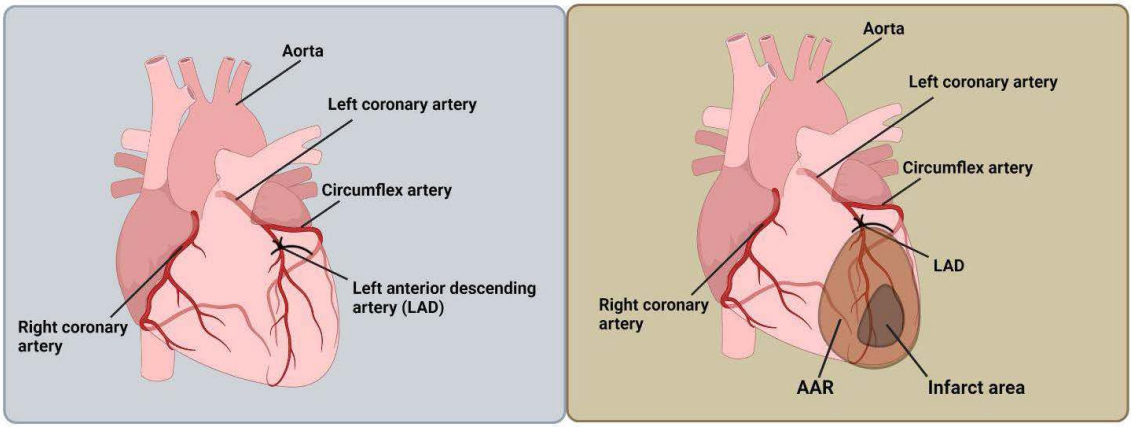

Fig. 11 Myocardial ischemia-reperfusion protocol and infarct size quantification

Myocardial ischemia-reperfusion protocol. The protocol consisted of 30 minutes of ligation of the left anterior descendent artery (LAD), as illustrated in the left image, followed by 24h of reperfusion. The infarct size was calculated as a percentage of the Area at risk (AAR), as illustrated in the right image. Created by Amanda Brum with Biorender.

2.14 Statistical analysis

Statistical analysis was carried out with GraphPad Prism 8. If not differently specified, the results are given as mean ± standard error of the mean (SEM). Pared or an unpaired Student's t-test was used to determine if the two groups of data were significantly different. Data were analyzed by 1-way or 2-way ANOVA to compare three or more groups, followed by Bonferroni's or Sidak's post hoc tests. The D'Agostino-Pearson test tested normal distribution, and $p \leq 0.05$ was considered statistically significant.

3 Results

3.1 NZO mice exhibit glucose intolerance, insulin resistance, and hyperinsulinemia

To investigate the impact of Pyk2 on eNOS regulation in insulin resistance with associated hyperinsulinemia conditions, we used a well-known murine model of insulin resistance and T2DM, the NZO mice. Therefore, our first aim was to characterize this mouse model's metabolic and cardiovascular system.

As demonstrated in Figure 12, the NZO mice exhibited a significantly higher body weight (BW: BL6 29±0,5 vs. NZO 51,6±0,7 $p<0.0001$) and heart weight (HW: BL6 173,6±4,7 vs. NZO 264,3±10,3 $p <0.0001$) compared with BL6 mice. Moreover, NZO mice exhibited higher fasting blood glucose concentration (BL6 136,9±4,9 vs. NZO 162,3±10,8 $p=0,039$) and higher fasting insulin plasma levels (BL6 0,61±0,15 vs. NZO 2,34±0,51 $p=0,009$) compared to BL6 mice.

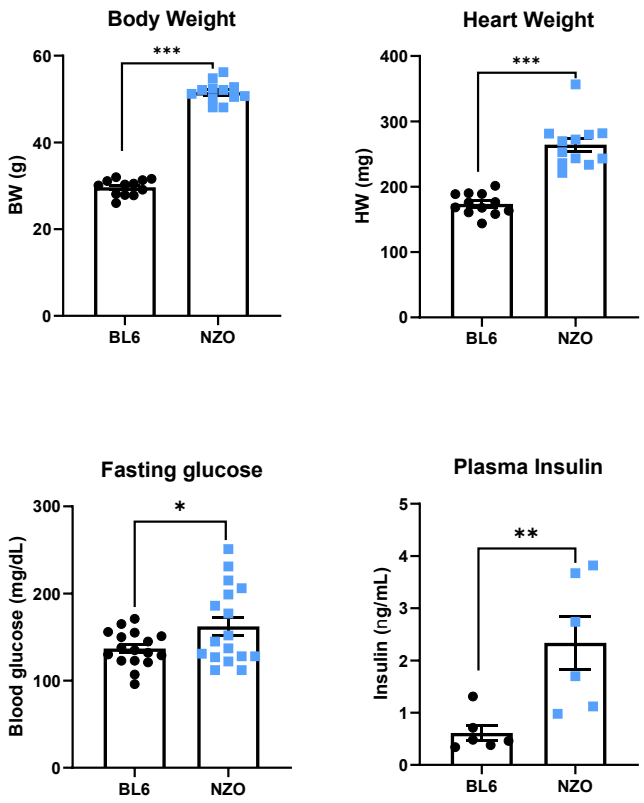

Fig. 12 Basal characterization

(A) NZO mice show higher body weight (BW) than BL6 mice. (B) NZO mice show higher heart weight (HW) compared to BL6 mice. BL6 and NZO n=12. (C) NZO shows higher fasting blood glucose than BL6 mice. BL6 and NZO n=17. (D) NZO mice show greater insulin plasma levels than BL6 mice. BL6 and NZO n=6. BL6 mice individuals' values are represented in black, and NZO mice individuals' values are represented in blue. Statistic: Unpaired t-test, data shown as mean± SEM. *p<0,05, **p<0,01, *** p<0,0001.

Furthermore, as demonstrated in Figure 13, the assessment of metabolic tolerance tests showed that NZO mice exhibit a significantly higher blood glucose concentration after glucose (AUC of GTT: BL6 21221±1957,7 vs. NZO 40036±3920,1 p=0,0010) and insulin administration (AUC of ITT: BL6 7413±224,6 vs. NZO 10903±1111,7 p=0,0096) compared to BL6 mice.

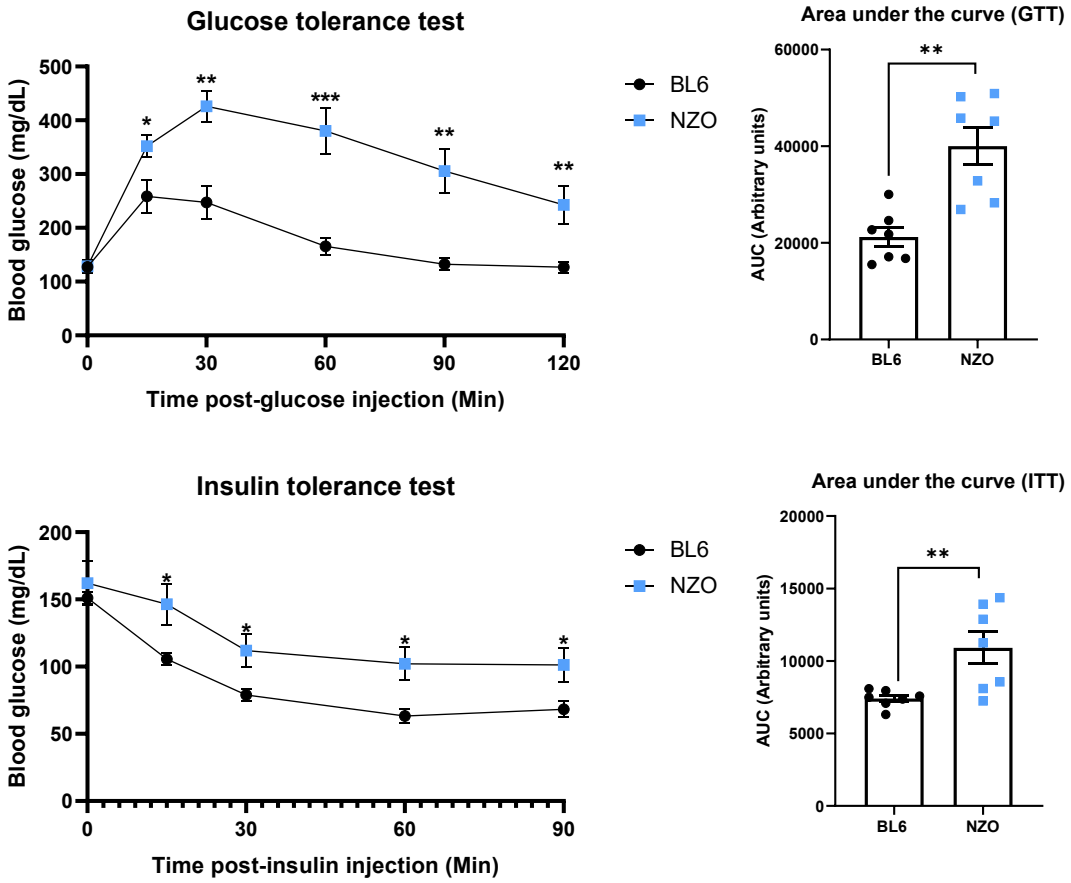

Fig. 13 NZO mice present insulin resistance and glucose intolerance

(A)Glucose tolerance test (GTT) shows that NZO mice present significant glucose intolerance compared to BL6 mice. The area under the curve (AUC) of GTT demonstrates that NZO mice show higher AUC compared to BL6 mice. (B) The insulin tolerance test (ITT) demonstrates that NZO mice present higher insulin resistance than BL6 mice. The area under the curve (AUC) of ITT), shows that NZO mice exhibit a significantly higher area under the curve compared to BL6 mice. BL6 mice individuals' values are represented in black, and NZO mice individuals' values are represented in blue. BL6 and NZO n=7. Unpaired t-test data are shown as mean± SEM. *p<0,05, **p<0,01, *** p<0,0001.

In addition, as demonstrated in Figure 14, the assessment of cardiac function by echocardiography showed that the NZO mice have similar heart rates (HR: BL6 vs. NZO p=0,34), cardiac output index (COI: BL6 vs. NZO p=0,53), stroke volume index (SVI: BL6 vs. NZO p=0,99), ejection fraction (EF: BL6 vs. NZO p=0,31), end-

systolic volume index (ESVI: BL6 vs. NZO p=0,17) and end-diastolic volume index (EDVI: BL6 vs. NZO p=0,28) to BL6 mice.

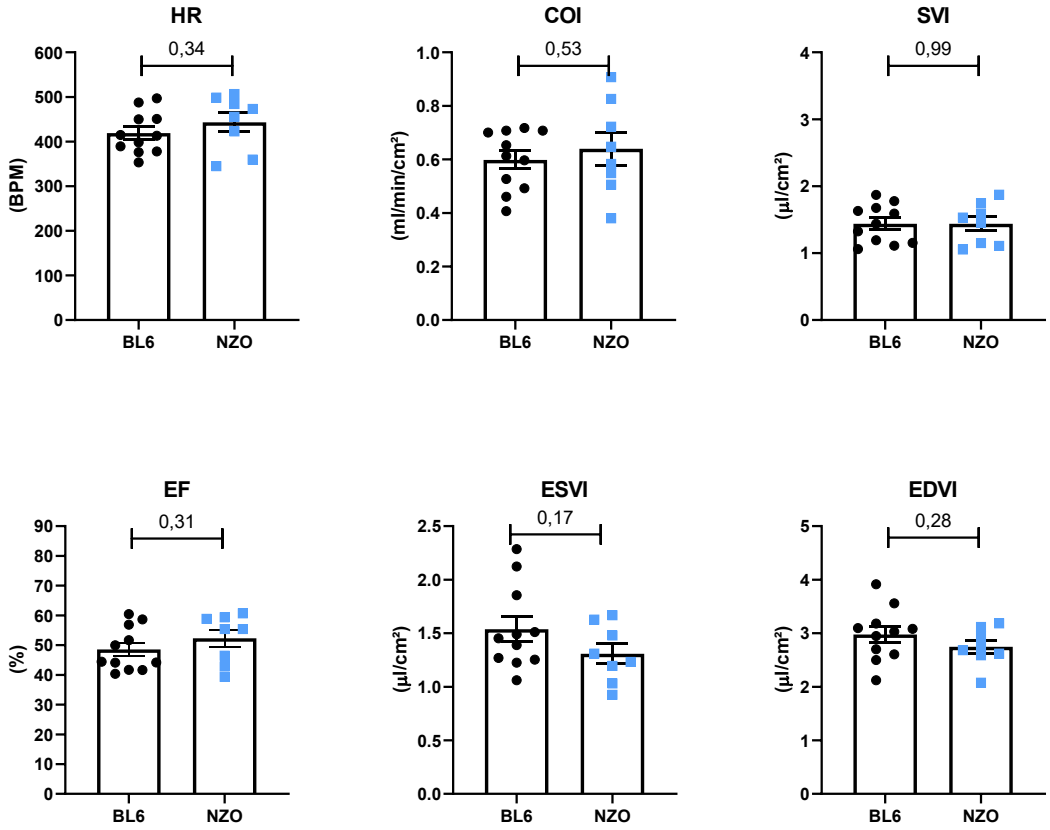

Fig. 14 Cardiac function assessed by echocardiography

A) Heart Rate (HR). B) Cardiac output index (COI). C) Stroke volume index (SVI). D) Ejection fraction (EF). E) End systolic volume index (ESVI). F) End diastolic volume index (EDVI). BL6 mice individuals' values are represented in black, and NZO mice individuals' values are represented in blue. BPM (beats per minute). BL6 and NZO n=8-11. Unpaired t-test data are shown as mean± SEM.

3.2 Insulin signaling pathway in skeletal muscle and cardiovascular tissues

Proteins involved in the insulin signaling pathway were investigated through insulin stimulation experiments to determine the sensibility of skeletal muscle and myocardium to insulin.

3.2.1 Skeletal muscle

The soleus muscle was used to determine the effects of insulin on skeletal muscle metabolism. Upon binding to its receptor, insulin can initiate two central signaling cascades: the metabolic pathway represented by AKT activation, resulting in GLUT-4 translocation, and the mitogenic pathway represented by ERK activation responsible for chronic insulin responses. As demonstrated in Figure 15, insulin increases the soleus phosphorylation of AKT on the ser473 side regardless of the group investigated (pAKT/GAPDH: BL6 fasting vs. BL6 insulin p=0,0056; NZO fasting vs. NZO insulin=0,01) (pAKT/AKT: BL6 fasting vs. BL6 insulin p=0,02; NZO fasting vs. NZO insulin=0,006). Furthermore, the fasting and insulin levels of p-AKT (BL6 fasting vs. NZO fasting p=0,9; BL6 insulin vs. NZO insulin=0,99) and total AKT (BL6 fasting vs. NZO fasting p=0,7; BL6 insulin vs. NZO insulin=0,11) were not different between the groups. However, in BL6 mice, the total AKT amount increased in response to insulin, whereas the AKT amount was not affected in response to insulin in the NZO mice (BL6 fasting vs. BL6 insulin p=0,03; NZO fasting vs. NZO insulin p=0,4).

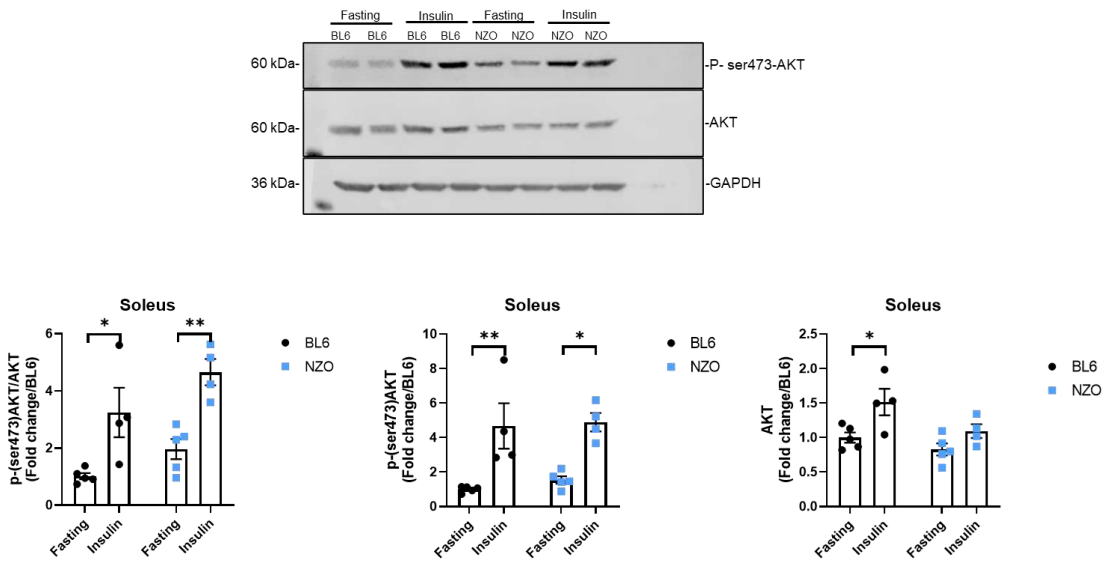

Fig. 15 Insulin increases the activation of AKT in the skeletal muscle

Western blot analysis of AKT expression after insulin stimulation in soleus. A) Representative Western blot signal of AKT levels. B) Ratio of p-AKT/AKT. C) Levels of p-ser473 AKT in response to insulin. D) AKT total protein amount. BL6 mice individuals' values are represented in black, and NZO mice individuals' values are represented in blue. BL6 and NZO n=4-5. Data are shown as fold change of BL6 (Fasting). Two-way ANOVA, Tukey's multiple comparison tests, data are shown as mean± SEM. *p<0,05, **p<0,01.

Furthermore, the activation levels of ERK in response to insulin were also investigated. As demonstrated in Figure 16, even though ERK activity form was nearly three-fold higher in the NZO mice fasting compared with BL6 fasting (p-ERK levels: BL6 1,0 ±0,19 vs. NZO 2,84± 1,18 p=0,38; ratio p-ERK/ERK: BL6 0,97±0,17 vs. NZO 2,82±1,09 p=0,23), ERK activity and total protein amount were not significantly different between the groups (ERK: BL6 vs. NZO p=0.99) nor affected by insulin stimulation (ERK: BL6 fasting vs. BL6 insulin p=0,87; NZO fasting vs. NZO insulin p=0,74).

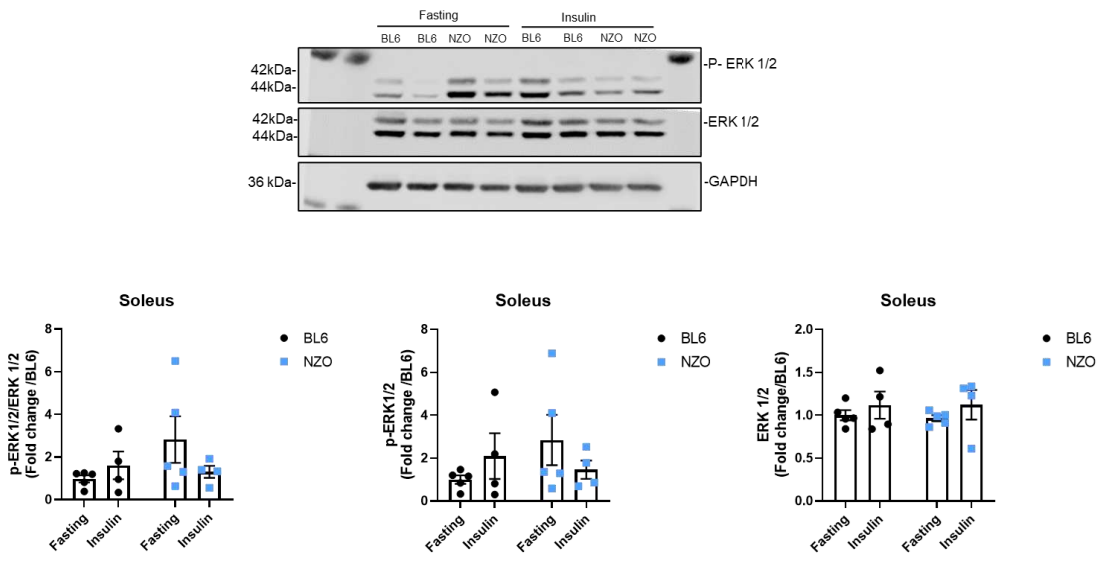

Fig. 16 Insulin does not affect ERK activation and protein amount in the skeletal muscle

Western blot analysis of ERK expression after insulin stimulation in soleus. A) Representative Western blot signal of ERK levels. B) Ratio of p-ERK/ERK. C) Levels of p-ERK1/2 in response to insulin. D) ERK total protein amount. BL6 mice individuals' values are represented in black, and NZO mice individuals' values are represented in blue. BL6 and NZO n=4-5. Data are shown as fold change of BL6 (Fasting). Two-way ANOVA, Tukey's multiple comparison tests, data are shown as mean± SEM.

To determine whether AKT-mediated GLUT4 translocation was preserved, two proteins that control the vesicular traffic of GLUT4 in response to insulin were investigated AS160 and TBC1D1. As demonstrated in Figure 17, phosphorylation of AS160 on thr642 was enhanced in response to insulin (BL6 fasting vs. BL6 insulin p=0,085; NZO fasting vs. NZO insulin p=0,0030). The total protein amount and the ratio p-thr642 AS160/AS160 were not significant between and within the groups. Furthermore, as demonstrated in Figure 18, insulin did not affect the levels of TBC1D1 phosphorylated on thr590 between and within the groups. When analyzed, the total protein amount after insulin stimulation in NZO mice showed a significant reduction of TBC1D1 compared with BL6 mice (BL6 vs. NZO p=0,034).

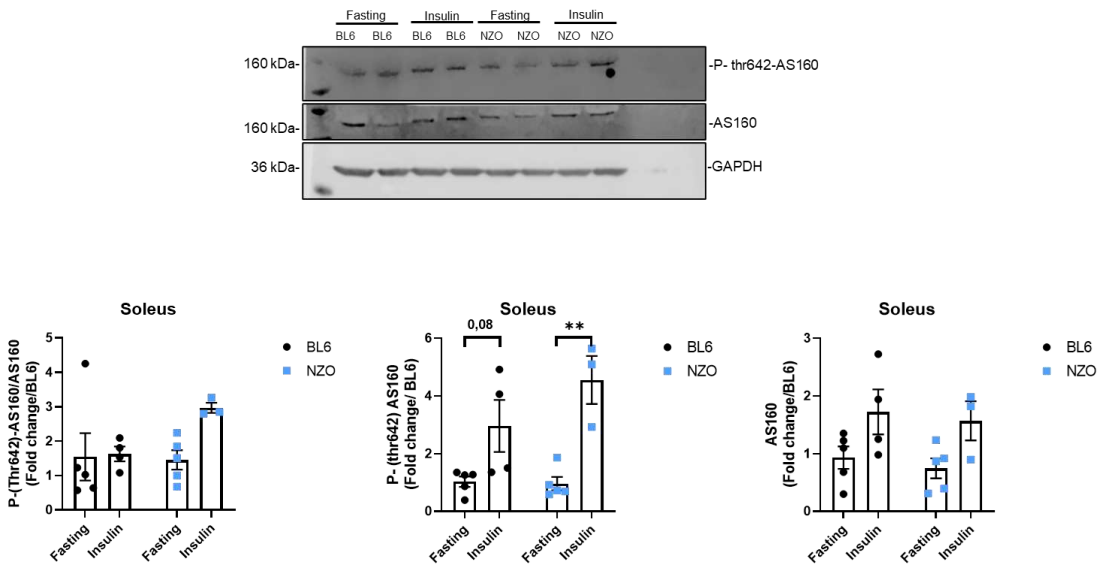

Fig. 17 Insulin increases AS160 activation in the skeletal muscle

Western blot analysis of AS160 expression after insulin stimulation in soleus. A) Representative Western blot signal of AS160 levels. B) Ratio of p-AS160/AS160. C) Levels of p-thr642 AS160 in response to insulin. D) AS160 total protein amount. BL6 mice individuals' values are represented in black, and NZO mice individuals' values are represented in blue. BL6 and NZO n=3-5. Data are shown as fold change of BL6 (Fasting). Two-way ANOVA, Tukey's multiple comparison tests, data are shown as mean± SEM. *p<0,05, **p<0,01.

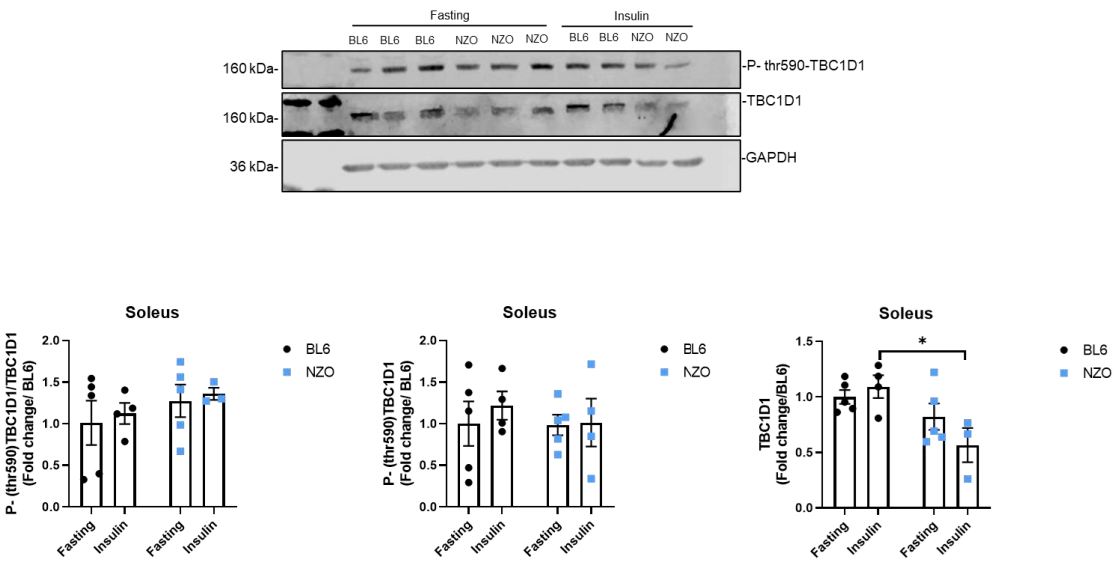

Fig. 18 Insulin does not affect TBC1D1 activation in the skeletal muscle

Western blot analysis of TBC1D1 expression after insulin stimulation in soleus. A) Representative Western blot signal of TBC1D1 levels. B) Ratio of p-TBC1D1/ TBC1D1. C) Levels of p-thr590 TBC1D1 in response to insulin. D) TBC1D1 total protein amount. BL6 mice individuals' values are represented in black, and NZO mice individuals' values are represented in blue. BL6 and NZO n=3-5. Data are shown as fold change of BL6 (Fasting). Two-way ANOVA, Tukey's multiple comparison tests, data are shown as mean± SEM. *p<0,05.

Next, Western blot analysis was performed to investigate whether insulin stimulation affects GLUT4 expression. As shown in Figure 19, insulin stimulation increases by 27% and 29% of the total amount in BL6 (BL6 fasting 1,0±0,07 vs. BL6 insulin 1,27±0,11) and NZO (NZO fasting 0,71±0,13 vs. NZO insulin 1,0±0,10) mice, respectively. Although no significant NZO mice exhibited 29% and 24% less GLUT4 total protein amount compared to BL6 mice fasting (BL6 1,0±0,07 vs. NZO 0,71±0,13) and after insulin stimulation (BL6 1,27±0,11 vs. NZO 1,0±0,10), respectively.

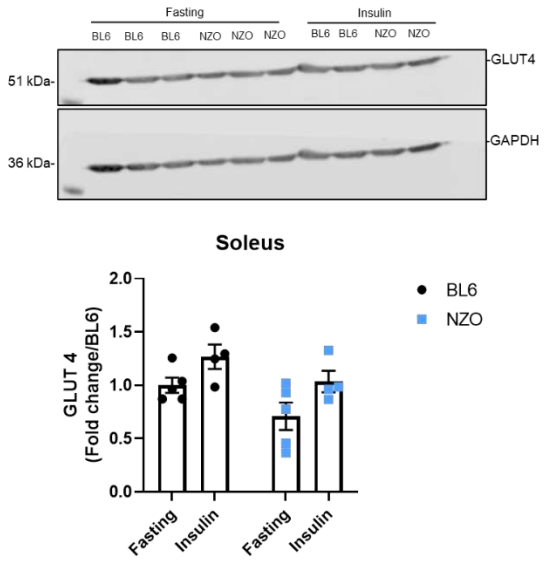

Fig. 19 GLUT4 amount in soleus

Western blot analysis of GLUT4 expression after insulin stimulation in soleus. A) Representative Western blot signal of GLUT4 levels. B) GLUT4 total protein amount. BL6 mice individuals' values are represented in black, and NZO mice individuals' values are represented in blue. BL6 and NZO n=4-5. Data are shown as fold change of BL6 (Fasting). Two-way ANOVA, Tukey's multiple comparison tests, data are shown as mean± SEM.

GSK3 is a relevant kinase that participates in several signaling cascades. In the skeletal muscle, the phosphorylation of GSK3 leads to glycogen synthesis in response to insulin. Therefore, it was investigated whether insulin stimulation affects the levels of GSK3 α/β in the soleus of the groups analyzed. As demonstrated in Figure 20, insulin stimulation increases the phosphorylation (ser21/9) of GSK3α/β by around 234% and 133% in BL6 (BL6 fasting 1,0±0,16 vs. BL6 insulin 3,34±0,7) and NZO (NZO fasting 1,78 ±0,4 vs. NZO insulin 2,37 ±0,4) respectively. Total GSK3 α/β was not different between and within the groups.

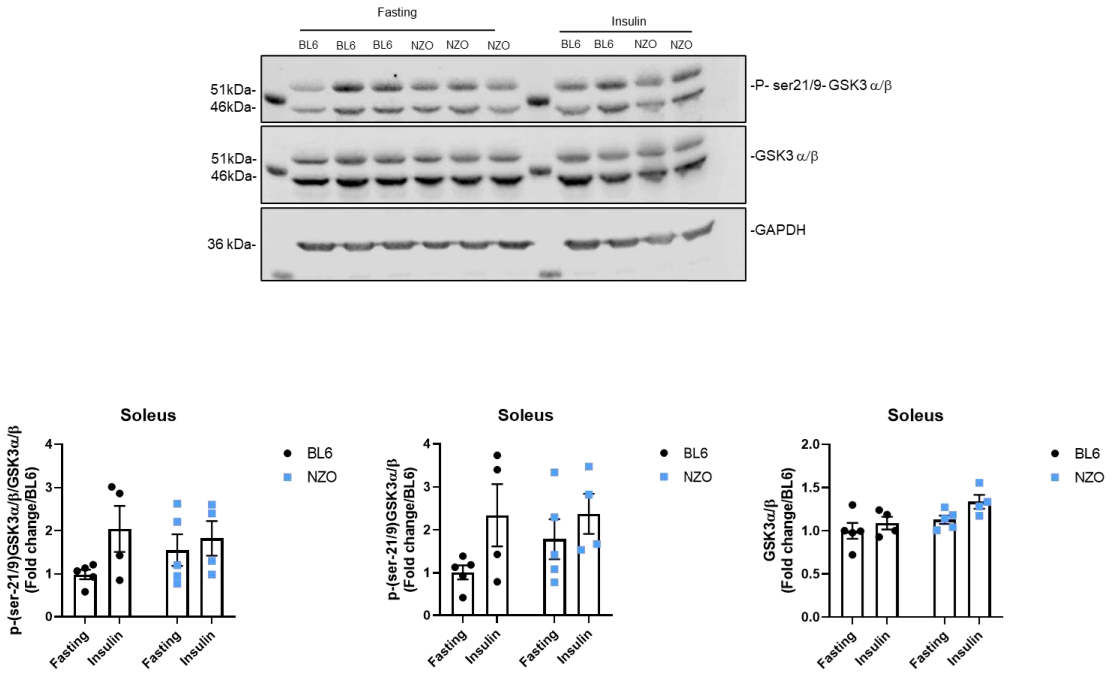

Fig. 20 Insulin does not affect GSK3 α/β levels in the skeletal muscle

Western blot analysis of GSK3 α/β expression after insulin stimulation in soleus. A) Representative Western blot signal of GSK3 α/β levels. B) Ratio of p-ser21/9-GSK3 α/β/GSK3 α/β. C) Levels of p-ser21/9- GSK3 α/β in response to insulin. D) GSK3 α/β total protein amount. BL6 mice individuals' values are represented in black, and NZO mice individuals' values are represented in blue. BL6 and NZO n=4-5. Data are shown as fold change of BL6 (Fasting). Two-way ANOVA, Tukey's multiple comparison tests, data are shown as mean± SEM.

3.2.2 Heart

In order to investigate whether the insulin resistance observed in the NZO mice extends to cardiovascular tissues, the effects of insulin in the heart were investigated. As shown in Figure 21, even though the NZO mice presented a lower AKT protein amount compared to BL6 mice (Fasting: BL6 1,0±0,09 vs. NZO 0,71±0,03 p=0,06; Insulin: BL6 1,0 ±0,09vs NZO 0,73±0,04 p=0,03), insulin increased the heart phosphorylation of AKT on the ser473 side regardless of the group investigated (pAKT/GAPDH: BL6 fasting vs. BL6 insulin p=0,0003; NZO fasting vs. NZO insulin=0,03). This effect was also demonstrated by the ratio p-ser473-AKT/AKT (pAKT/AKT: BL6 fasting vs. BL6 insulin p=0,002; NZO fasting vs. NZO insulin=0,015) within the groups.

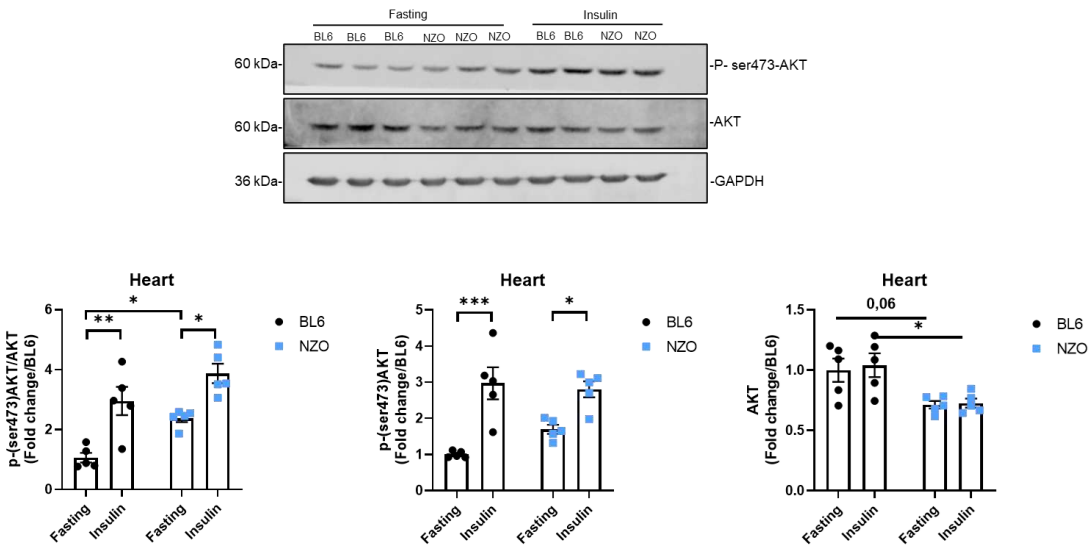

Fig. 21 Insulin increases the activation of AKT in the heart

Western blot analysis of AKT expression after insulin stimulation in the heart. A) Representative Western blot signal of AKT levels. B) Ratio of p-AKT/AKT. C) Levels of p-ser473 AKT in response to insulin. D) AKT total protein amount. BL6 mice individuals' values are represented in black, and NZO mice individuals' values are represented in blue. BL6 and NZO n=5. Data are shown as fold change of BL6 (Fasting). Two-way ANOVA, Tukey's multiple comparison tests, data are shown as mean± SEM. *p<0,05, **p<0,01, *** p<0,0001.

Moreover, as demonstrated in Figure 22, similarly to what was found in skeletal muscle, insulin did not affect the activation (p-ERK/GAPDH: BL6 fasting vs. BL6 insulin p=0,65; NZO fasting vs. NZO insulin p=0,99) and protein amount of ERK(ERK/GAPDH: BL6 fasting vs. BL6 insulin p>0,9; NZO fasting vs. NZO insulin p=0,40) in the heart. Furthermore, ERK activity (Fasting: BL6 vs. NZO p=0,98; Insulin: BL6 vs. NZO p=0,52) and total protein amount(Fasting: BL6 vs. NZO p=0,99; Insulin: BL6 vs. NZO p=0,30) were not significantly different between the groups.

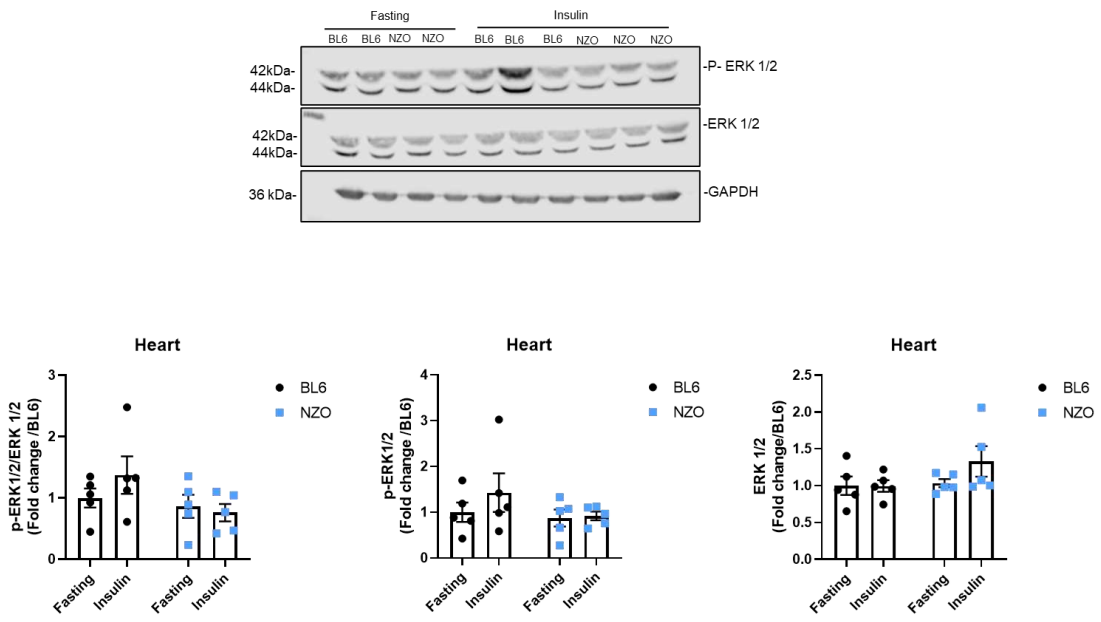

Fig. 22 Insulin does not affect ERK activation and protein amount in the heart

Western blot analysis of ERK expression after insulin stimulation in the heart. A) Representative Western blot signal of ERK levels. B) Ratio of p-ERK/ERK. C) Levels of p-ERK1/2 in response to insulin. D) ERK total protein amount. BL6 mice individuals' values are represented in black, and NZO mice individuals' values are represented in blue. BL6 and NZO n=5. Data are shown as fold change of BL6 (Fasting). Two-way ANOVA, Tukey's multiple comparison tests, data are shown as mean± SEM.

The measurement of AS160 activity and expression in the heart demonstrated (Figure 23) that the thr642 phosphorylation AS160 ratio was significantly increased in response to insulin in BL6 mice (BL6 fasting vs. BL6 insulin p=0,005). In contrast, it was not significantly different in NZO mice (NZO fasting vs. NZO insulin p=0,39). Furthermore, insulin increased 120% (BL6 fasting 1,0±0,14 vs. BL6 insulin 2,23±0,5) of p-thr642 AS160 while it increased only 19% (NZO fasting 1,5±0,3 vs. NZO 1,8±0,3 insulin) in the NZO mice. The total protein amount and the ratio p-thr642 AS160/AS160 were not significant between the groups.

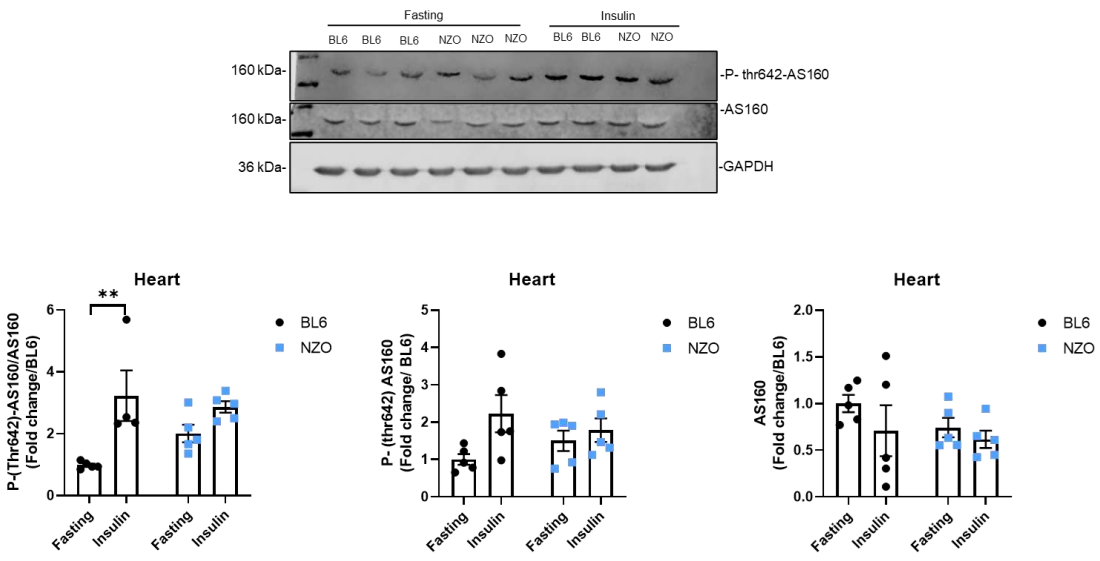

Fig. 23 Insulin increases AS160 activation in the skeletal muscle

Western blot analysis of AS160 expression after insulin stimulation in the heart. A) Representative Western blot signal of AS160 levels. B) Ratio of p-AS160/AS160. C) Levels of p-thr642 AS160 in response to insulin. D) AS160 total protein amount. BL6 mice individuals' values are represented in black, and NZO mice individuals' values are represented in blue. BL6 and NZO n=5. Data are shown as fold change of BL6 (Fasting). Two-way ANOVA, Tukey's multiple comparison tests, data are shown as mean± SEM. **p<0,01.

Furthermore, as demonstrated in Figure 24, insulin increased the levels of TBC1D1 phosphorylated on thr590 by 64% and 128% in BL6 (BL6 fasting 0±0,09 vs. BL6 insulin1,64±0,4) and NZO (NZO fasting 0,63±0,24 vs. NZO insulin1,44±0,22), respectively. The total TBC1D1 protein was not significantly different between and within the groups regardless of insulin stimulation. In addition, as shown in Figure 25, insulin did not affect the expression of GLUT4 in the heart.

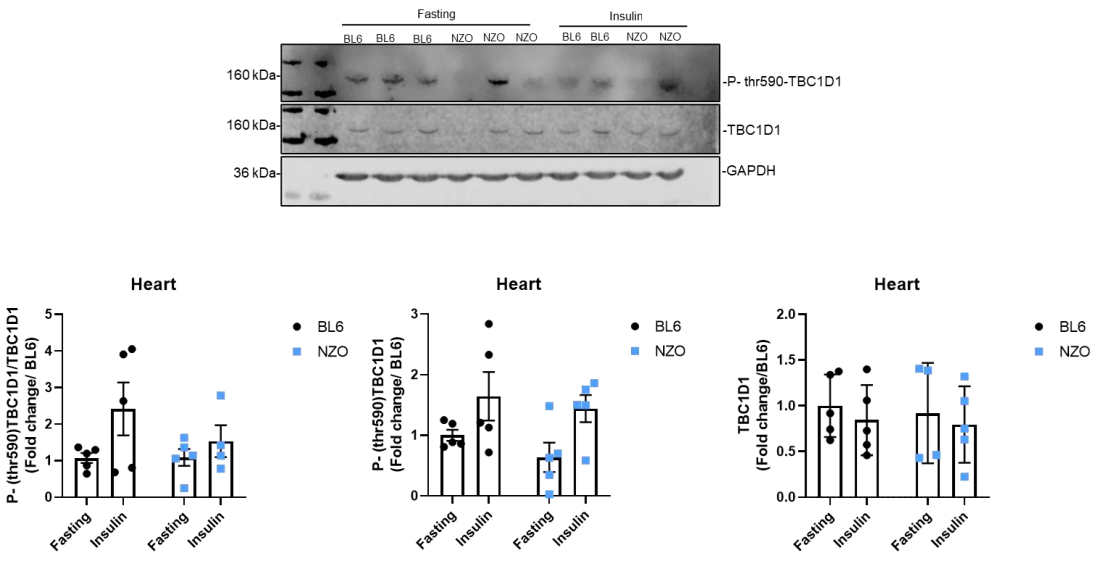

Fig. 24 TBC1D1 expression in the heart

Western blot analysis of TBC1D1 expression after insulin stimulation in the heart. A) Representative Western blot signal of TBC1D1 levels. B) Ratio of p-TBC1D1/ TBC1D1. C) Levels of p-thr590 TBC1D1 in response to insulin. D) TBC1D1 total protein amount. BL6 mice individuals' values are represented in black, and NZO mice individuals' values are represented in blue. BL6 and NZO n=4-5. Data are shown as fold change of BL6 (Fasting). Two-way ANOVA, Tukey's multiple comparison tests, data are shown as mean± SEM.

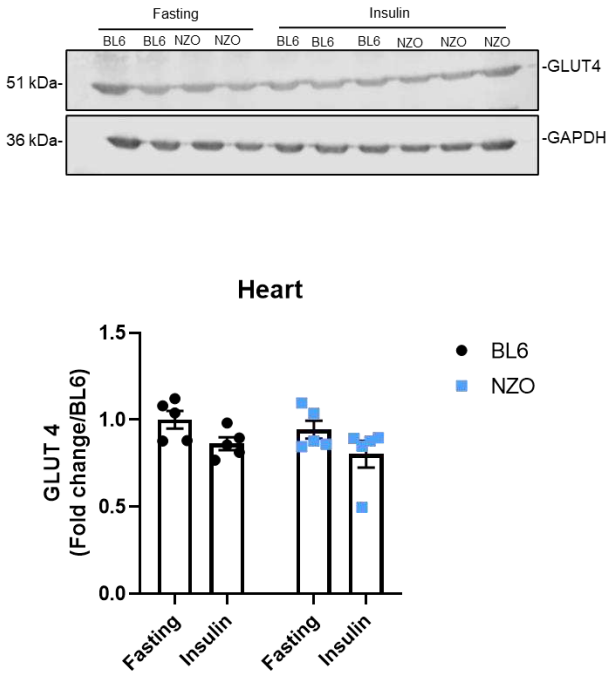

Fig. 25 Insulin did not affect the expression of GLUT4 in the heart.

Western blot analysis of GLUT4 expression after insulin stimulation in the heart. A) Representative Western blot signal of GLUT4 levels. B) GLUT4 total protein amount. BL6 mice individuals' values are represented in black, and NZO mice individuals' values are represented in blue. BL6 and NZO n=4-5. Data are shown as fold change of BL6 (Fasting). Two-way ANOVA, Tukey's multiple comparison tests, data are shown as mean± SEM.

The measurement of GSK3 α/β activity and expression in the heart demonstrated (Fig. 26) that the phosphorylation (ser21/9) of the GSK3α/β and its ratio was significantly increased in response to insulin in BL6 mice (p-ser21/9-GSK3α/β/GAPDH: BL6 fasting vs. BL6 insulin p=0,03; p-ser21/9-GSK3α/β/GSK3: BL6 fasting vs. BL6 insulin p=0,014;). In contrast, it was not significantly different in NZO mice (p-ser21/9-GSK3α/β/GAPDH: NZO fasting vs. NZO insulin p>0,99; p-ser21/9-GSK3α/β/GSK3: NZO fasting vs. NZO insulin p=0,99). Total GSK3 α/β was not different between and within the groups.

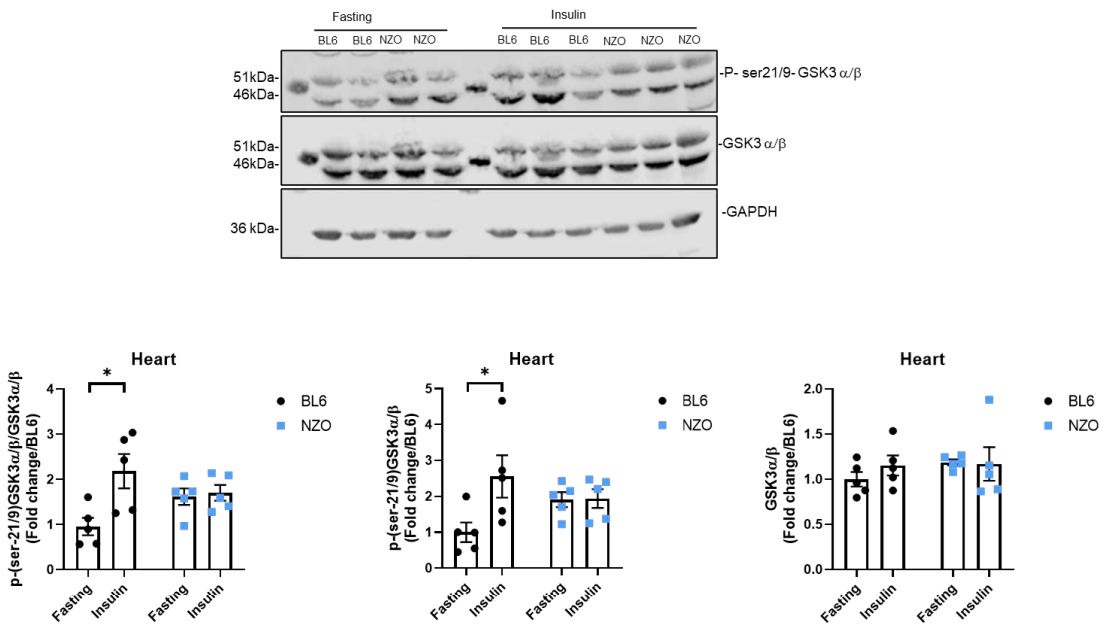

Fig. 26 Insulin does not affect GSK3 α/β levels in the heart of NZO mice

Western blot analysis of GSK3 α/β expression after insulin stimulation in the heart. A) Representative Western blot signal of GSK3 α/β levels. B) Ratio of p-ser21/9-GSK3 α/β/GSK3 α/β. C) Levels of p-ser21/9- GSK3 α/β in response to insulin. D) GSK3 α/β total protein amount. BL6 mice individuals' values are represented in black, and NZO mice individuals' values are represented in blue. BL6 and NZO n=5. Data are shown as fold change of BL6 (Fasting). Two-way ANOVA, Tukey's multiple comparison tests, data are shown as mean± SEM.

Furthermore, the impact of insulin on the expression and activity of eNOS was investigated (Fig.27). Insulin did not affect the activity (p-ser-eNOS/GAPDH: BL6 fasting vs. BL6 insulin p=0,99; NZO fasting vs. NZO insulin p=0,99) and expression of eNOS (eNOS/GAPDH: BL6 fasting vs. BL6 insulin p=0,64; NZO fasting vs. NZO insulin p=0,99) in the heart. However, the NZO mice showed around 40% lower p-ser eNOS (p-eNOS Fasting: BL6 1,0±0,11 vs. NZO 0,58±0,19; Insulin BL6 1,03±0,16 vs. NZO 0,56±0,15) and 20-30% lower total eNOS (eNOS Fasting: BL6 1,00±0,10 vs. NZO 0,82±0,09; Insulin BL6 1,17±0,11 vs. NZO 0,83±0,1) compared to BL6.

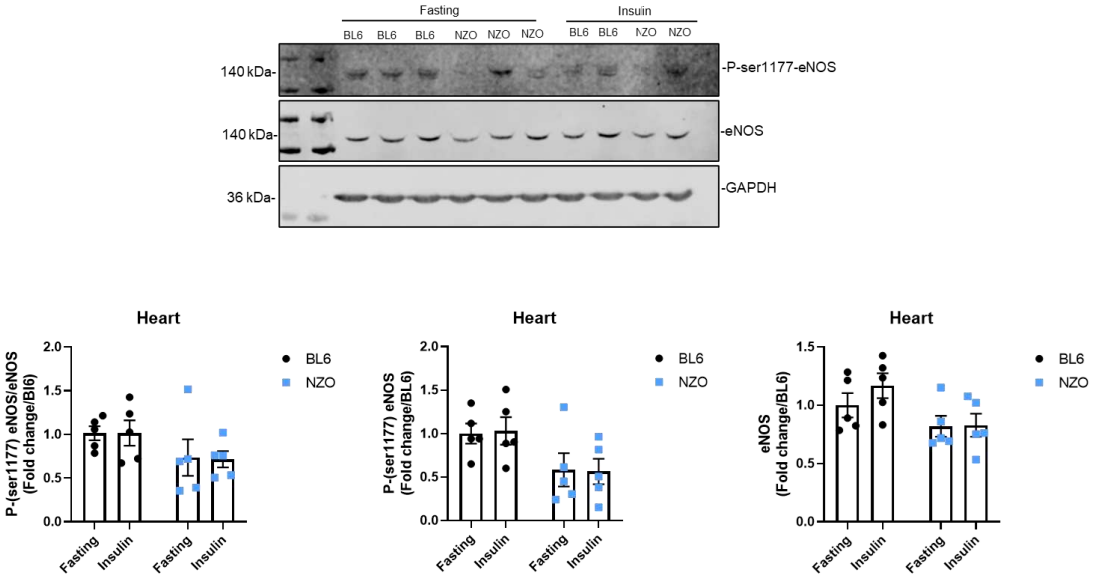

Fig. 27 Insulin does not affect eNOS levels in the heart

Western blot analysis of eNOS expression after insulin stimulation in the heart. A) Representative Western blot signal of eNOS levels. B) Ratio of p-ser1177-eNOS/eNOS. C) Levels of p-ser1177-eNOS in response to insulin. D) eNOS total protein amount. BL6 mice individuals' values are represented in black, and NZO mice individuals' values are represented in blue. BL6 and NZO n=5. Data are shown as fold change of BL6 (Fasting). Two-way ANOVA, Tukey's multiple comparison tests, data are shown as mean± SEM.

3.3 Pyk2 inhibition leads to a regain in endothelial function in NZO mice

To determine endothelial function *in vivo*, FMD was performed. According to the FMD premise, a healthy endothelium responds to increased fluid shear stress by enhancing NO production. Subsequently, NO dissipation induces the relaxation of the vascular smooth muscle layer, leading to vasodilation and intensifying tissue perfusion. This phenomenon is well demonstrated in the BL6 FMD curve (Fig. 28, black line), in which a preserved endothelial function resulted in vasodilation with around 20% increased vessel diameter (Max dilation BL6 19,59±1,76%) after vessel occlusion. However, the NZO mice demonstrated a lack of endothelial-dependent dilatory response after vessel occlusion (Max dilation NZO 4,05±0,73%;

Fig. 28, blue line) with reduced maximum dilution compared to BL6 mice (BL6 19,59±1,76% vs. NZO 4,05±0,73% p <0,0001).

Furthermore, to investigate the role of Pyk2 in regulating endothelial function in insulin resistance, we administrated a pharmacological Pyk2 inhibitor prior to the endothelial function assessment. Interestingly, the use of Pyk2 inhibitor resulted in the regaining of endothelial-dependent dilatory response in NZO mice, demonstrated as increased responsiveness to fluid shear stress during the FMD assessment (Fig. 28, red line) and increased maximal dilation (Max dilation NZO 4,05±0,73% vs. NZO+Pyk2-I 20,26±3,17% p= 0,0032) similar to the one observed in BL6 mice (BL6 19,59±1,76% vs. NZO+Pyk2-I 20,26±3,17% p=0,65). Nonetheless, Pyk2 inhibition did not affect the endothelial function of BL6 mice (Fig. 28 green line: BL6 19,59±1,76 vs. BL6+Pyk2-I 15,97±3,50 p=0,99).

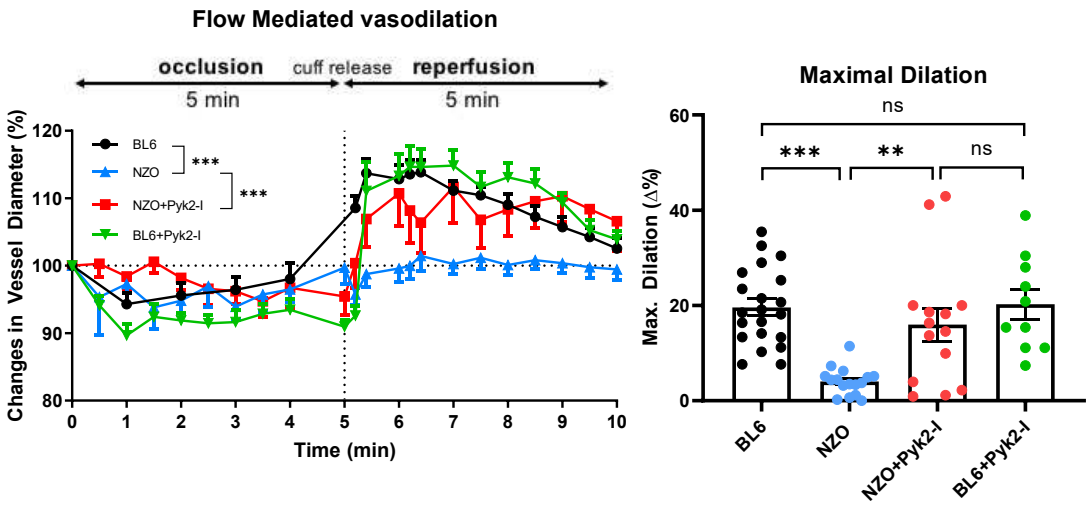

Fig. 28 Assessment of endothelial function *in vivo*

Endothelial function assessment by Flow-mediated vasodilation (FMD). Changes of iliac artery diameter during 5 minutes of ischemia following 5 minutes of reperfusion (Left). Maximal dilation response after cuff release (reperfusion phase) (right). One-way ANOVA, Tukey's multiple comparison tests, data are shown as mean± SEM. **p<0,01, *** p<0,0001, ns= no significant. BL6 n=21, BL6+Pyk2-I n=10, NZO n=16, NZO+Pyk2-I n=14.

3.4 Pyk2 inhibition normalizes NZO mice´s arterial blood pressure

To evaluate whether Pyk2 inhibition affects systemic hemodynamics in our mouse model, an invasive blood pressure assessment was performed. NZO mice show increased systolic blood pressure (BL6 91,8±3,3 vs. NZO 112,1±4,2 p=0,003) with a significant increase in mean arterial blood pressure (BL6 75,4±3,3 vs. NZO 88,8±1,8 p=0,006), and total peripheral resistance (BL6 3,1±0,2 vs. NZO 4,2±0,2 p=0,0026) (Fig. 29) compared to BL6 mice. Furthermore, Pyk2 inhibitor administration resulted in a significant decrease in systolic blood pressure (BL6 91,8±3,3 vs. NZO+Pyk2-I 92,0±3,8 p=0,99; NZO 112,1±4,2 vs. NZO+Pyk2-I 92,0±3,8 p=0,006), mean arterial pressure (BL6 75,4±3,3 vs. NZO+Pyk2-I 69,9±3,7 p=0,41; NZO 88,8±1,8 vs. NZO+Pk2-I 69,9±3,7 p=0,0006), and total peripheral resistance (BL6 3,1±0,2 vs. NZO+Pyk2-I 2,7±0,3 p=0,50; NZO 4,2±0,2 vs. NZO+Pk2-I 2,7±0,3 p=0,0004) in NZO mice.

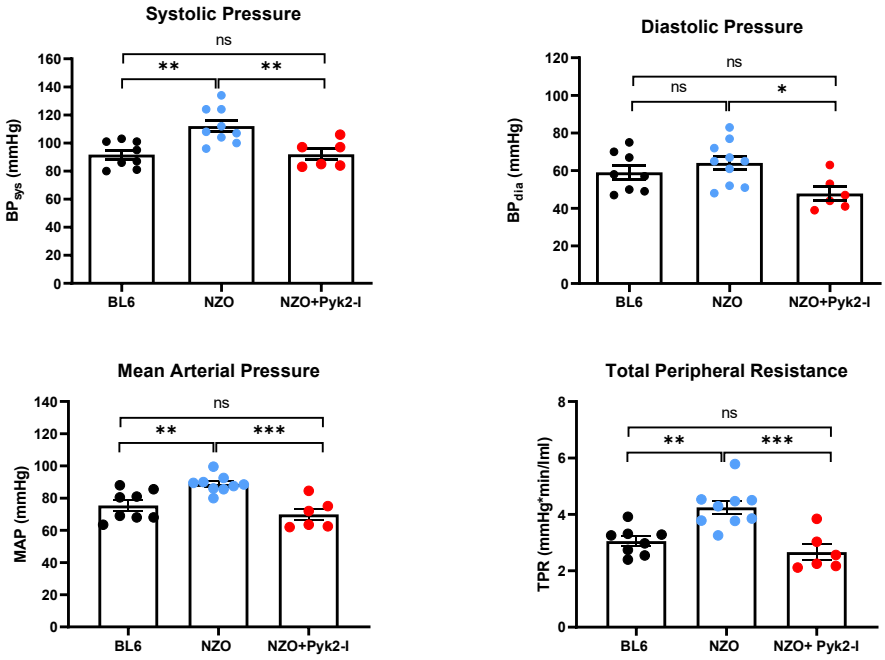

Fig. 29 Systemic hemodinamics

Systemic hemodynamics changes assessed by Millar catheter. A) Systolic blood pressure, B) diastolic blood pressure, C) Mean arterial blood pressure (MAP), D) total peripheral resistance

(TPR). One-way ANOVA, Tukey's multiple comparison tests, data are shown as mean± SEM. **p<0,01, *** p<0,0001, ns= no significant. BL6 n=8, NZO n=9-10 NZO+Pyk2-I n=6.

3.5 Pyk2 inhibition alleviates p-Tyr656-induced eNOS abrogation in NZO mice heart

This chapter investigates the mechanism by which hyperinsulinemia and insulin resistance affect Pyk2 expression and its capacity to regulate eNOS in cardiovascular tissues. As shown in Figure 30, although NZO mice showed a significantly lower total Pyk2 amount in the heart (BL6 vs. NZO p<0,001), NZO mice showed substantially higher Pyk2 activity than BL6 mice (Phospho-Pyk2/GAPDH: BL6 vs. NZO p=0,015 and Phospho-Pyk2/Pyk2 ratio- p=0,002).

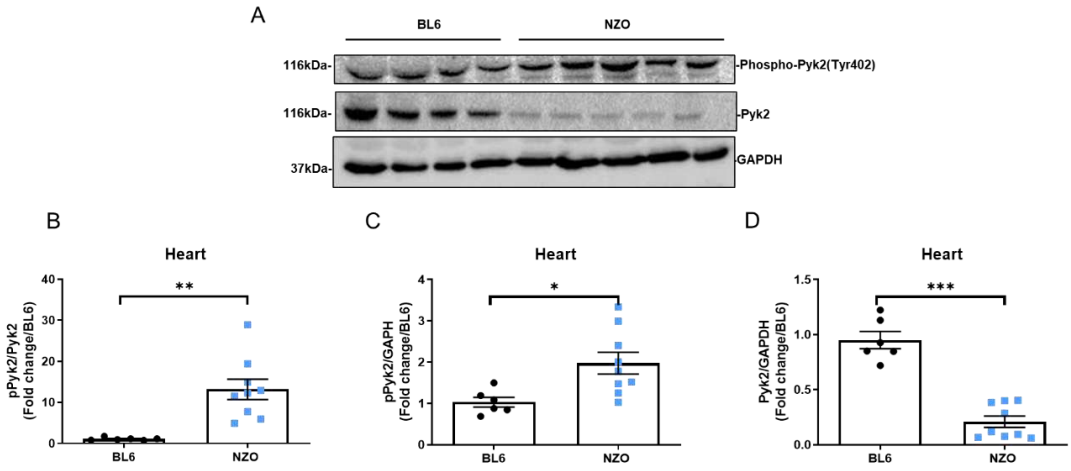

Fig. 30 Pyk2 expression and function in the heart

Western blot analysis of Pyk2 expression in the heart. A) Representative Western blot signal of Pyk2 levels. B) Ratio of p-(Tyr402) Pyk2/ Pyk2. C) Levels of p-(Tyr402) Pyk2. D) Pyk2 total protein amount. BL6 mice individuals' values are represented in black, and NZO mice individuals' values are represented in blue. BL6 n=6 and NZO n=9. Data are shown as fold change of BL6. Unpaired t-test data are shown as mean± SEM. *p<0,05, **p<0,01,*** p<0,0001, ns= no significant.

Furthermore, we investigated whether increased Pyk2 activity modulates eNOS activity in NZO mice. Therefore, we evaluated the levels of eNOS phosphorylated on its inhibitory side, Tyr656 (in mouse), and on its stimulatory site, ser1177, in the hearts of NZO mice. Interestingly, NZO mice showed higher levels of eNOS

phosphorylated on its inhibitory (tyr656) side when compared with BL6 mice (BL6 vs. NZO p=0,034) (Fig. 31). Importantly, the administration of the Pyk2 inhibitor reduced the levels of eNOS phosphorylation on Tyr656 on NZO mice hearts (NZO vs. NZO+Pyk2-I p=0,002) to a level comparable to BL6 mice (BL6 1,0±0,1 vs. NZO+Pyk2-I 0,9±0,1 p=0,78). Moreover, the Pyk2 inhibitor did not affect BL6 mice Phospho (tyr656) eNOS levels (Fig. 31).

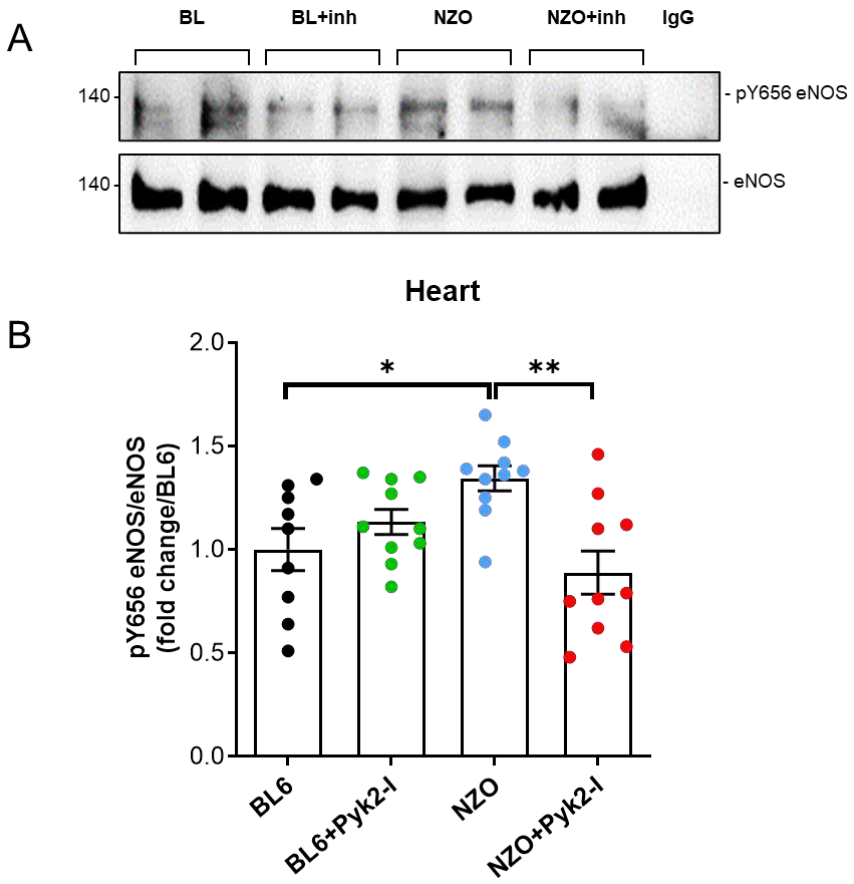

Fig. 31 Levels of eNOS phosphorylated on its inhibitory site

Immunoprecipitation of p-tyr656 eNOS in the heart. A) Representative Western blot signal of eNOS levels. B) Ratio of p-tyr656 eNOS/eNOS. BL6 n=9, BL6+Pyk2-I n=10, NZO n=10, NZO+ BL6+Pyk2-I n=10. Data are shown as fold change of BL6. One-way ANOVA, Tukey's multiple comparison tests, data are shown as mean± SEM. *p<0,05, **p<0,01.

In addition, we investigate whether eNOS stimulation, represented by p-ser1177, is preserved in NZO mice. NZO mice hearts showed a slightly reduced (17%) total eNOS amount (BL6 1,0±0,15 vs. NZO 0,83±0,07) and a significantly decreased eNOS phosphorylated in ser1177 (Fig.32, p-ser eNOS: BL6 vs. NZO p=0,026;p-ser eNOS/eNOS ratio: BL6 vs. NZO p=0,03) compared to BL6 mice.

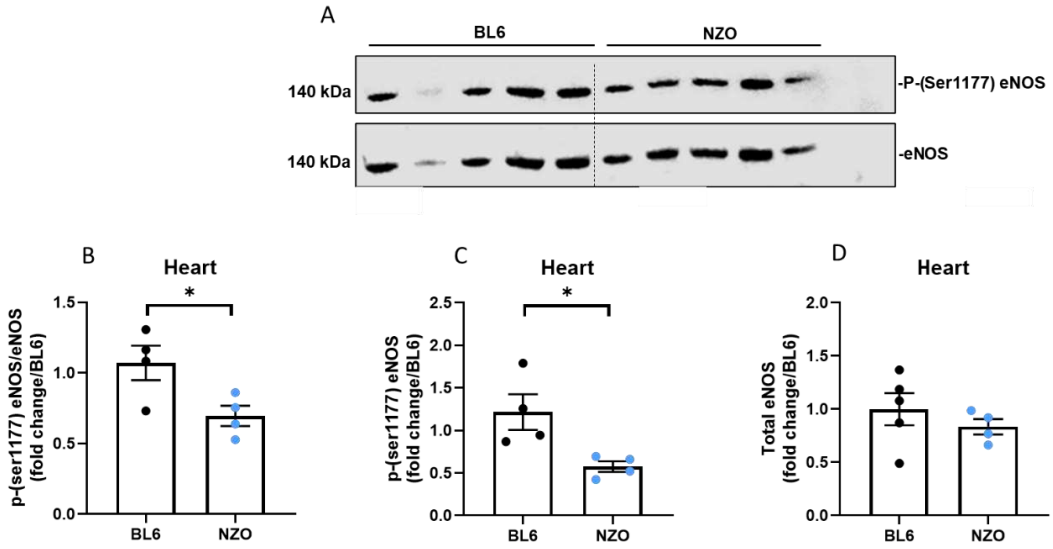

Fig. 32 Heart levels of eNOS phosphorylated on its stimulatory site

Western blot analysis of eNOS expression in the heart. A) Representative Western blot signal of eNOS levels. B) Ratio of p-(ser1177) eNOS/ eNOS. C) p-(ser1177) eNOS. D) eNOS total protein amount. BL6 mice individuals' values are represented in black, and NZO mice individuals' values are represented in blue. BL6 and NZO n=4. Data are shown as fold change of BL6. Unpaired t-test data are shown as mean± SEM. *p<0,05.

In addition, we investigate the circulating levels of the inert end products of NO metabolism nitrite (NO_2^-) and Nitrate (NO_3^-). Furthermore, we next investigate whether Pyk2 inhibition could alter the circulation of nitrite and nitrate levels in our mice models. As shown in Figure 33, although not significant, NZO mice showed reduced plasma nitrite levels compared to BL6 mice (BL6 214,2±19,9 nM vs. NZO 173,7±14,9 nM). Interestingly, the use of the Pyk2 inhibitor increased nitrite levels by around onefold in NZO mice compared to NZO mice (NZO 173,7±14,9 nM vs.

NZO+Pyk2-I 365,9±104,5 nM). Furthermore, plasma nitrate levels did not change regardless of Pyk2 inhibition between the groups.

Moreover, to investigate the potential of the rIPC maneuver as a protocol to increase NO output, we include a group that received the rIPC maneuver protocol. As demonstrated in Figure 33, the rIPC maneuver increased plasma levels in BL6 mice (BL6 214,2±19,9 nM vs. BL6+rIPC 352,6±35,3nM). However, rIPC did not change nitrite levels in NZO mice (NZO 173,7±14,9 nM vs. NZO+rIPC 120±45,3nM). Importantly, BL6+rIPC showed significantly higher plasma levels than the NZO+rIPC group (BL6+rIPC vs. NZO+rIPC p=0,039). However, the rIPC maneuver in combination with the Pyk2 inhibitor did not change plasma nitrite levels in NZO mice. Furthermore, plasma nitrate levels did not change regardless of Pyk2 inhibition and the rIPC maneuver between the groups.

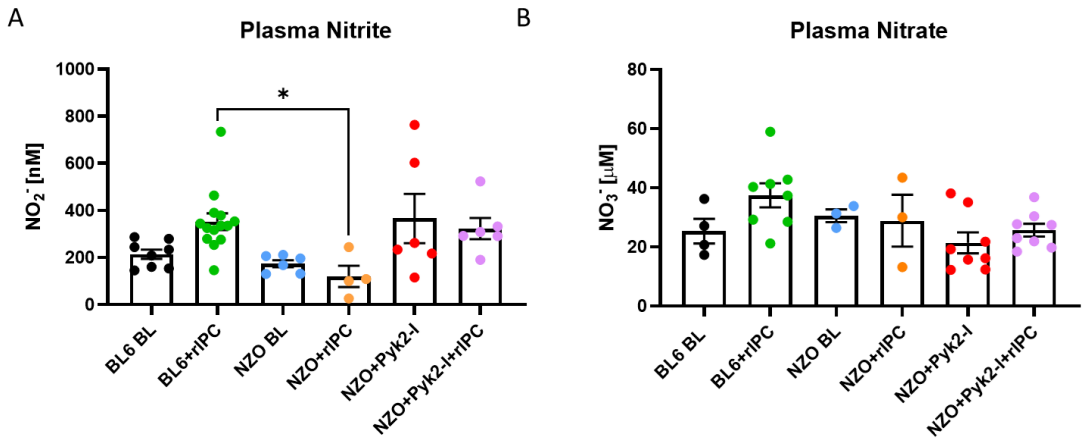

Fig. 33 Nitric oxide metabolites plasma levels

Circulating levels of NO metabolites. A) Nitrite Plasma levels quantified by CLD. B) Nitrate plasma levels quantified by ENO30.One-way ANOVA, Tukey's multiple comparison tests, data are shown as mean± SEM. *p<0,05. BL6 n=8, BL6+rIPC n=14, NZO n=6, NZO+rIPC n=4, NZO+Pyk2 n=6, NZO+Pyk2-I+rIPC n=6.

3.6 Pyk2 inhibition restores the loss of cardioprotection mediated by rIPC in NZO mice

As mentioned previously, cardiovascular diseases are the leading cause of death among diabetes patients. Therefore, investigating new therapies that alleviate detrimental cardiovascular outcomes in diabetic patients is crucial. Therefore, our next aim was to determine whether Pyk2 inhibition affects the heart responsiveness to the cardioprotective effects of rIPC.

Hence, when submitted to myocardial ischemia-reperfusion surgery, as shown in Figure 34, NZO mice demonstrated significantly larger infarct sizes compared to BL6 mice (BL6+IR 24,77±2,63% vs. NZO+IR 39,58±2,02%, p= 0,004). Furthermore, the administration of the Pyk2 inhibitor did not affect the infarct sizes in either of the groups (BL6+IR 24,77±2,63% vs. BL6+Pyk2-I 28,05±2,33%, p=0,77; NZO+IR 39,58±2,02% vs. NZO+Pyk2-I 40,82±4,84%, p=0,99). The area at risk was similar among the groups (BL6+IR 48,59±1,77%, NZO+IR 49,10±1,99%, BL6+Pyk2-I 44,67± 2,05%, NZO+Pyk2-I 55,35±2,48%). However, the group NZO+Pyk2-I exhibited a larger area at risk (55,35±2,48%) compared to the group BL6+Pyk2-I (44,67± 2,05%) (BL6+Pyk2-I vs NZO+Pyk2-I p=0,043). In addition, the cardiac function assessment before post-myocardial ischemia-reperfusion surgery demonstrated a reduction of ejection fraction in NZO and BL6 mice regardless of Pyk2 inhibition (Table 3). BL6 mice presented a significant decrease in EF (BL6 vs. BL6 post-IR p= 0.0422) and SVI (BL6 vs. BL6 post-IR p= 0.0131), followed by increased ESVI (BL6 vs. BL6 post-IR p= 0.0302) 24h after infarct. NZO mice showed a significant reduction of EF (NZO vs. NZO post-IR p= 0.0007), SVI (NZO vs. NZO post-IR p= 0.0002), and COI (NZO vs. NZO post-IR p= 0.0022) and increased in ESVI (NZO vs. NZO post-IR p= 0.0369).

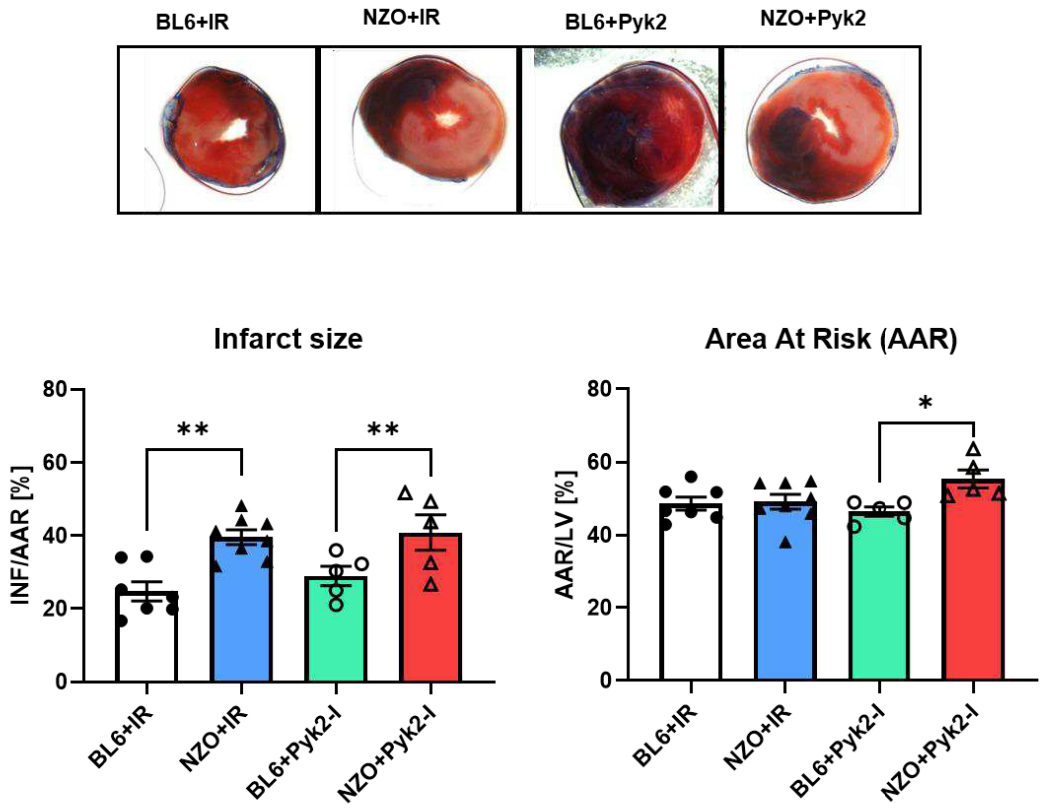

Fig. 34 NZO mice exhibit larger myocardial infarct sizes

Myocardial ischemia-reperfusion injury (30 min/24h). A) Representative infarct area picture performed by TTC staining technique (infarct area represented by the faded area). B) Infarct sizes (IS) are shown as the percentage of the area at risk (AAT). C) AAT is shown as the percentage of the left ventricle (LV). One-way ANOVA, Tukey's multiple comparison tests, data are shown as mean± SEM. *p<0,05, **p<0,01.N=6-8.

Table 3 Echocardiography of mice subjected to myocardial ischemia-reperfusion surgery (± Pyk2 inhibition)

BL6	**IR (n=7)**			**Pyk2-I (n=6)**		
Parameters	Baseline	Post AMI	p-value	Baseline	Post AMI	p-value
HR(bpm)	407 ± 25	463 ± 51	0.0943	432 ± 47	445 ± 56	0.5917
EF (%)	52.7 ± 7.16	37.8 ± 8.09	**0.0422**	51.4 ± 7.28	39.3 ± 4.59	**0.0368**
ESVI (µL/cm²)	1.36 ± 0.13	1.65 ± 0.26	**0.0302**	1.31 ± 0.25	1.49 ± 0.23	0.1129
EDVI (µL/cm²)	2.89 ± 0.24	2.58 ± 0.39	0.2318	2.59 ± 0.24	2.8 ± 0.32	0.0581
SVI (µl/cm²)	1.64 ± 0.31	1.13 ± 0.17	**0.0131**	1.28 ± 0.41	1.11 ± 0.33	0.0631
COI (mL/min/cm²)	0.62 ± 0.12	0.53 ± 0.22	0.0593	0.58 ± 0.08	0.63 ± 0.08	0.2903
NZO	**IR (n=8)**			**Pyk2-I (n=8)**		
Parameters	Baseline	Post AMI	p-value	Baseline	Post AMI	p-value
HR(bpm)	474 ± 31	480 ± 69	0.1746	459 ± 41	475 ± 35	0.4778
EF (%)	52.3 ± 8.2	34.3 ± 8.8	**0.0007**	51.4 ± 8.2	42.2 ± 11.6	**0.0244**
ESVI (µL/cm²)	1.31 ± 0.27	1.75 ± 0.52	**0.0369**	1.26 ± 0.29	1.24 ± 0.14	0.5616
EDVI (µL/cm²)	2.75 ± 0.35	2.63 ± 0.53	0.4042	2.42 ± 0.29	2.08 ± 0.15	**0.0332**
SVI (µl/cm²)	1.54 ± 0.31	0.88 ± 0.18	**0.0002**	1.57 ± 0.12	0.91 ± 0.20	**0.0092**
COI (mL/min/cm²)	0.64 ± 0.17	0.44 ± 0.11	**0.0022**	0.64 ± 0.09	0.63 ± 0.15	0.9098

Ischemia-reperfusion (IR), Pyk2 inhibition (Pyk2-I), heart rate (HR), ejection fraction (EF), end-systolic volume index (ESVI), end-diastolic volume index (EDVI), stroke volume index (SVI), cardiac output index (COI). Pared t-test. Data shown as mean ± standard deviation, p-value ≤0,05 is marked in **bold**.

Moreover, as demonstrated in Figure 35, the rIPC maneuver significantly reduced infarct sizes in BL6 mice (BL6+IR 24,77±2,63% vs. BL6+rIPC 11,40±0,55%, p= 0,0002), whereas rIPC maneuver failed to reduce infarct sizes in NZO mice (NZO+IR 39,58±2,02% vs. NZO+rIPC 36,04±4,98%, p= 0,74). Notably, the use of exogenous nitrite significantly reduced infarct sizes in BL6 (BL6+IR 24,77±2,63% vs. BL6+Nitrite 14,69±1,30%,p= 0,0023) and NZO (NZO+IR 39,58±2,02% vs. NZO+Nitrite 21,95±2,64%,p=0,017) mice. The area at risk was not different among the groups (BL6+IR 48,59±1,77%, BL6+rIPC 48,89 ±2,09%, BL6 nitrite 52,82± 3,16%, NZO+IR 49,10±1,99%, NZO+ rIPC 47,08±2,76%, NZO Nitrite 48,08±2,73%, NZO+Pyk2-I 55,35±2,48%, NZO+PYK2-I+rIPC 52,70±1,85%, NZO+Nitrite+Pyk2-I 43,99±1,65%).

Interestingly, Pyk2 inhibition in combination with rIPC maneuver significantly decreased infarct sizes in NZO mice (NZO+PYK2-I 40,82±4,84% vs. NZO+PYK2-I+rIPC 21,50±3,34%,p= 0,0037, Fig.36). Similarly, the use of Pyk2 in combination with nitrite also reduced infarct sizes in NZO mice (NZO+PYK2-I 40,82±4,84% vs.

NZO+Nitrite+Pyk2-I 24,58±2,07%,p= 0,0161, Fig.36). This similar effect in limit infarct sizes between rIPC maneuver and nitrite was observed in BL6 (BL6+rIPC 11,40±0,55% vs. BL6+Nitrite 14,69±1,30%,p=0,43) and NZO (NZO+PYK2-I+rIPC 21,50±3,34% vs. NZO+Nitrite+Pyk2-I 24,58±2,07%, p=0,79) mice. As demonstrated in Table 4, rIPC maneuver and nitrite preserved cardiac function in BL6 mice after ischemic insult. Interestingly, rIPC failed to preserve cardiac function in NZO mice, whereas rIPC combined with Pyk2 inhibition preserved the cardiac function in NZO mice similarly to nitrite.

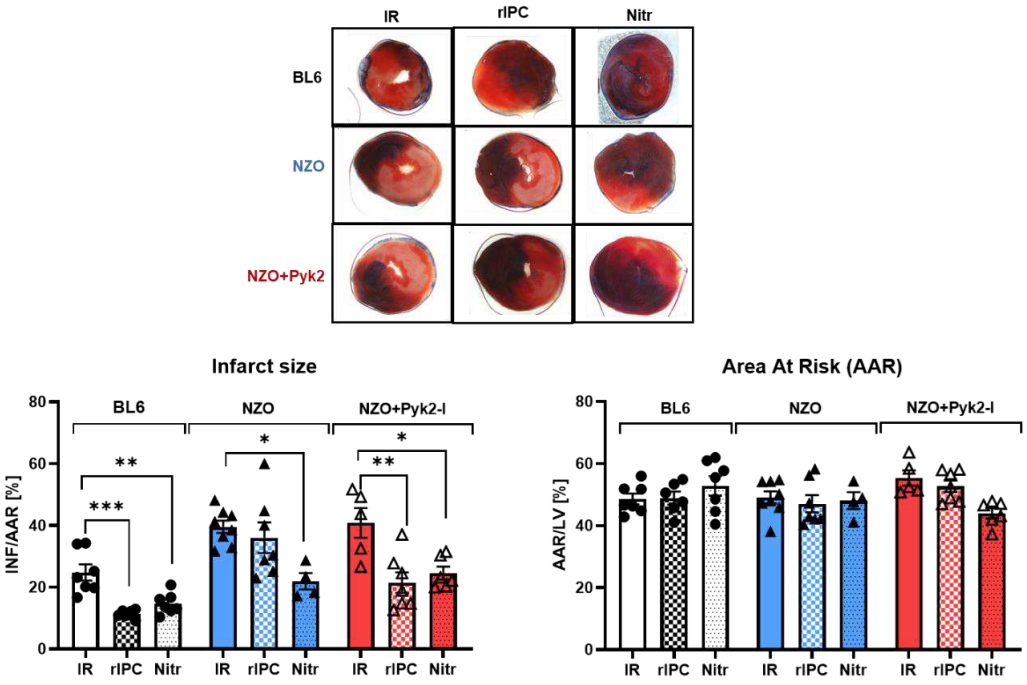

Fig. 35 Pyk2 inhibition restoures rIPC-mediated cardioprotection in NZO mice

Myocardial ischemia-reperfusion injury (30 min/24h). A) Representative infarct area picture performed by TTC staining technic (infarct area represented by the faded area). B) Infarct sizes (IS) are shown as the percentage of the area at risk (AAT). C) AAT are shown as the percentage of the left ventricle (LV). One-way ANOVA, Tukey's multiple comparison tests, data are shown as mean± SEM. *p<0,05, **p<0,01,*** p<0,0001.N=4-8.

Table 4 Echocardiography of mice subjected to myocardial ischemia-reperfusion (rIPC and nitrite groups)

BL6	**rIPC (n=6)**			**Nitrite (n=7)**		
Parameters	Baseline	Post AMI	p-value	Baseline	Post AMI	p-value
HR(bpm)	449 ± 30	493 ± 48	0.1098	433 ± 65	509 ± 47	0.0756
EF (%)	51.5 ± 10.5	46.9 ± 10.3	0.1823	53.6 ± 3.84	50.4 ± 6.29	0.0688
ESVI (µL/cm²)	1.62 ± 0.84	2.42 ± 0.64	0.1034	1.76 ± 0.5	1.47 ± 0.44	0.1798
EDVI (µL/cm²)	3.23 ± 0.94	3.82 ± 0.79	0.1199	3.08 ± 0.72	3.11 ± 0.86	0.8657
SVI (µl/cm²)	1.61 ± 0.49	1.40 ± 0.43	0.3656	1.32 ± 0.23	1.64 ± 0.53	0.1094
COI (mL/min/cm²)	0.72 ± 0.23	0.69 ± 0.23	0.7949	0.57 ± 0.11	0.84 ± 0.31	0.0904
NZO	**rIPC (n=6)**			**Nitrite (n=5)**		
Parameters	Baseline	Post AMI	p-value	Baseline	Post AMI	p-value
HR(bpm)	428 ± 44	455 ± 51	0.055	454 ± 27	442 ± 34	0.4976
EF (%)	51.1 ± 7.8	30.7 ± 11.7	**0.0176**	51.9 ± 12.3	50 ± 11.6	0.1622
ESVI (µL/cm²)	1.29 ± 0.34	1.91 ± 0.63	**0.0396**	1.12 ± 0.41	1.06 ± 0.31	0.3033
EDVI (µL/cm²)	2.64 ± 0.63	2.7 ± 0.58	0.4336	2.42 ± 0.39	2.19 ± 0.25	0.1025
SVI (µl/cm²)	1.35 ± 0.44	0.8 ± 0.2	**0.0482**	1.29 ± 0.33	1.13 ± 0.25	0.1027
COI (mL/min/cm²)	0.52 ± 0.16	0.37 ± 0.11	0.093	0.6 ± 0.12	0.59 ± 0.13	0.4007
NZO+Pyk2-I	**rIPC (n=7)**			**Nitrite (n=6)**		
Parameters	Baseline	Post AMI	p-value	Baseline	Post AMI	p-value
HR(bpm)	456 ± 27	440 ± 49	0.4036	411 ± 72	478 ± 28	0.0735
EF (%)	53.9 ± 12.8	54.6 ± 11.1	0.9165	58.4 ± 11.4	52 ± 9.1	**0.0152**
ESVI (µL/cm²)	1.11 ± 0.41	0.88 ± 0.21	0.3383	0.73 ± 0.26	0.73 ± 0.19	0.9743
EDVI (µL/cm²)	2.38 ± 0.37	1.98 ± 0.34	0.1474	1.79 ± 0.26	1.53 ± 0.26	0.2123
SVI (µl/cm²)	1.37 ± 0.31	1.1 ± 0.35	0.327	1.36 ± 0.32	1.18 ± 0.19	0.1296
COI (mL/min/cm²)	0.58 ± 0.14	0.48 ± 0.16	0.2222	0.43 ± 0.11	0.39 ± 0.08	0.3062

Remote ischemic preconditioning (rIPC), Pyk2 inhibition (Pyk2-I), heart rate (HR), ejection fraction (EF), end-systolic volume index (ESVI), end-diastolic volume index (EDVI), stroke volume index (SVI), cardiac output index (COI). Pared t-test. Data shown as mean ± standard deviation, p-value ≤0,05 is marked in **bold**.

Furthermore, we investigated whether the mechanism in which Pyk2 inhibition leads to improved cardioprotection following rIPC occurs in an eNOS-dependent manner. Therefore, we repeated the myocardial ischemia-reperfusion groups that presented reduced infarct sizes and added a NO scavenger (CPTIO). As demonstrated in Figure 36, the use of CPTIO increased the infarct sizes in BL6 that received rIPC maneuver and nitrite (BL6+rIPC 11,40±0,55% vs. BL6+CPTIO+rIPC 31,05±1,83%, p<0,0001; BL6+Nitrite 14,69±1,30% vs. BL6+CPTIO+Nitrite 33,69±1,61%, p<0,0001), demonstrating the potential role of NO in reducing infarct sizes in these groups. Furthermore, the use of nitrite also increased the infarct sizes and NZO that received nitrite and the NZO that received Pyk2 inhibitor and

rIPC(NZO+Nitrite 21,95±2,64% vs. NZO+Nitrit+CPTIO 43,65±3,16%,p= 0,0014; NZO+PYK2-I+rIPC 21,50±3,34% vs. NZO+Pyk2-I+CPTIO+rIPC 40,48±2,22%,p= 0,0014). In addition, the AAR was not significantly different between the groups (BL6+rIPC 48,89±2,09%, BL6+CPTIO+rIPC 46,02±0,91%, BL6 nitrite 52,82± 3,16%, BL6+CPTIO+Nitrite 49,28 ±2,21%, NZO Nitrite 48,08±2,73%, NZO+Nitrite+CPTIO 49,43±2,06%, NZO+PYK2-I+rIPC 52,70±1,85%, NZO+Pyk2-I+CPTIO+rIPC 46,36±2,63%). Importantly, all effects of rIPC and nitrite in maintaining cardiac function post-IR were abrogated in the groups that received CPTIO (Table 5).

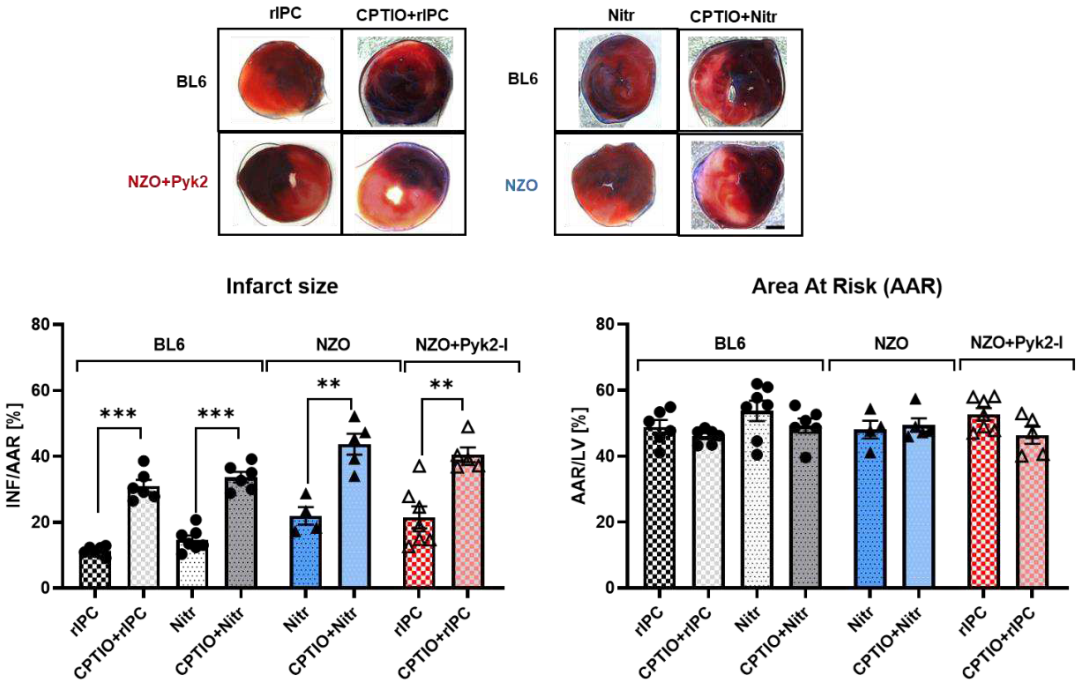

Fig. 36 CPTIO abolishes rIPC and nitrite reduction of infarct sizes

Myocardial ischemia-reperfusion injury (30 min/24h). A) Representative infarct area picture performed by TTC staining technique (infarct area represented by the faded area). B) Infarct sizes (IS) are shown as the percentage of the area at risk (AAT). C) AAT are shown as the percentage of the left ventricle (LV). One-way ANOVA, Tukey's multiple comparison tests, data are shown as mean± SEM. **p<0,01,*** p<0,0001.N=4-8.

Table 5 Echocardiography of mice subjected to myocardial ischemia-reperfusion (CPTIO groups)

BL6	**rIPC+CPTIO (n=6)**			**Nitrite+CPTIO (n=6)**		
Parameters	Baseline	Post AMI	p-value	Baseline	Post AMI	p-value
HR(bpm)	448 ± 49	476 ± 38	0.7298	439 ± 47	461 ± 55	0.6014
EF (%)	51.8 ± 6.12	41.5 ± 3.1	**0.005**	51.5 ± 5.67	41.3 ± 4.56	**0.0346**
ESVI (µL/cm²)	1.41 ± 0.3	1.54 ± 0.3	0.2727	1.68 ± 0.41	1.76 ± 0.36	0.5095
EDVI (µL/cm²)	2.8 ± 0.25	2.46 ± 0.42	**0.0367**	2.95 ± 0.54	2.59 ± 0.58	0.1364
SVI (µl/cm²)	1.4 ± 0.23	0.93 ± 0.23	**0.0039**	1.27 ± 0.39	0.83 ± 0.27	0.0643
COI (mL/min/cm²)	0.73 ± 0.09	0.6 ± 0.13	**0.008**	0.58 ± 0.2	0.63 ± 0.2	0.6027
NZO	**Nitrite+CPTIO (n=5)**			**Pyk2+rIPC+CPTIO (n=5)**		
Parameters	Baseline	Post AMI	p-value	Baseline	Post AMI	p-value
HR(bpm)	434 ± 46	442 ± 51	0.7704	415 ± 54	449 ± 51	0.0577
EF (%)	49.4 ± 9.04	38.3 ± 6.48	**0.0264**	51.8 ± 5.69	38.2 ± 3.13	**0.0148**
ESVI (µL/cm²)	1.36 ± 0.17	1.61 ± 0.14	0.1151	1.06 ± 0.44	1.15 ± 0.18	0.8737
EDVI (µL/cm²)	2.41 ± 0.14	2.29 ± 0.15	0.2551	1.88 ± 0.4	2.11 ± 0.29	0.8026
SVI (µl/cm²)	1.05 ± 0.17	0.68 ± 0.11	**0.0109**	1.22 ± 0.13	0.85 ± 0.18	0.0535
COI (mL/min/cm²)	0.6 ± 0.14	0.45 ± 0.1	**0.0078**	0.64 ± 0.84	0.42 ± 0.04	0.4223

Remote ischemic preconditioning (rIPC), Pyk2 inhibition (Pyk2-I), nitric oxide scavenger (CPTIO), heart rate (HR), ejection fraction (EF), end-systolic volume index (ESVI), end-diastolic volume index (EDVI), stroke volume index (SVI), cardiac output index (COI). Pared t-test. Data shown as mean ± standard deviation, p-value ≤0,05 is marked in **bold.**

Additionally, to evaluate whether the protective effect of rIPC on myocardial ischemia-reperfusion injury also involves neural activation, we repeated the rIPC groups with mice that had a transection of the femoral nerve. The transection of the femoral nerve diminished the efficiency of rIPC-induced reduction of infarct sizes in BL6 mice (BL6+IR 24,77±2,63% vs. BL6+rIPC 11,40±0,55%, p= 0,0002; BL6+IR 24,77±2,63% vs. BL6+rIPC+F.nerve 17,56±2,18%, p=0,06). In the rIPC groups, the transection of the femoral nerve alone was responsible for an increased 6% of the infarct sizes in BL6 mice (BL6+rIPC 11,40±0,55% vs. BL6+rIPC+F.nerve 17,56±2,18%). Importantly, this effect was also observed in NZO mice that received Pyk2 inhibitor (NZO+PYK2-I+rIPC 21,50±3,34% vs. NZO+Pyk+rIPC+F.nerve 26,26±2,80%, p=0,06; Fig.37) but not in native NZO mice (NZO+rIPC 36,04±4,98% vs. NZO+rIPC+F.nerve 39,14±2,77%, p=0,82). The AAR was similar among the groups (BL6+IR 48,59±1,77%, BL6+rIPC 48,89±2,09%, BL6+rIPC+F.nerve 47,05±2,91%, NZO+IR49,10±1,99%, NZO+ rIPC 47,08±2,76%, NZO+rIPC+F.

nerve 45,46±1,67%, NZO+Pyk2-I 55,35±2,48%, NZO+PYK2-I+rIPC 52,70±1,85%, NZO+Pyk+rIPC+ F.nerve 47,36±2,39%; Fig.37).

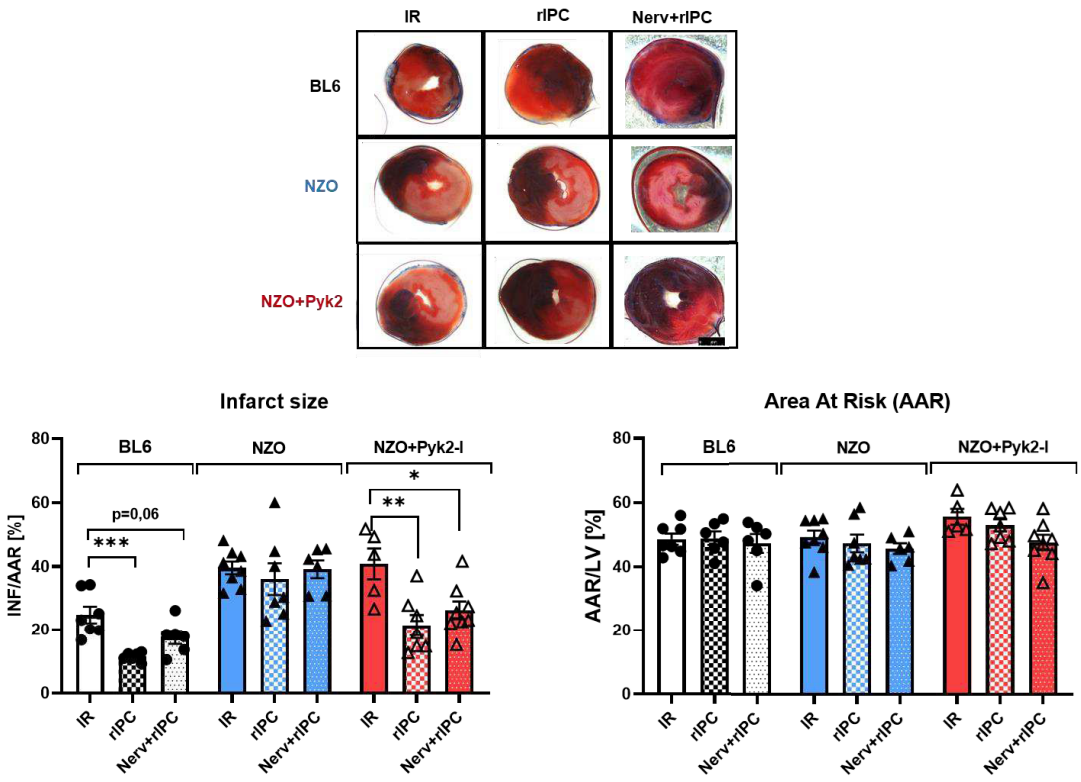

Fig. 37 Neural signaling does not play a role in rIPC-induced cardioprotection

Myocardial ischemia-reperfusion injury (30 min/24h). A) Representative infarct area picture performed by TTC staining technique (infarct area represented by the faded area). B) Infarct sizes (IS) are shown as the percentage of the area at risk (AAT). C) AAT are shown as the percentage of the left ventricle (LV). One-way ANOVA, Tukey's multiple comparison tests, data are shown as mean± SEM. *p<0,05, **p<0,01,*** p<0,0001.N=6-8.

Next, to investigate whether proteins involved in the RISK/ MAPK signaling pathways play a role in the rIPC-mediated cardioprotection in our mice, we performed ischemia-reperfusion protocols with the presence of U0126, an inhibitor of MAPK signaling. The use of U0126 prior to the surgery did not affect the infarct sizes of the BL6+IR and NZO+IR groups (BL6+IR 24,77±2,63% vs. BL6+U0126 28,88±2,97%,p=0,7; NZO+IR 39,58±2,02% vs. NZO+U0126 40,07±3,19%, p=0,99; NZO+Pyk2-I 40,82±4,84% vs. NZO+Pyk2+U0126 38,90 ±2,75%, p=0,97; Fig.38). However, the use of U0126 significantly increased the infarct sizes

of the groups that received rIPC maneuver (BL6+rIPC 11,40±0,55% vs. BL6+U0126+rIPC 25,62±3,37%, p=0,006; NZO+Pyk2-I+rIPC 21,50±3,34% vs. NZO + Pyk2+rIPC+U0126 38,72±3,31%,p=0,0098; Fig.38), suggesting that the ERK1/2 signaling pathway also participates in the mechanism in which rIPC mediates cardioprotection. All the AAR was similar between the groups (BL6+IR 48,59±1,77%, BL6+U0126 48,29±1,09%, BL6+rIPC 48,89 ±2,09%, BL6+ rIPC+U0126 47,61±1,69%, NZO+IR 49,10±1,99%, NZO+U0126 48,50±1,01%, NZO+ rIPC 47,08±2,76%, NZO+rIPC+U0126 48,35±1,66%, NZO+Pyk2-I 55,35±2,48%, NZO+Pyk2+U0126 46,03±1,56%, NZO+PYK2-I+rIPC 52,70±1,85%, NZO+ Pyk2+rIPC+U0126 47,94±1,01%). As illustrated in Table 6, the use of U0126 did not affect the cardiac function of BL6 and NZO mice. However, NZO mice that received Pyk2 inhibitor and U0126 presented impairment of cardiac function regardless of rIPC maneuver (EF: NZO+Pyk2+U0126 vs. NZO+Pyk2+U0126 post-IR p= 0.0024; NZO+Pyk2+U0126+rIPC vs. NZO+Pyk2+U0126+rIPC post-IR p= 0.0116).

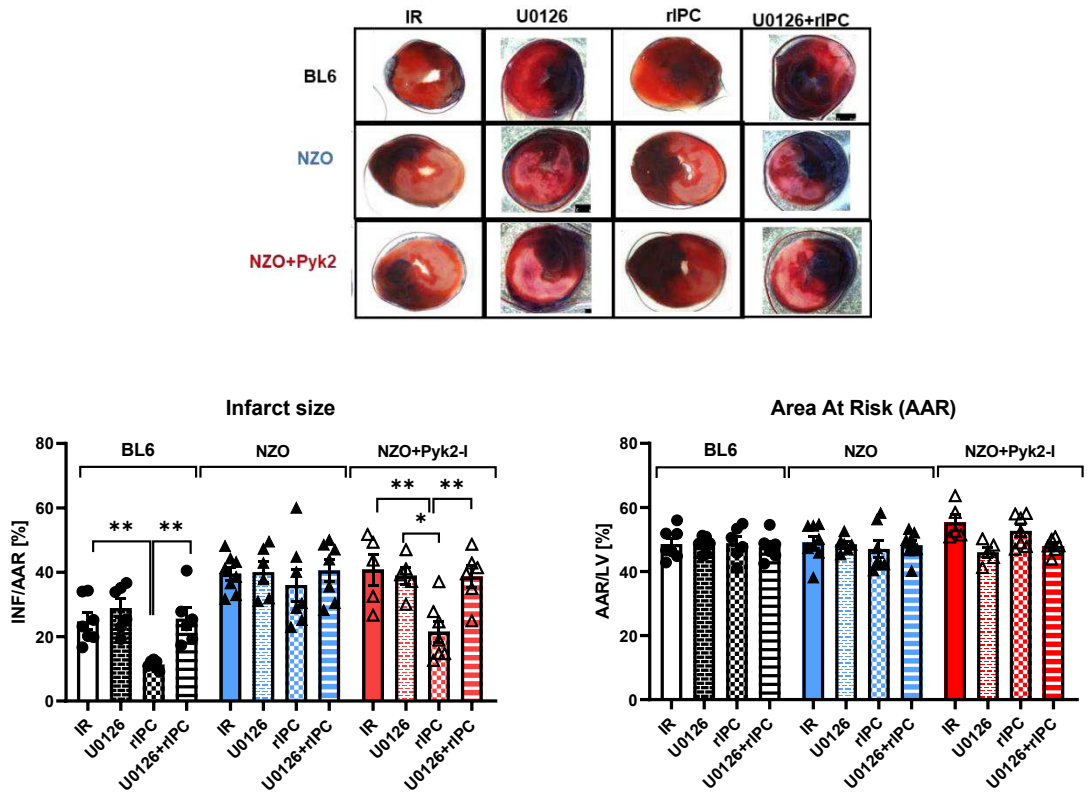

Fig. 38 Relevance of RISK signaling pathway for rIPC-induced cardioprotection

Myocardial ischemia-reperfusion injury (30 min/24h). A) Representative infarct area picture performed by TTC staining technique (infarct area represented by the faded area). B) Infarct sizes (IS) are shown as the percentage of the area at risk (AAT). C) AAT are shown as the percentage of the left ventricle (LV). One-way ANOVA, Tukey's multiple comparison tests, data are shown as mean± SEM. *p<0,05, **p<0,01,***.N=5-8.

Table 6 Echocardiography of mice subjected to myocardial ischemia-reperfusion (U0126 groups)

BL6	**U0126 (n=6)**			**U0126+rIPC (n=6)**		
Parameters	Baseline	Post AMI	p-value	Baseline	Post AMI	p-value
HR(bpm)	430±23	505±41	**0.0095**	450±19	479±45	0,073
EF (%)	43.59±6.2	46.25±8.1	0.4984	53.75±5.9	45.19±10	0,1398
ESVI (µL/cm²)	1.49±0.35	1.49±0.34	0,9924	1.27±0.47	1.51±0.29	0,2541
EDVI (µL/cm²)	2.64±0.37	2.8±0.59	0,6453	2.71±0.76	2.78±0.55	0,825
SVI (µl/cm²)	1.14±0.13	1.31±0.42	0,3358	1.44±0.31	1.27±0.47	0,4766
COI (mL/min/cm²)	0.29±0.05	0.66±0.20	0,0606	0.65±0.15	0.63±0.27	0,8414
NZO	**U0126 (n=5)**			**U0126+rIPC (n=5)**		
Parameters	Baseline	Post AMI	p-value	Baseline	Post AMI	p-value
HR(bpm)	433±60	434±100	0.9910	441±39	448±63	0,9663
EF (%)	44.6±8.44	38.43±7.01	0.3205	46.5±7.30	49.35±3.45	0,1538
ESVI (µL/cm²)	1.74±0.50	1.82±0.48	0.8129	1.30±0.32	1.33±0.18	0,5884
EDVI (µL/cm²)	3.11±0.56	2.93±0.53	0.5718	2.46±0.32	2.62±0.3	0,6293
SVI (µl/cm²)	1.38±0.21	1.12±0.17	0.0683	1.16±0.15	1.29±0.17	**0,0427**
COI (mL/min/cm²)	0.59±0.10	0.47±0.09	**0.0384**	0.51±0.07	0.59±0.16	0,2462
NZO+Pyk2-I	**U0126 (n=5)**			**U0126+rIPC (n=7)**		
Parameters	Baseline	Post AMI	p-value	Baseline	Post AMI	p-value
HR(bpm)	413±57.3	525±70	**0,0095**	451±48	430±58	0,0722
EF (%)	53±8.3	43.4±10.7	**0,0024**	45.13±3.74	36.42±5.2	**0,0116**
ESVI (µL/cm²)	1.38±0.64	1.57±0.7	0,4736	1.38±0.32	1.50±0.23	**0,0443**
EDVI (µL/cm²)	2.87±0.8	2.70±0.92	0,6754	2.53±0.56	2.39±0.47	0,4448
SVI (µl/cm²)	1.49±0,20	1.13±0.32	0,0662	1.15±0.26	0.88±0.26	**0,0324**
COI (mL/min/cm²)	0.62±0.12	0.59±0.17	0,692	0.53±0.17	0.38±0.17	**0,0127**

Remote ischemic preconditioning (rIPC), Pyk2 inhibition (Pyk2-I), Mitogen-activated protein kinase inhibitor (U0126), heart rate (HR), ejection fraction (EF), end-systolic volume index (ESVI), end-diastolic volume index (EDVI), stroke volume index (SVI), and cardiac output index (COI). Pared t-test. Data shown as mean ± standard deviation, p-value ≤0,05 is marked in **bold.**

4 Discussion

This study investigated the role of Pyk2-mediated regulation of eNOS and its consequences for endothelial function and endothelial-dependent remote cardioprotection in insulin resistance and hyperinsulinemia conditions. Pyk2-mediated eNOS negative regulation was hypothesized to be the key mechanism

involved in endothelial dysfunction and blunted rIPC-induced cardioprotection observed in insulin resistance. Therefore, the following aims were proposed to address this hypothesis: 1-Perform the cardiac and metabolic characterization of a murine model of insulin resistance and hyperinsulinemia exhibiting endothelial dysfunction. 2-Determine the effect of Pyk2-inhibition on endothelial function and systemic hemodynamics. 3-Investigate the role of Pyk2-induced eNOS regulation and function. 4-Analyze the role of Pyk2 and its inhibition on eNOS-dependent remote cardioprotection.

The main findings of this study (Fig. 39) are the following:

1-NZO mice showed systemic insulin resistance, glucose intolerance, hyperinsulinemia, hypertension, increased peripheral resistance, endothelial dysfunction, and preserved cardiac function.

2-Pyk2 inhibition effectively rescued endothelial-dependent dilatory response and normalized arterial blood pressure and peripheral resistance in diabetic NZO mice.

3-The mechanism involved in Pyk2-mediated eNOS regulation occurs due to increased tyr657 phosphorylation, which abolishes eNOS functionality and its capacity to produce NO properly. Pyk2 inhibition alleviates eNOS abrogation by reducing Pyk2-mediated tyr657 phosphorylation on eNOS, which restores NO bioavailability.

4-Pyk2 inhibition restores the cardioprotective effects of rIPC in NZO mice subjected to myocardial ischemia-reperfusion insult. The mechanism involved in this process occurs in a NO and MAPK/RISK pathway-dependent manner with minor participation of neural signaling.

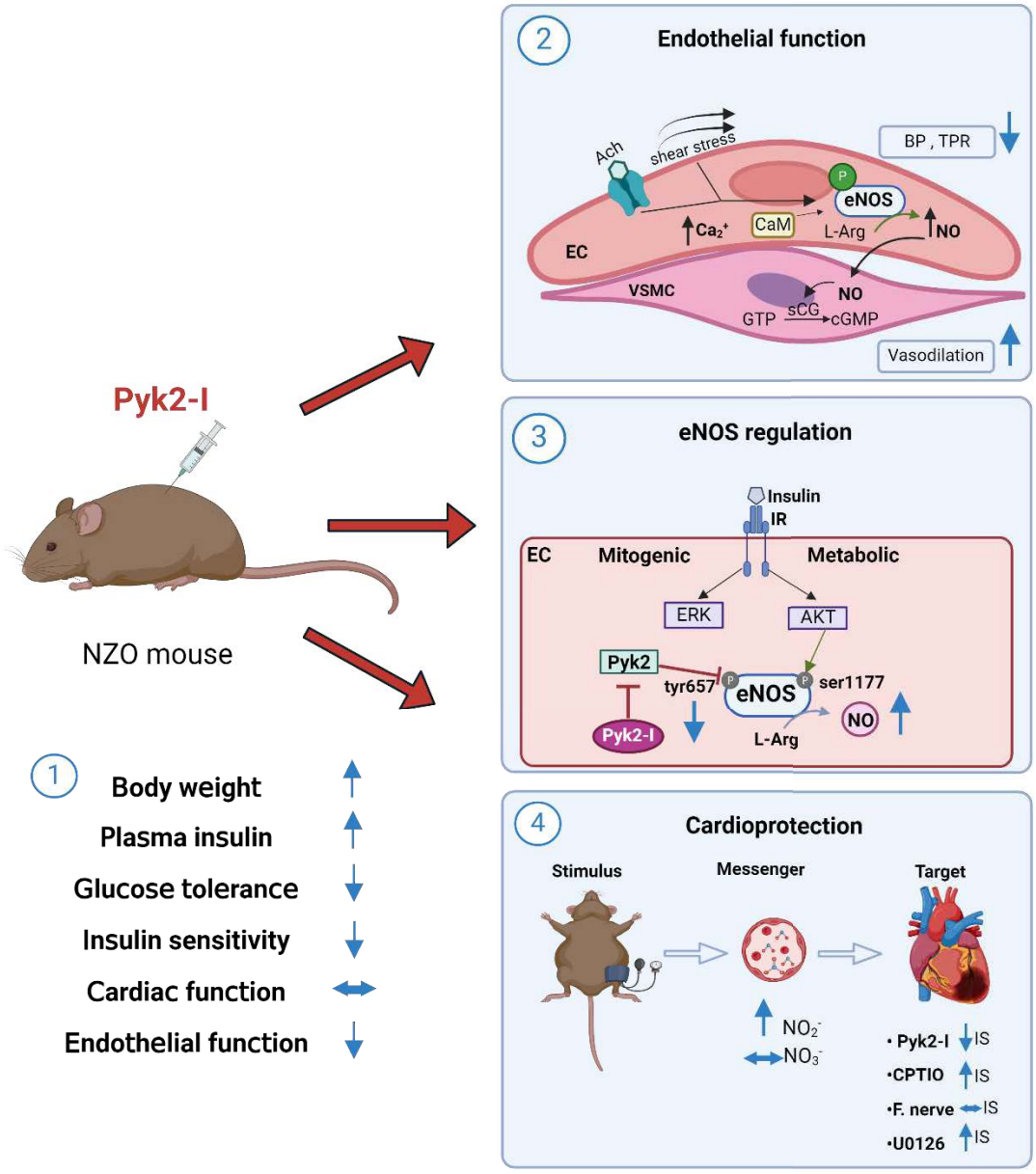

Fig. 39 Main findings of the research project

The main findings of the present study are: 1) NZO mice showed systemic insulin resistance, glucose intolerance, hyperinsulinemia, hypertension, increased peripheral resistance, endothelial dysfunction, and preserved cardiac function. 2) Pyk2 inhibition effectively rescued endothelial-dependent dilatory response and normalized arterial blood pressure and peripheral resistance in the NZO mice. 3)The mechanism involved in Pyk2-mediated eNOS regulation occurs due to increased tyr657 phosphorylation, which abolishes eNOS functionality and its capacity to produce NO properly. Pyk2 inhibition alleviates eNOS abrogation by reducing Pyk2-mediated tyr657 phosphorylation on eNOS, which restores NO bioavailability.4)Pyk2 inhibition restores the

cardioprotective effects of rIPC in NZO mice subjected to myocardial ischemia-reperfusion insult. The mechanism involved in this process occurs in a NO and MAPK/RISK pathway-dependent manner with minor participation of neural signaling. Endothelial cell (EC), vascular smooth muscle cells (VSMC), Blood pressure (BP), total peripheral resistance (TPR), Nitrite (NO_2-), nitrate (NO_3-), Infarct size (IS), 2-(4-carboxyphenyl)-4,4,5,5-tetramethylimidazoline-1-oxyl-3-oxide. (CPTIO), femoral nerve transection (F.nerve).Created by Amanda Brum with Biorender.

4.1 Cardiometabolic characterization of the NZO mice

Diabetes mellitus and insulin resistance are strongly associated with the development of endothelial dysfunction and increased cardiovascular risk. However, the underlying mechanism of this phenomenon remains unclear. Therefore, choosing a proper murine model that mimics the conditions observed in patients is crucial to investigating pathological mechanisms and uncovering potential therapeutic target molecules. Hence, we decided on the NZO mice as our murine model in this study.

The NZO mouse is an inbred strain, a well-known model for studying obesity, T2DM, insulin resistance, and metabolic syndrome (Crofford and Davis 1965, Ortlepp, Kluge et al. 2000, Altenhofen, Khuong et al. 2023). NZO mice develop polygenic obesity and glucose intolerance, and around 50% of the males develop T2DM. When fed with a standard chow diet, the onset of T2DM occurs approximately 16-20 weeks, whereas, on a high-fat diet, this process is accelerated by three weeks (Leiter, Reifsnyder et al. 1998, Haskell, Flurkey et al. 2002, Jürgens, Neschen et al. 2007). In addition, NZO mice also develop insulin resistance, hyperinsulinemia, dyslipidemia, and hypertension (Veroni, Proietto et al. 1991, Ortlepp, Kluge et al. 2000, Kluge, Scherneck et al. 2012). Furthermore, preliminary data from our working group demonstrated that NZO mice develop endothelial dysfunction in an age-dependent manner, with onset at 15 to 20 weeks of age (Data not shown).

In accordance with the literature (Ferreras, Kelada et al. 1994, Ortlepp, Kluge et al. 2000, Cho, Kim et al. 2007), our data indicated the NZO mice develop obesity, hypertension, hyperinsulinemia, hyperglycemia, impaired glucose tolerance,

systemic insulin resistance, and hypertension. In addition, the Western blot analysis indicates that although the skeletal muscle of the NZO mice remains sensitive to insulin, the heart of these mice exhibits signs of impairment of insulin-induced phosphorylation of AS160 and GSK3α/β. Furthermore, the NZO mice also presented a decreased expression of eNOS in the heart, which may affect the heart endothelial cells' ability to produce NO and participate in the maintenance of endothelial function in those mice.

Altogether, our metabolic and cardiac characterization confirms that the NZO mice exhibit systemic insulin resistance and hyperinsulinemia followed by impaired endothelial and preserved cardiac function. Thus, this data suggests that the NZO is a suitable mouse model for investigating the role of Pyk2 on eNOS regulation, endothelial function, and endothelial-dependent remote cardioprotection under insulin resistance and hyperinsulinemia conditions. This fact is essential to increase the possibility of future translation of our results into clinical practice.

4.2 Pyk2 inhibition restores endothelial function in NZO mice

Endothelial function is a marker of cardiovascular health, and its dysfunction has been shown to aggravate cardiovascular risk. Patients with T2DM and non-diabetics with insulin resistance develop endothelial dysfunction prior to cardiovascular events, indicating endothelial dysfunction as a hallmark of future cardiovascular complications (Takeda, Matoba et al. 2020). Therefore, improving endothelial function is key to alleviating cardiovascular risk and complications in those individuals.

The primary approach to determining endothelial function is assessing endothelial-dependent relaxation response to shear stress (FMD, *in vivo*) and acetylcholine (aortic rings or myograph, *ex vivo*). In those methods, a blunted relaxation response to those stimuli is considered endothelial dysfunction. The present study demonstrated, for the first time *in vivo*, the impairment of endothelial-dependent

vasorelaxation response to shear stress in NZO mice. These results align with experiments by Marchesi and colleagues (Marchesi, Ebrahimian et al. 2009), which showed that the NZO mice have endothelial dysfunction demonstrated as impaired endothelial-dependent relaxation response to acetylcholine. In addition, Marchesi's study also showed eNOS uncoupling, reduced NO output, and increased perivascular oxidative stress as the leading cause of NZO mice endothelial dysfunction.

Moreover, the lack of vasodilation observed in NZO mice during the FMD assessment was comparable to those observed in eNOS knockout (eNOS KO) mice and BL6 mice that received the NOS inhibitor, previously by our working group (Erkens, Kramer et al. 2015). This data determined that the dilatory response observed during the FMD occurs in an eNOS-dependent matter. This data suggests that the impairment in dilatory response observed in NZO mice occurs due to an impairment of eNOS activity/function that leads to a dysfunctional vessel response to fluid shear stress. Additionally, this data supports our hypothesis that the endothelial dysfunction observed in NZO mice occurs due to an abolishing of eNOS function, resulting in reduced eNOS-dependent vasodilation in those mice.

Interestingly, those data are consistent with the studies performed by Fisslthaler and Loot (Fisslthaler, Loot et al. 2008, Loot, Schreiber et al. 2009), which demonstrated that oxidative stress and insulin lead to endothelial dysfunction and reduced NO output. This mechanism occurs mainly due to Pyk2-mediated eNOS inhibition through tyr657 phosphorylation. Interestingly, our results support their observations, in which the inhibition of Pyk2 restored the endothelial-dependent relaxation response to shear stress and acetylcholine despite the insulin resistance hyperinsulinemic status of NZO mice (Erkens, Duse et al. 2023).

Several studies have shown that insulin-dependent vasodilation response occurs by AKT-mediated serine1177 phosphorylation on eNOS (Fisslthaler, Loot et al. 2008, Symons, McMillin et al. 2009, Heiss, Rodriguez-Mateos et al. 2015). Indeed, a recent study performed by Akther and colleagues demonstrated that UCD-T2DM

rats have impaired endothelial function caused mainly by reduced insulin-mediated AKT-eNOS phosphorylation (Akther, Razan et al. 2021). However, studies showed that insulin also mediates eNOS inhibition through Pyk2-mediated tyrosine 657 phosphorylation, which results in eNOS inhibition regardless of parallel eNOS stimulation (Viswambharan, Yuldasheva et al. 2017). Fisslthaler and colleagues have shown that Pyk2 mediates eNOS phosphorylation on tyr657(Human)/tyr656(mouse) within the FMN binding domain, which leads to a direct inhibitory effect resulting in impairment in the generation of NO, O_2^- or citrulline (Fisslthaler, Loot et al. 2008). This data was supported by Viswambharan et al. (2017), who have shown that the endothelial-specific over-sensibility to insulin leads to endothelial dysfunction due to eNOS abrogation mediated by Pyk2 overactivity followed by increased eNOS phosphorylation on tyr657 side (Viswambharan, Yuldasheva et al. 2017). Our data is in line with those previous studies, as we demonstrated that the NZO mice developed endothelial dysfunction mainly due to a reduction in eNOS activity as a result of an increased Pyk2 activity followed by higher phosphorylation of eNOS on its inhibitory site tyr656. Pyk2 inhibitor reduces eNOS inhibition by tyr656 phosphorylation and limits endothelial dysfunction caused by insulin resistance and hyperinsulinemia.

Additionally, this data was validated by our *ex vivo* findings, assessed by aortic rings. The aortas of NZO mice showed reduced endothelial-dependent relaxation responses to acetylcholine compared to BL6 mice. In line with the *in vivo* assessment, the use of Pyk2 inhibitor restores the dose-response sensibility to acetylcholine in NZO mice, demonstrated as a regain of vessel relaxation response to acetylcholine (Erkens, Duse et al. 2023). This data supports the *in vivo* assessment of endothelial function and determines an abrogation of eNOS-dependent vasodilation on NZO mice. Therefore, these results demonstrated that the NZO mice have endothelial dysfunction, characterized by a lack of responsiveness to eNOS-dependent dilatory stimuli such as fluid shear stress and acetylcholine. The use of Pyk2 inhibitor restores the endothelial function of these mice, suggesting Pyk2 as the primary negative regulator of eNOS activity in this

mouse model. Furthermore, this data supports our hypothesis that Pyk2 modulates eNOS-dependent vasodilation and endothelial function in insulin-resistance conditions.

Furthermore, this data is in line with previous studies in which the pharmacological Pyk2 inhibition or its gene knockdown improved endothelial function and eNOS activity by alleviating eNOS inhibition (Bibli, Zhou et al. 2017, Viswambharan, Yuldasheva et al. 2017). Additionally, Murphy et al. (2019) have shown that using FAK/Pyk2 inhibitor decreases vascular inflammation and limits macrophage infiltration in the vessel walls of a mouse model of atherosclerosis (Murphy, Jeong et al. 2019). Similarly, Zhang and colleagues (Zhang, Yang et al. 2021) recently showed that Pyk2 is overexpressed in the artery wall of atherosclerotic mice, and the inhibition of Pyk2 or the inhibition of mitochondrial calcium uniporter pathway reduces cell death, decreases oxidative stress, mitochondrial disruption and limit the development of atherosclerosis.

Collectively, our data indicate Pyk2 as the main responsible for eNOS regulation and the development of endothelial dysfunction in insulin resistance conditions. Furthermore, the inhibition of Pyk2 alleviates the deleterious impact of hyperinsulinemia/insulin resistance on endothelial function, implying the inhibition of this molecule as a promising therapeutic target.

4.2.1 Pyk2 Inhibition and Systemic Hemodynamics

Endothelial eNOS has been shown to regulate vascular tone, inflammation, cell adhesion, coagulation, and blood pressure. Furthermore, studies have demonstrated that the impairment of endothelial-dependent vasodilation and reduced NO output correlate to increased blood pressure (Dharmashankar and Widlansky 2010, Brandes 2014). Indeed, studies with eNOS KO mice demonstrated the relevance of endothelial eNOS and NO bioavailability for blood pressure regulation (Shesely, Maeda et al. 1996, Leo, Suvorava et al. 2021). These results reinforce our data, which shows that the NZO mice exhibit endothelial dysfunction followed by increased mean arterial blood pressure and total peripheral

resistance. This data corroborates the findings of Marchesi et al., which observed endothelial dysfunction and eNOS abrogation followed by high systolic blood pressure in NZO mice (Marchesi, Ebrahimian et al. 2009). Together, this data supports our hypothesis that impaired eNOS function is the key phenomenon involved in cardiovascular alterations in NZO mice.

Interestingly, the inhibition of Pyk2 alleviated the abrogation of eNOS and restored endothelial function, which in turn directly normalized arterial blood pressure and peripheral resistance in the NZO mice. These results indicate the importance of a functional eNOS for supporting and maintaining a healthy endothelium and overall cardiovascular system. Also, it highlights how the rescue of eNOS functionality can immensely cause positive effects on endothelial function, systemic hemodynamics, and cardiovascular health in diabetes-related conditions. Therefore, this data indicates that the administration of Pyk2 inhibitor alleviates hypertension well established in the NZO mice, decreasing the blood pressure to levels similar to those found in BL6 mice.

Collectively, we demonstrate that the NZO mouse presents insulin resistance with related hyperinsulinemia, preserved cardiac function, endothelial dysfunction, and hypertension. When given Pyk2 inhibition, these mice exhibit a significant improvement in endothelial function and arterial blood pressure, suggesting that Pyk2 has an essential role in modulating endothelium-dependent relaxation and regulating arterial blood pressure in insulin-resistance conditions.

4.3 Pyk2-inhibition restores rIPC-induced cardioprotection in NZO mice

4.3.1 Remote ischemia preconditioning mediating cardioprotection

Research has highlighted the importance of non-invasive strategies such as rIPC in reducing infarction sizes and protecting the myocardium against ischemic insult (Chai, Liu et al. 2014, Heinen, Behmenburg et al. 2018, Rossello, He et al. 2018). However, as demonstrated in this study, a functional endothelial is mandatory for

rIPC efficacy in decreasing myocardial infarct sizes. For instance, our BL6 mice results showed that the endothelial function is preserved under healthy conditions, and thereby, rIPC can reduce infarct sizes. Conversely, the rIPC maneuver fails to mediate cardioprotection in the endothelial dysfunction condition, as demonstrated in the NZO mice. These results corroborate recent studies that showed that comorbidities that impair endothelial function, such as diabetes (Chien, Wen et al. 2020), hyperglycemia (Feige, Roth et al. 2022), and aging (Heinen, Behmenburg et al. 2018) abolish the cardioprotective effect of rIPC. Interestingly, once the NZO mice regain their endothelial function, they also regain their endothelial capacity to participate in remote organ protection and, consequently, rIPC-mediated infarct size reduction. These results corroborate the studies of van den Munckhof and Seeger (van den Munckhof, Riksen et al. 2013, Seeger, Benda et al. 2016), which demonstrated that reduced flow-mediated vasorelaxation is associated with abrogated ischemic preconditioning efficacy and aggravated I/R injury, indicating that a healthy endothelial function is essential for ischemic preconditioning effectiveness in reducing infarct sizes. Moreover, Zhao and Xue demonstrated that rIPC, besides decreasing infarct sizes, also decreases inflammation, apoptosis, and tissue damage (Zhao, Xue et al. 2019).

Furthermore, regardless of the rIPC maneuver, NZO mice exhibited larger infarct sizes than BL6 mice. In addition, the larger infarct sizes in NZO mice were combined with a slight decrease in circulating nitrite levels. Importantly, using Pyk2 inhibitor in combination with the rIPC maneuver reduced infarct sizes and increased the circulating levels of nitrite in these mice. This data supports the previously described impairment of eNOS function in NZO mice and validates the relevance of endothelial-dependent NO release in rIPC-mediate cardioprotection. Furthermore, this data indicates nitrite as a circulatory messenger that participates in the organ protective effect of rIPC. The collective data is consistent with Rassaf and colegues (Rassaf, Totzeck et al. 2014), which showed that nitrite plasma levels are essential for rIPC-induced cardioprotection.

Additionally, this indication was validated by using exogenous nitrite or NO scavenging in our mouse models, implying that the cardioprotective effect of rIPC occurs in a NO-dependent manner. Interestingly, the rIPC maneuver and nitrite equally preserved the cardiac function following myocardial infarction, whereas using NO scavenger CPTIO abrogates these positive effects. This data highlights the relevance of NO for organ protection and functional recovery following myocardial infarction.

4.3.2 The mechanism involved in rIPC-mediated cardioprotection

Several studies have been investigating the potential humoral factors responsible to rIPC-mediate cardioprotection. Among the main circulatory messages proposed, NO metabolites, i.e., nitrite and nitrate, are among the most studied (Rassaf, Totzeck et al. 2014, Andreadou, Iliodromitis et al. 2015). The present study demonstrated that functional endothelial eNOS and adequate NO bioavailability are crucial for rIPC-induced cardioprotection in healthy and insulin resistance/hyperinsulinemia conditions.

For instance, our data have shown that the rIPC maneuver promotes cardioprotection in BL6 and NZO mice, granting that the latter regained endothelial function and eNOS functionality by Pyk2 inhibition. Similarly, using exogenous nitrite demonstrated the same positive effects in reducing infarct sizes, supporting the relevance of NO metabolites in promoting cardioprotection. Importantly, this cardioprotection effect was abolished in the presence of a NO scavenger, indicating that this cardioprotective effect occurs in a NO-dependent manner. Similarly, Abu-Amara and Yang et al. have shown (Abu-Amara, Yang et al. 2011) that eNOS KO mice have bigger infarct sizes and blunted rIPC-mediated cardioprotection than BL6 mice, indicating that eNOS is crucial for organ protection phenomenon. Furthermore, Kidd et al. (Kidd, Dobrucki et al. 2000) also demonstrated that the NO deficit is a determinant for the increase of cerebral infarct size. Indeed, studies have shown that NO can trigger several organ protection mechanisms, including direct regulation of protein modification by nitrosylation. This process has anti-

inflammatory and antioxidant effects, protecting protein residues against oxidation and I/R injury (Kohr, Sun et al. 2011, Heusch 2015). In line with these results, Bibli et al. (2017) recently showed that Pyk2 inhibition alleviated eNOS inhibition and enhanced NO disponibility, leading to decreased cardiac damage following ischemia and reperfusion injury in the heart of C57Bl/6 mice (Bibli, Zhou et al. 2017). In addition, the pharmacological inhibition of Pyk2 or its gene knockdown limited cell damage and increased NO output in a culture of cardiomyocytes.

In contrast, our data illustrate that besides Pyk2 inhibition restoring eNOS functionality, this effect on its own is not enough to induce cardioprotection in insulin resistance/hyperinsulinemia conditions. Therefore, this data indicates that physical stimuli such as rIPC maneuver or physical exercise are necessary to increase NO production and exceed the harmful effects of insulin resistance and hyperinsulinemia. Similar conclusions were drawn by Landman and colleagues (Landman, Uthman et al. 2022), who recently demonstrated that rIPC maneuvers and handgrip exercises could significantly decrease circulating proinflammatory biomarkers in patients with cerebral small vessel disease.

In addition, Rassaf and Totzeck (Rassaf, Totzeck et al. 2014) demonstrated the relevance of NO metabolites as a circulating messenger in rIPC-induced cardioprotection. In addition, these authors further show that this organ's protective effects are transferable by plasma transference between species. Furthermore, this conditioning signal transference was also successfully achieved by Feige and Roth et al. (Feige, Roth et al. 2022), demonstrating that the plasma of healthy individuals receiving rIPC significantly decreased the myocardial infarct sizes of Wistar rats. This data validates and illustrates the presence of circulatory factors that induce cardioprotection, supporting the humoral messenger theory and our results. In addition, Feige and colleagues also specified that this protective effect was abolished under hyperglycemic conditions. This data corroborates with studies that observed failure in rIPC mediating organ protection under insulin resistance and diabetic conditions (Chien, Wen et al. 2020). Furthermore, our results reinforce this

pattern, in which the cardioprotective response induced by the rIPC maneuver is abolished in insulin resistance conditions.

Moreover, research has suggested that neural signaling is also involved in rIPC-mediated cardioprotection. This mechanism involves afferent somatic nerves, sympathetic nerves in the periphery that stimulate the valgus nerves that induce organ protection (Yang, Shakil et al. 2019). Indeed, Redington and colleagues (Redington, Disenhouse et al. 2012) demonstrated that femoral nerve stimulation produces a similar release of circulatory cardioprotective factors as the rIPC maneuver. Furthermore, these authors identified that a neural connection in the limb is necessary for rIPC-mediated cardioprotection. Our data demonstrated that the femoral nerve transection slightly decreased the potency of rIPC-induced reduction of infarct sizes in BL6 mice but not in native NZO mice. This data suggests that humoral and neural signaling are involved in reducing infarct sizes under healthy conditions. However, rIPC-induced stimulation of cardioprotective signaling is abrogated under diabetic-related conditions. In addition, our results indicate that rIPC-mediated cardioprotection occurs mainly due to humoral signaling and with minor participation of neural signaling in NZO mice that received Pyk2 inhibition. This data suggests that in diabetes related conditions, there is abrogation in rIPC-mediated cardioprotection due to impairments in the humoral and neural signaling. Pyk2 inhibition restoures endothelial function and endothelial-dependent capacity to respond to rIPC stimulus regardless of neural signaling, supporting the existance of a humoral factor.

Furthermore, previous data from Lim et al. (Lim, Yellon et al. 2010) demonstrated that transection of the femoral nerve just partially limits the reduction of infarct sizes mediated by rIPC. Also, resectioning the femoral and sciatic nerve is necessary to completely abolish the cardioprotective effects of rIPC. On the other hand, Lim et al. also demonstrated that the occlusion of the femoral artery completely abolishes the cardioprotective effects of rIPC, indicating an essential humoral mechanism. This data corroborates with our data, indicating that although the humoral and

neuronal signaling pathways might be present in the mechanism of rIPC-mediated cardioprotection, humoral signaling is dominant in reducing infarct sizes.

Moreover, research has shown that the upregulation of proteins involved in cellular survival also participates in the mechanism of ischemic preconditioning-induced organ protection (Kalakech, Hibert et al. 2014, Wang, Zhang et al. 2016, Heusch 2017). This phenomenon's primary survival signaling pathways are the RISK and the SAVE signaling pathways. The proteins involved in the RISK pathway are PI3K, AKT, ERK, and GSK3β, whereas the proteins involved in the SAVE pathway consist of AKT, STAT3, and TNFα (Heusch 2017, Heinen, Behmenburg et al. 2018). These two signaling pathways act mainly in the modulation of mitochondrial function, reducing the opening of transitioning pores and promoting cell survival (Turrell, Thaitirarot et al. 2014).

In the present study, to determine the participation of the RISK signaling pathway in the rIPC-mediated cardioprotection mechanism, a MAPK inhibitor (U0126) was used. Our data indicate that rIPC-mediated cardioprotective effects were abolished after MAPK inhibition. Importantly, this effect was observed in all groups in which rIPC mediated the reduction of infarct sizes. This data indicates that the RISK signaling pathway is necessary for rIPC-induced cardioprotection. These results align with the findings of Hu and colleagues, who also demonstrated that liver rIPC maneuver protects the heart against I/R injury, sudden cardiac death, and cardiac arrhythmia by an ERK/GSK3β dependent signaling pathway (Hu, Hu et al. 2016). In addition, Hu et al. also showed that using U0126 or GSK-3β inhibitors completely abolished liver rIPC-mediated cardioprotection (Hu, Hu et al. 2016), supporting the relevance of RISK signaling pathway for rIPC-mediated cardioprotection.

Interestingly, Heinen et al.(Heinen, Behmenburg et al. 2018) observed that the plasma of young volunteers submitted to the rIPC maneuver increases the phosphorylation of GSK-3β in rat myocytes. The GSK-3β phosphorylation is accompanied by inhibition of the opening of mitochondrial transition pores, reducing mitochondrial disruption and cell death. Similar conclusions regarding the activation of RISK signaling were found by Davidson et al. (Davidson, Riquelme et

al. 2018). Davidson and colleagues demonstrated that endothelial-derived exosomes from endothelial cells subjected to ischemic preconditioning promote cardioprotection in cardiomyocytes subjected to simulated ischemia and reperfusion. However, this protective effect was abolished in the presence of U0126, suggesting that the cardioprotective effects depend on ERK1/2 MAPK signaling (Davidson, Riquelme et al. 2018). This data supports our results and highlights the RISK signaling pathway as an essential effector of rIPC-mediated cardioprotection. Together, our data suggest Pyk2 inhibition is a potential treatment to restore rIPC-mediated cardioprotection in NZO mice. Furthermore, our data indicate that the cardioprotective effects of rIPC occur in a NO-dependent manner, with minor participation of neural signaling and having the RISK signaling pathway as the primary end effector of rIPC-induced cardioprotection.

In conclusion, Pyk2 inhibition is a potential strategy to restore eNOS functionality in insulin resistance and hyperinsulinemic conditions. The regain of eNOS function acts directly, improving endothelial function, normalizing blood pressure, and increasing the participation of the endothelium in remote organ protection. To our knowledge, our results indicate for the first time that Pyk2 is an essential negative regulator of eNOS in insulin resistance and a key molecule for inducing endothelial dysfunction and increased cardiovascular risk in T2DM-related conditions. Therefore, our data indicates Pyk2 modulation as a potential candidate for future therapies to decrease diabetes-related cardiovascular complications.

Nevertheless, more studies are needed to understand the effects and safety of chronic Pyk2 inhibition and investigate its impact on other organs and animal models.

5 References

Abu-Amara, M., S. Y. Yang, A. Quaglia, P. Rowley, B. Fuller, A. Seifalian and B. Davidson (2011). "Role of endothelial nitric oxide synthase in remote ischemic preconditioning of the mouse liver." Liver Transpl **17**(5): 610-619.

Adeva-Andany, M. M., J. Martínez-Rodríguez, M. González-Lucán, C. Fernández-Fernández and E. Castro-Quintela (2019). "Insulin resistance is a cardiovascular risk factor in humans." Diabetes Metab Syndr **13**(2): 1449-1455.

Aikawa, R., M. Nawano, Y. Gu, H. Katagiri, T. Asano, W. Zhu, R. Nagai and I. Komuro (2000). "Insulin prevents cardiomyocytes from oxidative stress-induced apoptosis through activation of PI3 kinase/Akt." Circulation **102**(23): 2873-2879.

Akash, M. S. H., K. Rehman and A. Liaqat (2018). "Tumor Necrosis Factor-Alpha: Role in Development of Insulin Resistance and Pathogenesis of Type 2 Diabetes Mellitus." J Cell Biochem **119**(1): 105-110.

Akther, F., M. R. Razan, S. Shaligram, J. L. Graham, K. L. Stanhope, K. N. Allen, J. P. Vázquez-Medina, P. J. Havel and R. Rahimian (2021). "Potentiation of Acetylcholine-Induced Relaxation of Aorta in Male UC Davis Type 2 Diabetes Mellitus (UCD-T2DM) Rats: Sex-Specific Responses." Front Physiol **12**: 616317.

Alp, N. J., M. A. Mcateer, J. Khoo, R. P. Choudhury and K. M. Channon (2004). "Increased Endothelial Tetrahydrobiopterin Synthesis by Targeted Transgenic GTP-Cyclohydrolase I Overexpression Reduces Endothelial Dysfunction and Atherosclerosis in ApoE-Knockout Mice." Arteriosclerosis, Thrombosis, and Vascular Biology **24**(3): 445-450.

Alp, N. J., S. Mussa, J. Khoo, S. Cai, T. Guzik, A. Jefferson, N. Goh, K. A. Rockett and K. M. Channon (2003). "Tetrahydrobiopterin-dependent preservation of nitric oxide–mediated endothelial function in diabetes by targeted transgenic GTP–cyclohydrolase I overexpression." Journal of Clinical Investigation **112**(5): 725-735.

Altenhofen, D., J. M. Khuong, T. Kuhn, S. Lebek, S. Görigk, K. Kaiser, C. Binsch, K. Griess, B. Knebel, B. F. Belgardt, S. Cames, S. Eickelschulte, T. Stermann, A. Rasche, R. Herwig, J. Weiss, H. Vogel, A. Schürmann, A. Chadt and H. Al-Hasani (2023). "E96V Mutation in the." Int J Mol Sci **24**(1).

American Diabetes Association, A. (2014). "Diagnosis and classification of diabetes mellitus." Diabetes Care **37 Suppl 1**: S81-90.

An, J., G. A. Nichols, L. Qian, M. A. Munis, T. N. Harrison, Z. Li, R. Wei, T. Weiss, S. Rajpathak and K. Reynolds (2021). "Prevalence and incidence of microvascular and macrovascular complications over 15 years among patients with incident type 2 diabetes." BMJ Open Diabetes Res Care **9**(1).

Andreadou, I., E. K. Iliodromitis, T. Rassaf, R. Schulz, A. Papapetropoulos and P. Ferdinandy (2015). "The role of gasotransmitters NO, H2S and CO in myocardial ischaemia/reperfusion injury and cardioprotection by preconditioning, postconditioning and remote conditioning." Br J Pharmacol **172**(6): 1587-1606.

Andreozzi, F., E. Laratta, C. Procopio, M. L. Hribal, A. Sciacqua, M. Perticone, C. Miele, F. Perticone and G. Sesti (2007). "Interleukin-6 impairs the insulin signaling pathway, promoting production of nitric oxide in human umbilical vein endothelial cells." Mol Cell Biol **27**(6): 2372-2383.

Andreozzi, F., E. Laratta, A. Sciacqua, F. Perticone and G. Sesti (2004). "Angiotensin II impairs the insulin signaling pathway promoting production of nitric oxide by inducing phosphorylation of insulin receptor substrate-1 on Ser312 and Ser616 in human umbilical vein endothelial cells." Circ Res **94**(9): 1211-1218.
Arcambal, A., J. Taïlé, P. Rondeau, W. Viranaïcken, O. Meilhac and M. P. Gonthier (2019). "Hyperglycemia modulates redox, inflammatory and vasoactive markers through specific signaling pathways in cerebral endothelial cells: Insights on insulin protective action." Free Radic Biol Med **130**: 59-70.
Balligand, J. L., O. Feron and C. Dessy (2009). "eNOS activation by physical forces: from short-term regulation of contraction to chronic remodeling of cardiovascular tissues." Physiol Rev **89**(2): 481-534.
Bansal, M. and P. P. Sengupta (2017). "How to interpret an echocardiography report (for the non-imager)?" Heart **103**(21): 1733-1744.
Basalay, M. V., S. M. Davidson, A. V. Gourine and D. M. Yellon (2018). "Neural mechanisms in remote ischaemic conditioning in the heart and brain: mechanistic and translational aspects." Basic Res Cardiol **113**(4): 25.
Baviera, M., S. Genovese, P. Colacioppo, N. Cosentino, A. Foresta, M. Tettamanti, I. Fortino, M. C. Roncaglioni and G. Marenzi (2022). "Diabetes mellitus duration and mortality in patients hospitalized with acute myocardial infarction." Cardiovascular Diabetology **21**(1).
Bedinger, D. H. and S. H. Adams (2015). "Metabolic, anabolic, and mitogenic insulin responses: A tissue-specific perspective for insulin receptor activators." Mol Cell Endocrinol **415**: 143-156.
Benedé-Ubieto, R., O. Estévez-Vázquez, P. Ramadori, F. J. Cubero and Y. A. Nevzorova (2020). "Guidelines and Considerations for Metabolic Tolerance Tests in Mice." Diabetes Metab Syndr Obes **13**: 439-450.
Bibli, S. I., Z. Zhou, S. Zukunft, B. Fisslthaler, I. Andreadou, C. Szabo, P. Brouckaert, I. Fleming and A. Papapetropoulos (2017). "Tyrosine phosphorylation of eNOS regulates myocardial survival after an ischaemic insult: role of PYK2." Cardiovasc Res **113**(8): 926-937.
Bjornstad, P., M. Schäfer, U. Truong, M. Cree-Green, L. Pyle, A. Baumgartner, Y. Garcia Reyes, A. Maniatis, S. Nayak, R. P. Wadwa, L. P. Browne, J. E. B. Reusch and K. J. Nadeau (2018). "Metformin Improves Insulin Sensitivity and Vascular Health in Youth With Type 1 Diabetes Mellitus." Circulation **138**(25): 2895-2907.
Boucher, J., A. Kleinridders and C. R. Kahn (2014). "Insulin receptor signaling in normal and insulin-resistant states." Cold Spring Harb Perspect Biol **6**(1).
Brandes, R. P. (2014). "Endothelial dysfunction and hypertension." Hypertension **64**(5): 924-928.
Bromage, D. I., J. M. Pickard, X. Rossello, O. J. Ziff, N. Burke, D. M. Yellon and S. M. Davidson (2017). "Remote ischaemic conditioning reduces infarct size in animal in vivo models of ischaemia-reperfusion injury: a systematic review and meta-analysis." Cardiovasc Res **113**(3): 288-297.
Bryan, N. S., T. Rassaf, R. E. Maloney, C. M. Rodriguez, F. Saijo, J. R. Rodriguez and M. Feelisch (2004). "Cellular targets and mechanisms of nitros(yl)ation: An insight into their nature and kinetics

in vivo." Proceedings of the National Academy of Sciences **101**(12): 4308-4313.
Bøtker, H. E., R. Kharbanda, M. R. Schmidt, M. Bøttcher, A. K. Kaltoft, C. J. Terkelsen, K. Munk, N. H. Andersen, T. M. Hansen, S. Trautner, J. F. Lassen, E. H. Christiansen, L. R. Krusell, S. D. Kristensen, L. Thuesen, S. S. Nielsen, M. Rehling, H. T. Sørensen, A. N. Redington and T. T. Nielsen (2010). "Remote ischaemic conditioning before hospital admission, as a complement to angioplasty, and effect on myocardial salvage in patients with acute myocardial infarction: a randomised trial." Lancet **375**(9716): 727-734.
Cadenas, S. (2018). "ROS and redox signaling in myocardial ischemia-reperfusion injury and cardioprotection." Free Radic Biol Med **117**: 76-89.
Cahill, P. A. and E. M. Redmond (2016). "Vascular endothelium – Gatekeeper of vessel health." Atherosclerosis **248**: 97-109.
Cao, B., H. Wang, C. Zhang, M. Xia and X. Yang (2018). "Remote Ischemic Postconditioning (RIPC) of the Upper Arm Results in Protection from Cardiac Ischemia-Reperfusion Injury Following Primary Percutaneous Coronary Intervention (PCI) for Acute ST-Segment Elevation Myocardial Infarction (STEMI)." Med Sci Monit **24**: 1017-1026.
Carr, M. E. (2001). "Diabetes mellitus: a hypercoagulable state." J Diabetes Complications **15**(1): 44-54.
Chai, Q., J. Liu and Y. Hu (2014). "Comparison of femoral and aortic remote ischaemia preconditioning for cardioprotection against myocardial ischaemia/reperfusion injury in a rat model." Interact Cardiovasc Thorac Surg **19**(6): 1013-1018.
Chandel, S., A. Sathis, M. Dhar, H. Giri, A. A. Nathan, S. K. R. Samawar, A. Gupta, J. Gopal, R. Harish, V. Mohan and M. Dixit (2020). "Hyperinsulinemia promotes endothelial inflammation via increased expression and release of Angiopoietin-2." Atherosclerosis **307**: 1-10.
Chang, C., Y. Zhao, G. Song and K. She (2018). "Resveratrol protects hippocampal neurons against cerebral ischemia-reperfusion injury via modulating JAK/ERK/STAT signaling pathway in rats." J Neuroimmunol **315**: 9-14.
Chen, C.-A., L. J. Druhan, S. Varadharaj, Y.-R. Chen and J. L. Zweier (2008). "Phosphorylation of Endothelial Nitric-oxide Synthase Regulates Superoxide Generation from the Enzyme." Journal of Biological Chemistry **283**(40): 27038-27047.
Chen, K., Z. Xu, Y. Liu, Z. Wang, Y. Li, X. Xu, C. Chen, T. Xia, Q. Liao, Y. Yao, C. Zeng, D. He, Y. Yang, T. Tan, J. Yi, J. Zhou, H. Zhu, J. Ma and C. Zeng (2017). "Irisin protects mitochondria function during pulmonary ischemia/reperfusion injury." Science Translational Medicine **9**(418): eaao6298.
Chen, R., B. Ovbiagele and W. Feng (2016). "Diabetes and Stroke: Epidemiology, Pathophysiology, Pharmaceuticals and Outcomes." Am J Med Sci **351**(4): 380-386.
Cheng, Y., P. Zhu, J. Yang, X. Liu, S. Dong, X. Wang, B. Chun, J. Zhuang and C. Zhang (2010). "Ischaemic preconditioning-regulated miR-21 protects heart against ischaemia/reperfusion injury via anti-apoptosis through its target PDCD4." Cardiovascular Research **87**(3): 431-439.
Chien, C. Y., T. J. Wen, Y. H. Cheng, Y. T. Tsai, C. Y. Chiang and C. T. Chien (2020). "Diabetes Upregulates Oxidative Stress and Downregulates Cardiac Protection to Exacerbate Myocardial Ischemia/Reperfusion Injury in Rats." Antioxidants (Basel) **9**(8).

Cho, K., S. I. Min, S. Ahn, S. K. Min, C. Ahn, K. S. Yu, I. J. Jang, J. Y. Cho and J. Ha (2017). "Integrative Analysis of Renal Ischemia/Reperfusion Injury and Remote Ischemic Preconditioning in Mice." J Proteome Res **16**(8): 2877-2886.
Cho, Y.-R., S. H. Ann, K.-B. Won, G.-M. Park, Y.-G. Kim, D. H. Yang, J.-W. Kang, T.-H. Lim, H.-K. Kim, J. Choe, S.-W. Lee, Y.-H. Kim, S.-J. Kim and S.-G. Lee (2019). "Association between insulin resistance, hyperglycemia, and coronary artery disease according to the presence of diabetes." Scientific Reports **9**(1).
Cho, Y. R., H. J. Kim, S. Y. Park, H. J. Ko, E. G. Hong, T. Higashimori, Z. Zhang, D. Y. Jung, M. S. Ola, K. F. Lanoue, E. H. Leiter and J. K. Kim (2007). "Hyperglycemia, maturity-onset obesity, and insulin resistance in NONcNZO10/LtJ males, a new mouse model of type 2 diabetes." Am J Physiol Endocrinol Metab **293**(1): E327-336.
Chouchani, E. T., V. R. Pell, A. M. James, L. M. Work, K. Saeb-Parsy, C. Frezza, T. Krieg and M. P. Murphy (2016). "A Unifying Mechanism for Mitochondrial Superoxide Production during Ischemia-Reperfusion Injury." Cell Metab **23**(2): 254-263.
Crofford, O. B. and C. K. Davis (1965). "Growth characteristics, glucose tolerance and insulin sensitivity of New

Zealand Obese mice." Metabolism **14**: 271-280.
da Costa, R. M., K. B. Neves, F. L. Mestriner, P. Louzada-Junior, T. Bruder-Nascimento and R. C. Tostes (2016). "TNF-α induces vascular insulin resistance via positive modulation of PTEN and decreased Akt/eNOS/NO signaling in high fat diet-fed mice." Cardiovasc Diabetol **15**(1): 119.
Davidson, S. M., J. A. Riquelme, Y. Zheng, J. M. Vicencio, S. Lavandero and D. M. Yellon (2018). "Endothelial cells release cardioprotective exosomes that may contribute to ischaemic preconditioning." Scientific Reports **8**(1).
Dellett, M., E. D. Brown, J. Guduric-Fuchs, A. O'Connor, A. W. Stitt, R. J. Medina and D. A. Simpson (2017). "MicroRNA-containing extracellular vesicles released from endothelial colony-forming cells modulate angiogenesis during ischaemic retinopathy." J Cell Mol Med **21**(12): 3405-3419.
Dharmashankar, K. and M. E. Widlansky (2010). "Vascular endothelial function and hypertension: insights and directions." Curr Hypertens Rep **12**(6): 448-455.
Doenst, T., A. Haverich, P. Serruys, R. O. Bonow, P. Kappetein, V. Falk, E. Velazquez, A. Diegeler and H. Sigusch (2019). "PCI and CABG for Treating Stable Coronary Artery Disease: JACC Review Topic of the Week." J Am Coll Cardiol **73**(8): 964-976.
Durante, W., M. H. Kroll, N. Christodoulides, K. J. Peyton and A. I. Schafer (1997). "Nitric Oxide Induces Heme Oxygenase-1 Gene Expression and Carbon Monoxide Production in Vascular Smooth Muscle Cells." Circulation Research **80**(4): 557-564.
Eddy, D., L. Schlessinger, R. Kahn, B. Peskin and R. Schiebinger (2009). "Relationship of insulin resistance and related metabolic variables to coronary artery disease: a mathematical analysis." Diabetes Care **32**(2): 361-366.
Edgerton, D. S. (2006). "Insulin's direct effects on the liver dominate the control of hepatic glucose production." Journal of Clinical Investigation **116**(2): 521-527.
ElSayed, N. A., G. Aleppo, V. R. Aroda, R. R. Bannuru, F. M. Brown, D. Bruemmer, B. S. Collins, M. E. Hilliard, D. Isaacs, E. L. Johnson, S. Kahan, K. Khunti, J. Leon, S. K. Lyons, M. L. Perry, P. Prahalad, R. E. Pratley, J. J. Seley, R. C. Stanton, R. A. Gabbay and on behalf of the American Diabetes Association (2023). "2. Classification and

Diagnosis of Diabetes: Standards of Care in Diabetes-2023." Diabetes Care **46**(Suppl 1): S19-S40.
Eltzschig, H. K. and T. Eckle (2011). "Ischemia and reperfusion--from mechanism to translation." Nat Med **17**(11): 1391-1401.
Erkens, R., D. Duse, A. Brum, A. Chadt, S. Becher, M. Siragusa, C. Quast, J. Müssig, M. Roden, M. Cortese-Krott, E. Lammert E, I. Fleming, C. Jung, H. Al-Hasani, G. Heusch and M. Kelm (2023). Inhibition of proline-rich-tyrosine kinase 2 restores cardioprotection by remote ischemic preconditioning in type 2 diabetes mellitus, Cold Spring Harbor Laboratory.
Erkens, R., C. M. Kramer, W. Lückstädt, C. Panknin, L. Krause, M. Weidenbach, J. Dirzka, T. Krenz, E. Mergia, T. Suvorava, M. Kelm and M. M. Cortese-Krott (2015). "Left ventricular diastolic dysfunction in Nrf2 knock out mice is associated with cardiac hypertrophy, decreased expression of SERCA2a, and preserved endothelial function." Free Radic Biol Med **89**: 906-917.
Erkens, R., T. Suvorava, C. M. Kramer, L. D. Diederich, M. Kelm and M. M. Cortese-Krott (2017). "Modulation of Local and Systemic Heterocellular Communication by Mechanical Forces: A Role of Endothelial Nitric Oxide Synthase." Antioxid Redox Signal **26**(16): 917-935.
Feige, K., S. Roth, R. M'Pembele, A. Galow, S. Koenig, M. Stroethoff, A. Raupach, G. Lurati Buse, A. M. Mathes, M. W. Hollmann, R. Huhn and C. Torregroza (2022). "Influence of Short and Long Hyperglycemia on Cardioprotection by Remote Ischemic Preconditioning-A Translational Approach." Int J Mol Sci **23**(23).
Fernández-Hernando, C. and Y. Suárez (2018). "MicroRNAs in endothelial cell homeostasis and vascular disease." Curr Opin Hematol **25**(3): 227-236.
Ferreras, L., A. S. Kelada, M. McCoy and J. Proietto (1994). "Early decrease in GLUT4 protein levels in brown adipose tissue of New Zealand obese mice." Int J Obes Relat Metab Disord **18**(11): 760-765.
Fisslthaler, B., A. E. Loot, A. Mohamed, R. Busse and I. Fleming (2008). "Inhibition of endothelial nitric oxide synthase activity by proline-rich tyrosine kinase 2 in response to fluid shear stress and insulin." Circ Res **102**(12): 1520-1528.
Fleming, I. (2010). "Molecular mechanisms underlying the activation of eNOS." Pflugers Arch **459**(6): 793-806.
Fleming, I. and R. Busse (2003). "Molecular mechanisms involved in the regulation of the endothelial nitric oxide synthase." Am J Physiol Regul Integr Comp Physiol **284**(1): R1-12.
Fleming, I., B. Fisslthaler, S. Dimmeler, B. E. Kemp and R. Busse (2001). "Phosphorylation of Thr(495) regulates Ca(2+)/calmodulin-dependent endothelial nitric oxide synthase activity." Circ Res **88**(11): E68-75.
Foster, D. B., J. E. Van Eyk, E. Marbán and B. O'Rourke (2009). "Redox signaling and protein phosphorylation in mitochondria: progress and prospects." J Bioenerg Biomembr **41**(2): 159-168.
Furchgott, R. F. and J. V. Zawadzki (1980). "The obligatory role of endothelial cells in the relaxation of arterial smooth muscle by acetylcholine." Nature **288**(5789): 373-376.
Förstermann, U. and W. C. Sessa (2012). "Nitric oxide synthases: regulation and function." Eur Heart J **33**(7): 829-837, 837a-837d.

Gao, F., E. Gao, T. L. Yue, E. H. Ohlstein, B. L. Lopez, T. A. Christopher and X. L. Ma (2002). "Nitric oxide mediates the antiapoptotic effect of insulin in myocardial ischemia-reperfusion: the roles of PI3-kinase, Akt, and endothelial nitric oxide synthase phosphorylation." Circulation **105**(12): 1497-1502.
Gao, Z., Z. Wang, H. Zhu, X. Yuan, M. Sun, J. Wang, M. Zuo, X. Cui, Y. Han, Y. Zhang, S. Yang, Y. Qin, J. Xu, J. Yang and B. Chang (2020). "Hyperinsulinemia contributes to impaired-glucose-tolerance-induced renal injury." Ther Adv Chronic Dis **11**: 2040622320916008.
Gourine, A. V., A. Gourine, S. Mastitskaya and G. Ackland (2010). Remote preconditioning reflex – a neural pathway of cardioprotection during myocardial ischaemia and reperfusion induced by remote ischaemic preconditioning. European Heart Journal Supplements **31:** 319.
Group, D. I. S. (2004). "Plasma insulin and cardiovascular mortality in non-diabetic European men and women: a meta-analysis of data from eleven prospective studies." Diabetologia **47**(7): 1245-1256.
Gu, X., Z. Liu, S. Gao, L. Ma, J. Chen, Z. Wang, A. Lu, Z. Wang, B. Wang and Y. Li (2021). "The Effects of Ischemic Preconditioning Supplementation on Endothelial Function: A Systematic Review and Meta-Analysis." Evidence-Based Complementary and Alternative Medicine **2021**: 1-9.
Gual, P., Y. Le Marchand-Brustel and J. F. Tanti (2005). "Positive and negative regulation of insulin signaling through IRS-1 phosphorylation." Biochimie **87**(1): 99-109.
Han, S., A. Mistry, J. S. Chang, D. Cunningham, M. Griffor, P. C. Bonnette, H. Wang, B. A. Chrunyk, G. E. Aspnes, D. P. Walker, A. D. Brosius and L. Buckbinder (2009). "Structural characterization of proline-rich tyrosine kinase 2 (PYK2) reveals a unique (DFG-out) conformation and enables inhibitor design." J Biol Chem **284**(19): 13193-13201.
Haskell, B. D., K. Flurkey, T. M. Duffy, E. E. Sargent and E. H. Leiter (2002). "The diabetes-prone NZO/HlLt strain. I. Immunophenotypic comparison to the related NZB/BINJ and NZW/LacJ strains." Lab Invest **82**(7): 833-842.
Hausenloy, D. J., R. K. Kharbanda, U. K. Møller, M. Ramlall, J. Aarøe, R. Butler, H. Bulluck, T. Clayton, A. Dana, M. Dodd, T. Engstrom, R. Evans, J. F. Lassen, E. F. Christensen, J. M. Garcia-Ruiz, D. A. Gorog, J. Hjort, R. F. Houghton, B. Ibanez, R. Knight, F. K. Lippert, J. T. Lønborg, M. Maeng, D. Milasinovic, R. More, J. M. Nicholas, L. O. Jensen, A. Perkins, N. Radovanovic, R. D. Rakhit, J. Ravkilde, A. D. Ryding, M. R. Schmidt, I. S. Riddervold, H. T. Sørensen, G. Stankovic, M. Varma, I. Webb, C. J. Terkelsen, J. P. Greenwood, D. M. Yellon, H. E. Bøtker and C.-E.-P. Investigators (2019). "Effect of remote ischaemic conditioning on clinical outcomes in patients with acute myocardial infarction (CONDI-2/ERIC-PPCI): a single-blind randomised controlled trial." Lancet **394**(10207): 1415-1424.
He, Y., H. Li, J. Yao, H. Zhong, Y. Kuang, X. Li and W. Bian (2021). "HO-1 knockdown upregulates the expression of VCAM-1 to induce neutrophil recruitment during renal ischemia-reperfusion injury." International Journal of Molecular Medicine **48**(4).
Heinen, A., F. Behmenburg, A. Aytulun, M. Dierkes, L. Zerbin, W. Kaisers, M. Schaefer, T. Meyer-Treschan, S. Feit, I. Bauer, M. W. Hollmann and R. Huhn (2018). "The release of cardioprotective humoral factors after remote ischemic preconditioning in humans is age- and sex-dependent." J Transl Med **16**(1): 112.

Heiss, C., A. Rodriguez-Mateos and M. Kelm (2015). "Central role of eNOS in the maintenance of endothelial homeostasis." Antioxid Redox Signal **22**(14): 1230-1242.
Hendgen-Cotta, U. B., M. W. Merx, S. Shiva, J. Schmitz, S. Becher, J. P. Klare, H. J. Steinhoff, A. Goedecke, J. Schrader, M. T. Gladwin, M. Kelm and T. Rassaf (2008). "Nitrite reductase activity of myoglobin regulates respiration and cellular viability in myocardial ischemia-reperfusion injury." Proc Natl Acad Sci U S A **105**(29): 10256-10261.
Heusch, G. (2013). "Cardioprotection: chances and challenges of its translation to the clinic." Lancet **381**(9861): 166-175.
Heusch, G. (2015). "Molecular basis of cardioprotection: signal transduction in ischemic pre-, post-, and remote conditioning." Circ Res **116**(4): 674-699.
Heusch, G. (2017). "Remote ischemic conditioning: the enigmatic transfer of protection." Cardiovasc Res **113**(1): 1-2.
Heusch, G., H. E. Bøtker, K. Przyklenk, A. Redington and D. Yellon (2015). "Remote ischemic conditioning." J Am Coll Cardiol **65**(2): 177-195.
Honka, M.-J., A. Latva-Rasku, M. Bucci, K. A. Virtanen, J. C. Hannukainen, K. K. Kalliokoski and P. Nuutila (2018). "Insulin-stimulated glucose uptake in skeletal muscle, adipose tissue and liver: a positron emission tomography study." European Journal of Endocrinology **178**(5): 523-531.
Hu, Z., S. Hu, S. Yang, M. Chen, P. Zhang, J. Liu and G. W. Abbott (2016). "Remote Liver Ischemic Preconditioning Protects against Sudden Cardiac Death via an ERK/GSK-3β-Dependent Mechanism." PLOS ONE **11**(10): e0165123.
IDF (2021). IDF DIABETES ATLAS.
Jiang, Z. Y., Y. W. Lin, A. Clemont, E. P. Feener, K. D. Hein, M. Igarashi, T. Yamauchi, M. F. White and G. L. King (1999). "Characterization of selective resistance to insulin signaling in the vasculature of obese Zucker (fa/fa) rats." J Clin Invest **104**(4): 447-457.
Jin, Y.-J., R. Chennupati, R. Li, G. Liang, S. Wang, A. Iring, J. Graumann, N. Wettschureck and S. Offermanns (2021). "Protein kinase N2 mediates flow-induced endothelial NOS activation and vascular tone regulation." Journal of Clinical Investigation **131**(21).
Johnsen, J., K. Pryds, R. Salman, B. Løfgren, S. B. Kristiansen and H. E. Bøtker (2016). "The remote ischemic preconditioning algorithm: effect of number of cycles, cycle duration and effector organ mass on efficacy of protection." Basic Res Cardiol **111**(2): 10.
Johnson, J. D. (2021). "On the causal relationships between hyperinsulinaemia, insulin resistance, obesity and dysglycaemia in type 2 diabetes." Diabetologia **64**(10): 2138-2146.
Jürgens, H. S., S. Neschen, S. Ortmann, S. Scherneck, K. Schmolz, G. Schüler, S. Schmidt, M. Blüher, S. Klaus, D. Perez-Tilve, M. H. Tschöp, A. Schürmann and H. G. Joost (2007). "Development of diabetes in obese, insulin-resistant mice: essential role of dietary carbohydrate in beta cell destruction." Diabetologia **50**(7): 1481-1489.
Kalakech, H., P. Hibert, D. Prunier-Mirebeau, S. Tamareille, F. Letournel, L. Macchi, F. Pinet, A. Furber and F. Prunier (2014). "RISK and SAFE signaling pathway involvement in apolipoprotein A-I-induced cardioprotection." PLoS One **9**(9): e107950.
Kalogeris, T., C. P. Baines, M. Krenz and R. J. Korthuis (2012). "Cell biology of ischemia/reperfusion injury." Int Rev Cell Mol Biol **298**: 229-317.

Kidd, G. A., L. W. Dobrucki, V. Brovkovych, D. F. Bohr and T. Malinski (2000). "Nitric oxide deficiency contributes to large cerebral infarct size." Hypertension **35**(5): 1111-1118.
Kim, J. A., M. Montagnani, K. K. Koh and M. J. Quon (2006). "Reciprocal relationships between insulin resistance and endothelial dysfunction: molecular and pathophysiological mechanisms." Circulation **113**(15): 1888-1904.
King, G. L., K. Park and Q. Li (2016). "Selective Insulin Resistance and the Development of Cardiovascular Diseases in Diabetes: The 2015 Edwin Bierman Award Lecture." Diabetes **65**(6): 1462-1471.
Kleinbongard, P., A. Dejam, T. Lauer, T. Rassaf, A. Schindler, O. Picker, T. Scheeren, A. Gödecke, J. Schrader, R. Schulz, G. Heusch, G. A. Schaub, N. S. Bryan, M. Feelisch and M. Kelm (2003). "Plasma nitrite reflects constitutive nitric oxide synthase activity in mammals." Free Radic Biol Med **35**(7): 790-796.
Kluge, R., S. Scherneck, A. Schürmann and H. G. Joost (2012). "Pathophysiology and genetics of obesity and diabetes in the New Zealand obese mouse: a model of the human metabolic syndrome." Methods Mol Biol **933**: 59-73.
Kohr, M. J., J. Sun, A. Aponte, G. Wang, M. Gucek, E. Murphy and C. Steenbergen (2011). "Simultaneous measurement of protein oxidation and S-nitrosylation during preconditioning and ischemia/reperfusion injury with resin-assisted capture." Circ Res **108**(4): 418-426.
Lan, R., H. Geng, P. K. Singha, P. Saikumar, E. P. Bottinger, J. M. Weinberg and M. A. Venkatachalam (2016). "Mitochondrial Pathology and Glycolytic Shift during Proximal Tubule Atrophy after Ischemic AKI." J Am Soc Nephrol **27**(11): 3356-3367.
Landman, T. R. J., L. Uthman, I. A. H. Hofmans, Y. Schoon, F. E. de Leeuw and D. H. J. Thijssen (2022). "Attenuated inflammatory profile following single and repeated handgrip exercise and remote ischemic preconditioning in patients with cerebral small vessel disease." Front Physiol **13**: 1026711.
Lang, R. M., L. P. Badano, V. Mor-Avi, J. Afilalo, A. Armstrong, L. Ernande, F. A. Flachskampf, E. Foster, S. A. Goldstein, T. Kuznetsova, P. Lancellotti, D. Muraru, M. H. Picard, E. R. Rietzschel, L. Rudski, K. T. Spencer, W. Tsang and J.-U. Voigt (2015). "Recommendations for Cardiac Chamber Quantification by Echocardiography in Adults: An Update from the American Society of Echocardiography and the European Association of Cardiovascular Imaging." Journal of the American Society of Echocardiography **28**(1): 1-39.e14.
Lassen, T. R., J. Just, M. V. Hjortbak, N. R. Jespersen, K. T. Stenz, T. Gu, Y. Yan, J. Su, J. Hansen, R. Bæk, M. M. Jørgensen, J. R. Nyengaard, S. B. Kristiansen, K. R. Drasbek, J. Kjems and H. E. Bøtker (2021). "Cardioprotection by remote ischemic conditioning is transferable by plasma and mediated by extracellular vesicles." Basic Res Cardiol **116**(1): 16.
Lawton, J. S., J. E. Tamis-Holland, S. Bangalore, E. R. Bates, T. M. Beckie, J. M. Bischoff, J. A. Bittl, M. G. Cohen, J. M. Dimaio, C. W. Don, S. E. Fremes, M. F. Gaudino, Z. D. Goldberger, M. C. Grant, J. B. Jaswal, P. A. Kurlansky, R. Mehran, T. S. Metkus, L. C. Nnacheta, S. V. Rao, F. W. Sellke, G. Sharma, C. M. Yong and B. A. Zwischenberger (2022). "2021 ACC/AHA/SCAI Guideline for Coronary Artery Revascularization: A Report of the American College of Cardiology/American Heart Association Joint Committee on Clinical Practice Guidelines." Circulation **145**(3).

Lee, Y., S. Chakraborty, C. J. Meininger and M. Muthuchamy (2018). "Insulin resistance disrupts cell integrity, mitochondrial function, and inflammatory signaling in lymphatic endothelium." Microcirculation **25**(7): e12492.
Leiter, E. H., P. C. Reifsnyder, K. Flurkey, H. J. Partke, E. Junger and L. Herberg (1998). "NIDDM genes in mice: deleterious synergism by both parental genomes contributes to diabetogenic thresholds." Diabetes **47**(8): 1287-1295.
Leo, F., T. Suvorava, S. K. Heuser, J. Li, A. LoBue, F. Barbarino, E. Piragine, R. Schneckmann, B. Hutzler, M. E. Good, B. O. Fernandez, L. Vornholz, S. Rogers, A. Doctor, M. Grandoch, J. Stegbauer, E. Weitzberg, M. Feelisch, J. O. Lundberg, B. E. Isakson, M. Kelm and M. M. Cortese-Krott (2021). "Red Blood Cell and Endothelial eNOS Independently Regulate Circulating Nitric Oxide Metabolites and Blood Pressure." Circulation **144**(11): 870-889.
Liang, W., C. Lin, L. Yuan, L. Chen, P. Guo, P. Li, W. Wang and X. Zhang (2019). "Preactivation of Notch1 in remote ischemic preconditioning reduces cerebral ischemia-reperfusion injury through crosstalk with the NF-κB pathway." J Neuroinflammation **16**(1): 181.
Lim, S. Y., D. M. Yellon and D. J. Hausenloy (2010). "The neural and humoral pathways in remote limb ischemic preconditioning." Basic Res Cardiol **105**(5): 651-655.
Liu, P., M. Begley, W. Michowski, H. Inuzuka, M. Ginzberg, D. Gao, P. Tsou, W. Gan, A. Papa, B. M. Kim, L. Wan, A. Singh, B. Zhai, M. Yuan, Z. Wang, S. P. Gygi, T. H. Lee, K.-P. Lu, A. Toker, P. P. Pandolfi, J. M. Asara, M. W. Kirschner, P. Sicinski, L. Cantley and W. Wei (2014). "Cell-cycle-regulated activation of Akt kinase by phosphorylation at its carboxyl terminus." Nature **508**(7497): 541-545.
Liu, X., H. Cao, J. Li, B. Wang, P. Zhang, X. Dong Zhang, Z. Liu, H. Yuan and Z. Zhan (2017). "Autophagy induced by DAMPs facilitates the inflammation response in lungs undergoing ischemia-reperfusion injury through promoting TRAF6 ubiquitination." Cell Death Differ **24**(4): 683-693.
Loot, A. E., J. G. Schreiber, B. Fisslthaler and I. Fleming (2009). "Angiotensin II impairs endothelial function via tyrosine phosphorylation of the endothelial nitric oxide synthase." J Exp Med **206**(13): 2889-2896.
Loukogeorgakis, S. P., A. T. Panagiotidou, M. W. Broadhead, A. Donald, J. E. Deanfield and R. J. MacAllister (2005). "Remote ischemic preconditioning provides early and late protection against endothelial ischemia-reperfusion injury in humans: role of the autonomic nervous system." J Am Coll Cardiol **46**(3): 450-456.
Manchurov, V., N. Ryazankina, T. Khmara, D. Skrypnik, R. Reztsov, E. Vasilieva and A. Shpektor (2014). "Remote ischemic preconditioning and endothelial function in patients with acute myocardial infarction and primary PCI." Am J Med **127**(7): 670-673.
Marchesi, C., T. Ebrahimian, O. Angulo, P. Paradis and E. L. Schiffrin (2009). "Endothelial nitric oxide synthase uncoupling and perivascular adipose oxidative stress and inflammation contribute to vascular dysfunction in a rodent model of metabolic syndrome." Hypertension **54**(6): 1384-1392.
Marso, S. P., T. Miller, B. D. Rutherford, R. J. Gibbons, M. Qureshi, A. Kalynych, M. Turco, H. P. Schultheiss, R. Mehran, M. W. Krucoff, A. J. Lansky and G. W. Stone (2007). "Comparison of myocardial reperfusion in patients undergoing percutaneous coronary intervention in ST-segment elevation acute myocardial infarction with versus without diabetes mellitus (from the EMERALD Trial)." Am J Cardiol **100**(2): 206-210.

Marín-Juez, R., S. Jong-Raadsen, S. Yang and H. P. Spaink (2014). "Hyperinsulinemia induces insulin resistance and immune suppression via Ptpn6/Shp1 in zebrafish." Journal of Endocrinology **222**(2): 229-241.
Middelbeek, R. J., M. A. Chambers, P. Tantiwong, J. T. Treebak, D. An, M. F. Hirshman, N. Musi and L. J. Goodyear (2013). "Insulin stimulation regulates AS160 and TBC1D1 phosphorylation sites in human skeletal muscle." Nutr Diabetes **3**: e74.
Miki, T., T. Itoh, D. Sunaga and T. Miura (2012). "Effects of diabetes on myocardial infarct size and cardioprotection by preconditioning and postconditioning." Cardiovasc Diabetol **11**: 67.
Minicucci, M. F., E. Farah, D. R. Fusco, A. L. Cogni, P. S. Azevedo, K. Okoshi, S. G. Zanati, B. B. Matsubara, S. A. Paiva and L. A. Zornoff (2014). "Infarct size as predictor of systolic functional recovery after myocardial infarction." Arq Bras Cardiol **102**(6): 549-556.
Mukamal, K. J., R. W. Nesto, M. C. Cohen, J. E. Muller, M. Maclure, J. B. Sherwood and M. A. Mittleman (2001). "Impact of diabetes on long-term survival after acute myocardial infarction: comparability of risk with prior myocardial infarction." Diabetes Care **24**(8): 1422-1427.
Muniyappa, R., H. Chen, M. Montagnani, A. Sherman and M. J. Quon (2020). "Endothelial dysfunction due to selective insulin resistance in vascular endothelium: insights from mechanistic modeling." Am J Physiol Endocrinol Metab **319**(3): E629-E646.
Munk, K., N. H. Andersen, M. R. Schmidt, S. S. Nielsen, C. J. Terkelsen, E. Sloth, H. E. Bøtker, T. T. Nielsen and S. H. Poulsen (2010). "Remote Ischemic Conditioning in Patients With Myocardial Infarction Treated With Primary Angioplasty." Circulation: Cardiovascular Imaging **3**(6): 656-662.
Murphy, J. M., K. Jeong, Y. A. R. Rodriguez, J. H. Kim, E. E. Ahn and S. S. Lim (2019). "FAK and Pyk2 activity promote TNF-alpha and IL-1beta-mediated pro-inflammatory gene expression and vascular inflammation." Sci Rep **9**(1): 7617.
Murry, C. E., R. B. Jennings and K. A. Reimer (1986). "Preconditioning with ischemia: a delay of lethal cell injury in ischemic myocardium." Circulation **74**(5): 1124-1136.
Nikoulina, S. E., T. P. Ciaraldi, S. Mudaliar, L. Carter, K. Johnson and R. R. Henry (2002). "Inhibition of glycogen synthase kinase 3 improves insulin action and glucose metabolism in human skeletal muscle." Diabetes **51**(7): 2190-2198.
Ormazabal, V., S. Nair, O. Elfeky, C. Aguayo, C. Salomon and F. A. Zuñiga (2018). "Association between insulin resistance and the development of cardiovascular disease." Cardiovascular Diabetology **17**(1).
Ortlepp, J. R., R. Kluge, K. Giesen, L. Plum, P. Radke, P. Hanrath and H. G. Joost (2000). "A metabolic syndrome of hypertension, hyperinsulinaemia and hypercholesterolaemia in the New Zealand obese mouse." Eur J Clin Invest **30**(3): 195-202.
Pacher, P., T. Nagayama, P. Mukhopadhyay, S. Bátkai and D. A. Kass (2008). "Measurement of cardiac function using pressure–volume conductance catheter technique in mice and rats." Nature protocols **3**(9): 1422-1434.
Pearce, L., S. M. Davidson and D. M. Yellon (2021). "Does remote ischaemic conditioning reduce inflammation? A focus on innate immunity and cytokine response." Basic Research in Cardiology **116**(1).

Pitsavos, C., M. Tampourlou, D. B. Panagiotakos, Y. Skoumas, C. Chrysohoou, T. Nomikos and C. Stefanadis (2007). "Association Between Low-Grade Systemic Inflammation and Type 2 Diabetes Mellitus Among Men and Women from the ATTICA Study." Rev Diabet Stud **4**(2): 98-104.
Posner, B. I. (2017). "Insulin Signalling: The Inside Story." Can J Diabetes **41**(1): 108-113.
Preis, S. R., S. J. Hwang, S. Coady, M. J. Pencina, R. B. D'Agostino, P. J. Savage, D. Levy and C. S. Fox (2009). "Trends in all-cause and cardiovascular disease mortality among women and men with and without diabetes mellitus in the Framingham Heart Study, 1950 to 2005." Circulation **119**(13): 1728-1735.
Rassaf, T., M. Totzeck, U. B. Hendgen-Cotta, S. Shiva, G. Heusch and M. Kelm (2014). "Circulating nitrite contributes to cardioprotection by remote ischemic preconditioning." Circ Res **114**(10): 1601-1610.
Reaven, G. (2012). "Insulin resistance and coronary heart disease in nondiabetic individuals." Arterioscler Thromb Vasc Biol **32**(8): 1754-1759.
Redington, K. L., T. Disenhouse, S. C. Strantzas, R. Gladstone, C. Wei, M. B. Tropak, X. Dai, C. Manlhiot, J. Li and A. N. Redington (2012). "Remote cardioprotection by direct peripheral nerve stimulation and topical capsaicin is mediated by circulating humoral factors." Basic Res Cardiol **107**(2): 241.
Robinson, A. C., J. Burke, S. Robinson, D. G. Johnston and R. S. Elkeles (1998). "The effects of metformin on glycemic control and serum lipids in insulin-treated NIDDM patients with suboptimal metabolic control." Diabetes Care **21**(5): 701-705.
Rossello, X., Z. He and D. M. Yellon (2018). "Myocardial Infarct Size Reduction Provided by Local and Remote Ischaemic Preconditioning: References Values from the Hatter Cardiovascular Institute." Cardiovasc Drugs Ther **32**(2): 127-133.
Roth, G. A., G. A. Mensah, C. O. Johnson, G. Addolorato, E. Ammirati, L. M. Baddour, N. C. Barengo, A. Z. Beaton, E. J. Benjamin, C. P. Benziger, A. Bonny, M. Brauer, M. Brodmann, T. J. Cahill, J. Carapetis, A. L. Catapano, S. S. Chugh, L. T. Cooper, J. Coresh, M. Criqui, N. DeCleene, K. A. Eagle, S. Emmons-Bell, V. L. Feigin, J. Fernández-Solà, G. Fowkes, E. Gakidou, S. M. Grundy, F. J. He, G. Howard, F. Hu, L. Inker, G. Karthikeyan, N. Kassebaum, W. Koroshetz, C. Lavie, D. Lloyd-Jones, H. S. Lu, A. Mirijello, A. M. Temesgen, A. Mokdad, A. E. Moran, P. Muntner, J. Narula, B. Neal, M. Ntsekhe, G. Moraes de Oliveira, C. Otto, M. Owolabi, M. Pratt, S. Rajagopalan, M. Reitsma, A. L. P. Ribeiro, N. Rigotti, A. Rodgers, C. Sable, S. Shakil, K. Sliwa-Hahnle, B. Stark, J. Sundström, P. Timpel, I. M. Tleyjeh, M. Valgimigli, T. Vos, P. K. Whelton, M. Yacoub, L. Zuhlke, C. Murray, V. Fuster and G.-N.-J. G. B. o. C. D. W. Group (2020). "Global Burden of Cardiovascular Diseases and Risk Factors, 1990-2019: Update From the GBD 2019 Study." J Am Coll Cardiol **76**(25): 2982-3021.
Roux, E., P. Bougaran, P. Dufourcq and T. Couffinhal (2020). "Fluid Shear Stress Sensing by the Endothelial Layer." Front Physiol **11**: 861.
Rui, L. (2014). "Energy metabolism in the liver." Compr Physiol **4**(1): 177-197.
Sakamoto, K. and G. D. Holman (2008). "Emerging role for AS160/TBC1D4 and TBC1D1 in the regulation of GLUT4 traffic." Am J Physiol Endocrinol Metab **295**(1): E29-37.
Saltiel, A. R. and C. R. Kahn (2001). "Insulin signalling and the regulation of glucose and lipid metabolism." Nature **414**(6865): 799-806.

Sanit, J., E. Prompunt, P. Adulyaritthikul, N. Nokkaew, P. Mongkolpathumrat, K. Kongpol, A. Kijtawornrat, S. Petchdee, S. Barrère-Lemaire and S. Kumphune (2019). "Combination of metformin and p38 MAPK inhibitor, SB203580, reduced myocardial ischemia/reperfusion injury in non-obese type 2 diabetic Goto-Kakizaki rats." Exp Ther Med **18**(3): 1701-1714.
Schmidt, C., L. Reitzle, R. Paprott, J. Bätzing and J. Holstiege (2021). "Diabetes mellitus and comorbidities - A cross-sectional study with control group based on nationwide ambulatory claims data." J Health Monit **6**(2): 19-35.
Seeger, J. P., N. M. Benda, N. P. Riksen, A. P. van Dijk, L. Bellersen, M. T. Hopman, N. T. Cable and D. H. Thijssen (2016). "Heart failure is associated with exaggerated endothelial ischaemia-reperfusion injury and attenuated effect of ischaemic preconditioning." Eur J Prev Cardiol **23**(1): 33-40.
Shesely, E. G., N. Maeda, H. S. Kim, K. M. Desai, J. H. Krege, V. E. Laubach, P. A. Sherman, W. C. Sessa and O. Smithies (1996). "Elevated blood pressures in mice lacking endothelial nitric oxide synthase." Proc Natl Acad Sci U S A **93**(23): 13176-13181.
Silva Rosa, S. C., N. Nayak, A. M. Caymo and J. W. Gordon (2020). "Mechanisms of muscle insulin resistance and the cross-talk with liver and adipose tissue." Physiological Reports **8**(19).
Siragusa, M. and I. Fleming (2016). "The eNOS signalosome and its link to endothelial dysfunction." Pflugers Arch **468**(7): 1125-1137.
Steensrud, T., J. Li, X. Dai, C. Manlhiot, R. K. Kharbanda, M. Tropak and A. Redington (2010). "Pretreatment with the nitric oxide donor SNAP or nerve transection blocks humoral preconditioning by remote limb ischemia or intra-arterial adenosine." Am J Physiol Heart Circ Physiol **299**(5): H1598-1603.
Sun, H., P. Saeedi, S. Karuranga, M. Pinkepank, K. Ogurtsova, B. B. Duncan, C. Stein, A. Basit, J. C. N. Chan, J. C. Mbanya, M. E. Pavkov, A. Ramachandaran, S. H. Wild, S. James, W. H. Herman, P. Zhang, C. Bommer, S. Kuo, E. J. Boyko and D. J. Magliano (2022). "IDF Diabetes Atlas: Global, regional and country-level diabetes prevalence estimates for 2021 and projections for 2045." Diabetes Res Clin Pract **183**: 109119.
Sun, H. J., Z. Y. Wu, X. W. Nie and J. S. Bian (2019). "Role of Endothelial Dysfunction in Cardiovascular Diseases: The Link Between Inflammation and Hydrogen Sulfide." Front Pharmacol **10**: 1568.
Symons, J. D., S. L. McMillin, C. Riehle, J. Tanner, M. Palionyte, E. Hillas, D. Jones, R. C. Cooksey, M. J. Birnbaum, D. A. McClain, Q. J. Zhang, D. Gale, L. J. Wilson and E. D. Abel (2009). "Contribution of insulin and Akt1 signaling to endothelial nitric oxide synthase in the regulation of endothelial function and blood pressure." Circ Res **104**(9): 1085-1094.
Tabák, A. G., M. Jokela, T. N. Akbaraly, E. J. Brunner, M. Kivimäki and D. R. Witte (2009). "Trajectories of glycaemia, insulin sensitivity, and insulin secretion before diagnosis of type 2 diabetes: an analysis from the Whitehall II study." The Lancet **373**(9682): 2215-2221.
Takeda, Y., K. Matoba, K. Sekiguchi, Y. Nagai, T. Yokota, K. Utsunomiya and R. Nishimura (2020). "Endothelial Dysfunction in Diabetes." Biomedicines **8**(7): 182.
Tatulian, S. A. (2015). "Structural Dynamics of Insulin Receptor and Transmembrane Signaling." Biochemistry **54**(36): 5523-5532.

Terwoord, J. D., M. L. Racine, C. M. Hearon, G. J. Luckasen and F. A. Dinenno (2021). "ATP and acetylcholine interact to modulate vascular tone and α." J Appl Physiol (1985) **131**(2): 566-574.
Tomschi, F., D. Niemann, W. Bloch, H. G. Predel and M. Grau (2018). "Ischemic Preconditioning Enhances Performance and Erythrocyte Deformability of Responders." Int J Sports Med **39**(8): 596-603.
Treiber, T., N. Treiber and G. Meister (2019). "Regulation of microRNA biogenesis and its crosstalk with other cellular pathways." Nat Rev Mol Cell Biol **20**(1): 5-20.
Turrell, H. E., C. Thaitirarot, H. Crumbie and G. Rodrigo (2014). "Remote ischemic preconditioning of cardiomyocytes inhibits the mitochondrial permeability transition pore independently of reduced calcium-loading or sarcKATP channel activation." Physiol Rep **2**(11).
van den Munckhof, I., N. Riksen, J. P. Seeger, T. H. Schreuder, G. F. Borm, T. M. Eijsvogels, M. T. Hopman, G. A. Rongen and D. H. Thijssen (2013). "Aging attenuates the protective effect of ischemic preconditioning against endothelial ischemia-reperfusion injury in humans." Am J Physiol Heart Circ Physiol **304**(12): H1727-1732.
Veroni, M. C., J. Proietto and R. G. Larkins (1991). "Evolution of insulin resistance in New Zealand obese mice." Diabetes **40**(11): 1480-1487.
Viswambharan, H., N. Y. Yuldasheva, A. Sengupta, H. Imrie, M. C. Gage, N. Haywood, A. M. Walker, A. Skromna, N. Makova, S. Galloway, P. Shah, P. Sukumar, K. E. Porter, P. J. Grant, A. M. Shah, C. X. Santos, J. Li, D. J. Beech, S. B. Wheatcroft, R. M. Cubbon and M. T. Kearney (2017). "Selective Enhancement of Insulin Sensitivity in the Endothelium In Vivo Reveals a Novel Proatherosclerotic Signaling Loop." Circ Res **120**(5): 784-798.
Waldron, G. J., H. Ding, F. Lovren, P. Kubes and C. R. Triggle (1999). "Acetylcholine-induced relaxation of peripheral arteries isolated from mice lacking endothelial nitric oxide synthase." British Journal of Pharmacology **128**(3): 653-658.
Wang, A., H. Zhang, Z. Liang, K. Xu, W. Qiu, Y. Tian, H. Guo, J. Jia, E. Xing, R. Chen, Z. Xiang and J. Liu (2016). "U0126 attenuates ischemia/reperfusion-induced apoptosis and autophagy in myocardium through MEK/ERK/EGR-1 pathway." Eur J Pharmacol **788**: 280-285.
Wang, J., S. Toan and H. Zhou (2020). "New insights into the role of mitochondria in cardiac microvascular ischemia/reperfusion injury." Angiogenesis **23**(3): 299-314.
Wang, S., R. Chennupati, H. Kaur, A. Iring, N. Wettschureck and S. Offermanns (2016). "Endothelial cation channel PIEZO1 controls blood pressure by mediating flow-induced ATP release." Journal of Clinical Investigation **126**(12): 4527-4536.
Wider, J., V. V. R. Undyala, P. Whittaker, J. Woods, X. Chen and K. Przyklenk (2018). "Remote ischemic preconditioning fails to reduce infarct size in the Zucker fatty rat model of type-2 diabetes: role of defective humoral communication." Basic Res Cardiol **113**(3): 16.
Wu, G., M. Chen, X. Wang, E. Kong, W. Yu, Y. Sun and F. Wu (2020). "Effect of remote ischemic preconditioning on hepatic ischemia-reperfusion injury in patients undergoing liver resection: a randomized controlled trial." Minerva Anestesiol **86**(3): 252-260.
Yang, J., F. Shakil and S. Cho (2019). "Peripheral Mechanisms of Remote Ischemic Conditioning." Cond Med **2**(2): 61-68.

Yang, N., L. Wu, Y. Zhao, N. Zou and C. Liu (2018). "MicroRNA-320 involves in the cardioprotective effect of insulin against myocardial ischemia by targeting survivin." Cell Biochem Funct **36**(3): 166-171.
Yuan, T., T. Yang, H. Chen, D. Fu, Y. Hu, J. Wang, Q. Yuan, H. Yu, W. Xu and X. Xie (2019). "New insights into oxidative stress and inflammation during diabetes mellitus-accelerated atherosclerosis." Redox Biol **20**: 247-260.
Zhang, Y., X. Yang, Z. Li, K. Bu, T. Li, Z. Ma, B. Wang, L. Ma, H. Lu, K. Zhang, L. Liu, Y. Zhao, Y. Zhu, J. Qin, J. Cui, S. Liu, P. Fan and X. Liu (2021). "Pyk2/MCU Pathway as a New Target for Reversing Atherosclerosis." Front Cell Dev Biol **9**: 651579.
Zhao, M., D. Finlay, I. Zharkikh and K. Vuori (2016). "Novel Role of Src in Priming Pyk2 Phosphorylation." PLoS One **11**(2): e0149231.
Zhao, Y., Y. Xue, Z. Liu, S. Ren, X. Guan, M. Li, X. Zhao, Y. Song and X. Ren (2019). "Role of the Janus kinase 2/signal transducers and activators of transcription 3 pathway in the protective effect of remote ischemia preconditioning against cerebral ischemia-reperfusion injury in rats." Neuroreport **30**(9): 664-670.

6 Acknowledgments

I would like to express my immense gratitude to Prof. Dr. med. Malte Kelm for granting me the invaluable opportunity to pursue my Ph.D. within the Cardiovascular Research Laboratory. The support and guidance I received during my doctoral studies have been truly exceptional. Thank you.

I am genuinely grateful to Prof. Dr. Eckhard Lammert for his unwavering support and guidance these past four years. Your mentorship has been invaluable for the success of this project.

I am profoundly grateful to Dr. med. Ralf Erkens, whose leadership and continuous support were essential for the success of this project. Thank you so much for having chosen me for this project. Your mentorship has been instrumental in shaping my doctoral journey.

Dr. med. Dragos Duse, your support, feedback, and assistance with the transportation of mice have been invaluable contributions to this work. Thank you.

I extend my heartfelt appreciation to Prof. Dr. Norbert Gerdes, Dr. Susanne Pfeiler, and Dr. Alexander Lang for your unwavering support and assistance during my time in the Cardiolab. The collaborative spirit and expertise you provided were essential.

To my colleagues at Cardiolab, I sincerely thank you for your support, which has been pivotal in making this project a reality. A special thanks goes to Stephanie Becher, whose invaluable assistance in the animal facility, surgical procedures, and Millar catheter experiments has been indispensable.

My gratitude extends to Hakima Ezzahoini, who has provided both technical expertise and emotional support throughout these four years. Your presence has been a constant source of strength.

Dr. Ramesh Chennupati, your guidance and feedback on analytical experiments have been invaluable. Thank you for sharing your knowledge and expertise.

I am also immensely grateful to the Medical Research School team, particularly Dr. Jessica Gätjens, for making my doctoral journey smoother. Your support was a beacon of light.

I sincerely thank the CRC1116 doctoral program team for their incredible support and efforts in enhancing our Ph.D. experiences. Your dedication has not gone unnoticed.

This project would have been impossible without the support of Prof. Dr. Hadi Al-Hasani and Dr. Alexandra Chadt. Your assistance with the NZO mice has been instrumental, and I am immensely grateful for your support.

I extend my appreciation to Prof. Dr. Ingrid Fleming and Dr. Mauro Siragusa for their support with the Pyk2 inhibition protocols and eNOS tyrosine phosphorylation experiments.

I am deeply grateful for the wonderful friends I have made since arriving in Germany. You all make life more enjoyable and the Ph.D. journey much easier. Thank you, Katerina, for your constant support, encouragement, love and belief in me. Your friendship has been a rock throughout this journey. Denada, you have truly been a gift from God on this path. I'm so grateful for your unwavering support, kindness, and for standing by my side every step of the way. My gratitude and heartfelt thanks also to Sara, Tanya, Isabella Maria, Vithya, Ashley, Angelina, Gabrielle, and Delsi. Your friendship has been a blessing, and I am forever grateful for your support and kindness.

I am forever grateful for your support and kindness. I would like to extend my gratitude to Isabella Gyamfi Poku, who, besides being a fantastic friend, also taught me essential methods used in this thesis (Echocardiography and FMD).

Martha Calazans, my dear friend, your intense support throughout my Ph.D. and the past 23 years of my life has meant the world to me. Thank you for always being there for me and loving me just as I am.

Larissa Oliveira, your support and kind words during my writing process have been a source of motivation. You are an example of dedication and strength. Thank you for believing in me and helping me realize I can do it. Your help in this process was invaluable.

Thanks to my boyfriend Sebastian, without whom I would never have moved to Germany. Thank you for believing in my dreams and sharing them with me. Thanks for your love and support, for never letting me give up, and for holding my hand when fear threatened to overpower me.

I am eternally grateful to Rita Keller for planting the seed of pursuing my Ph.D. in Germany and embracing me as her daughter. Your strength and kindness have left a memorable mark on my life, and I will forever miss you. I also want to express immense gratitude to Helmut Keller for treating me like a daughter and providing great support and encouragement throughout this journey. Your love and kindness have been a tremendous blessing.

Thank you so much to my parents and God (Rom.11:36) for their support, guidance, unconditional love, and for believing in me when I could not do it. Your boundless love has carried me through the most challenging moments of this journey. I will never forget all the sacrifices you made so I could have a good education. I extend my thanks to my entire family for their incredible support and encouragement. To Guilherme, Nathalia, Vó Elza and Vô Moacyr, Vó Rita and Vô João, Tia Carol, Tia Solange, Tia Lucia, Tia Rita, Marcella, Vitoria, Alex, Alan, Priscila, Aninha, Brenno, Bruno, Julio and all the family and friends who have wished me luck, your collective support has been a driving force behind my success.